Physics – Uspekhi **51** (11) 1091 – 1121 (2008)

REVIEWS OF TOPICAL PROBLEMS

PACS numbers: **12.60.–i**, **29.40.–n**, **95.35.+d**

The search for dark matter particles

V A Ryabov, V A Tsarev, A M Tskhovrebov

DOI: 10.1070/PU2008v051n11ABEH006599

Contents

1. Introduction **1091**
2. Evidence of dark matter **1092**
3. Candidates for DM particles **1094**
3.1 Neutrinos; 3.2 Weakly interacting massive particles (WIMPs); 3.3 Superweakly interacting massive particles (SWIMPs); 3.4 Exotic baryonic candidates for DM particles; 3.5 Magnetic monopoles; 3.6 Mirror particles
4. The search for DM particles in collider experiments **1099**
5. Indirect methods of the search for DM particles: detection of WIMP annihilation products **1100**
5.1 Detection of neutrinos with neutrino telescopes; 5.2 Detection of photons with gamma-telescopes; 5.3 Balloon and satellite experiments to observe positrons and antiprotons
6. Direct detection of WIMPs **1106**
6.1 Charge detectors; 6.2 Scintillation detectors; 6.3 Cryogenic heat detectors; 6.4 Overheated droplet detectors and superconducting granule detectors; 6.5 Combined light and heat detectors; 6.6 Combined heat and ionization detectors; 6.7 Combined light and ionization detectors
7. Detection of strongly interacting DM **1113**
8. New promising methods for the detection of DM particles **1114**
8.1 Acoustic detection of massive charged DM particles in satellite experiments; 8.2 Two-channel cryogenic magnetic calorimeter
9. Conclusion **1117**
References **1118**

Abstract. **Evidence of dark matter in the Universe is discussed and the most popular candidates for dark matter particles are reviewed. The review is mainly devoted to numerous experiments, both underway and planned, on the search for dark matter particles. Various experimental methods are discussed, including those involving direct registration of dark matter particles with the detector and those where the products of dark matter decay and annihilation are registered.**

1. Introduction

Detection of dark matter (DM), i.e., matter emitting no light and unobservable with telescopes, is crucial for cosmology, astrophysics, and elementary particle physics [1]. Recent astrophysical and cosmological measurements have demonstrated that ordinary matter comprises less than 5% of the total energy density in the Universe, while the nature of the remaining 95% is unknown. This fact is one more example from the history of science, which abounds in situations where researchers had to recognize that the outside world they thought they knew so well proved to be but a small fraction of the still unexplored Universe. Numerous experiments in search of dark matter particles are presently underway in many countries (Fig. 1). In none of them, however, have these particles thus far been detected. The search for DM particles and detailed studies of their properties require joint efforts of experts working in different fields of accelerator and nonaccelerator physics and astrophysics, as well as the use of a range of mutually complementary methods.

Direct detection of DM particles coming in from the galactic halo would give evidence that these particles constitute the hidden mass of the Universe. Creation of new particles in accelerator experiments would open up possibilities for their comprehensive investigation. Finally, indirect detection of astrophysical signals from the putative annihilation of DM particles would provide important information, e.g., about the DM distribution. At the same time, it is clear that indirectly measured signals are often difficult to distinguish from signals produced by astrophysical sources. Generally speaking, detailed studies of DM particles require the development and manufacture of sophisticated detectors, the creation of materials free from radioactive admixtures, and building underground laboratories protected from cosmic background radiation.

V A Ryabov, V A Tsarev, A M Tskhovrebov Lebedev Physical Institute, Russian Academy of Sciences,
Leninskii prosp. 53, 119991 Moscow, Russian Federation
Tel. (7-499) 132 24 52, (7-499) 135 42 95. Fax (7-499) 135 24 52
E-mail: ryabov@x4u.lebedev.ru, tsarev@x4u.lebedev.ru, tshovrebov@rambler.ru

Received 18 March 2008, revised 20 August 2008
Uspekhi Fizicheskikh Nauk **178** (11) 1129 – 1163 (2008)
DOI: 10.3367/UFNr.0178.200811a.1129
Translated by Yu V Morozov; edited by A M Semikhatov

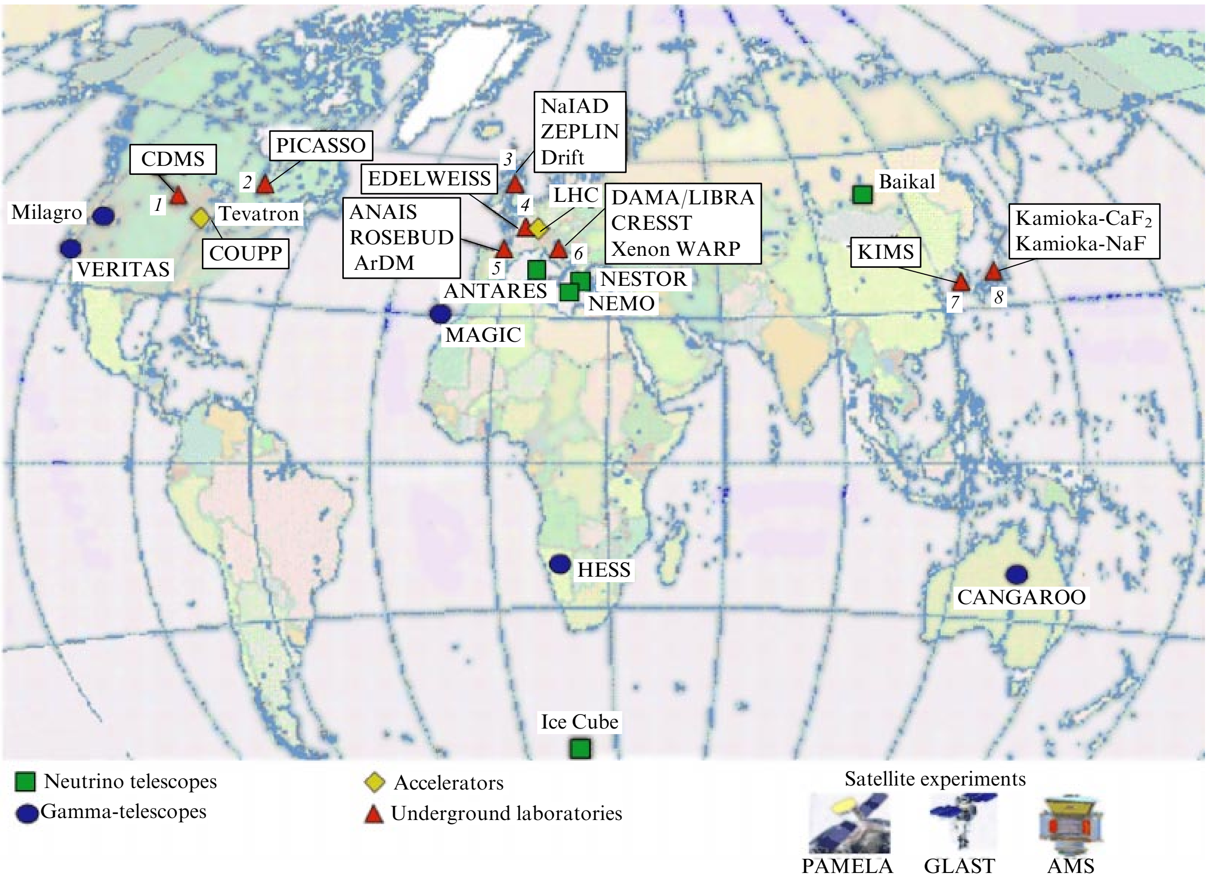

Figure 1. Geographic location of instruments for the search of DM mentioned in this review. Neutrino telescopes: ANTARES (Astronomy with a Neutrino Telescope and Abyss environmental RESearch), NESTOR (Neutrino Extended Submarine Telescope with Oceanographic Research), NEMO (NEutrino Mediterranean Observatory), Ice Cube, Baikal (Baikal Deep-Water Neutrino Telescope, BDNT). Gamma telescopes: Milagro, VERITAS (Very Energetic Radiation Imaging Telescope Array System), MAGIC (Major Atmospheric Imaging Cherenkov), HESS (High Energy Stereoscopic System), CANGAROO (Collaboration of Australia and Nippon (Japan) for a GAmma Ray Observatory in the Outback). Accelerators: Tevatron (Fermi National Accelerator Laboratory, FNAL), LHC (Large Hadron Collider, CERN). Underground laboratories: *1*, Soudan, USA, CDMS detector (Cryogenic Dark Matter Search); *2*, Sudbury, Canada, PICASSO detector (Project In Canada to Search for Supersymmetric Objects); *3*, Boulby, UK, detectors: NaIAD (NaI Advanced Detector), ZEPLIN (ZonEd Proportional scintillation in LIquid Noble gases), Drift; *4*, Modan, France, detector EDELWEISS (Expérience pour Détecter Les WIMPs en Site Souterrain); *5*, Canfranc, Spain, detectors: ANAIS (Annual modulation with NaI's), ROSEBUD (Rare Objects Search with Bolometers UndergrounD), ArDM (Argon Dark Matter); *6*, Gran-Sacco, Italy, detectors: DAMA/LIBRA (Dark MAtter/Large sodium Iodide Bulk for RAre processes), CRESST (Cryogenic Rare Event Search with Superconducting Thermometers), Xenon, WARP (Wimp ARgon Programme); *7*, Yang Yang, South Korea, detector KIMS (Korea Invisible Mass Search); *8*, Kamiokande, Japan, detectors: Kamioka-CaF_2(Eu), Kamioka-NaF. Detector COUPP (Chicagoland Observatory for Underground Particle Physics) located in the tunnel of the Tevatron NuMI neutrino channel (Neutrinos at the Main Injector). Also shown are satellite experiments: PAMELA (Payload for Antimatter Matter Exploration and Light-nuclei Astrophysics), GLAST (Gamma-ray Large Apace Telescope), AMS (Alpha Magnetic Spectrometer).

The problem of DM and the arguments for the existence of DM are briefly reviewed in Section 2. Favored candidates for DM particles are considered in Section 3. Detailed discussion of various aspects of theoretical models is beyond the scope of this publication. More comprehensive information can be found in the original works referred to in the text below. Sections 2 and 3 are intended to provide just a glimpse of the wide spectrum of ideas proposed to explain DM. In the bulk of the review, numerous experiments on the search for dark matter particles, both on-going and planned ones, are discussed. Section 4 concerns collider experiments and Section 5 is focused on the use of 'indirect' methods based on the detection of annihilation and decay products of DM particles. Direct detection of weakly and strongly interacting DM particles is discussed in Sections 6 and 7, respectively. Section 7 additionally describes certain new methods for the detection of DM particles. The Conclusion illustrates prospects for DM detection in future experiments.

2. Evidence of dark matter

The astronomer F Zwicky was the first to postulate the existence of DM in 1933 based on the results of investigations of galactic clusters [2]. Zwicky measured the dispersion of velocities of individual galaxies in the Coma cluster and suggested that a large amount of invisible matter is necessary to keep them gravitationally bound together. A great variety of self-consistent astrophysical and cosmological data have been obtained since that time, giving unquestionable evidence of the existence of DM on different scales of the Universe. A detailed discussion of various aspects of the nature of DM can be found in monograph [3].

The most direct and convincing evidence of DM on the galactic scale has been given by the analysis of galactic rotational curves or plots of orbital velocities of stars and gas versus their distance from the galactic center. The stars and the gas revolve around the center of a galaxy. For

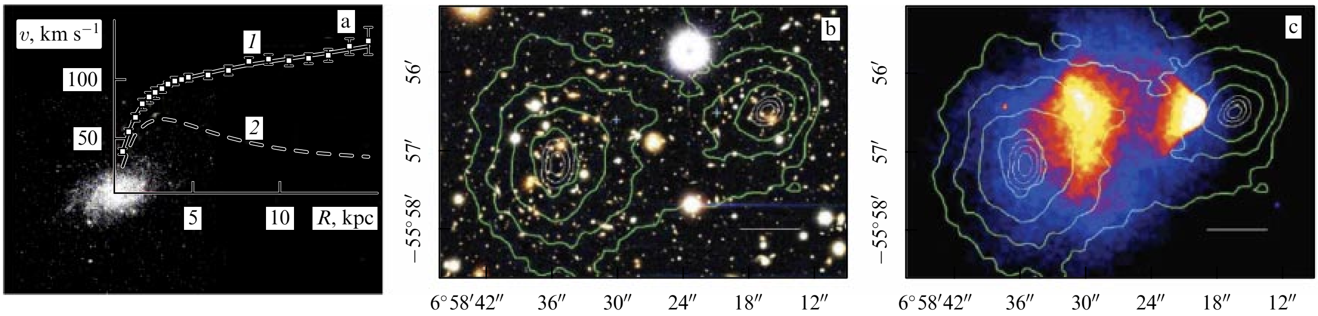

Figure 2. (a) Rotation curves for the M33 galaxy [4]: *1*, the observed curve, *2*, theoretical curve of the glowing galactic disk. (b) Optical and (c) X-ray images of cluster 1E0657-558 obtained with the Hubble and Chandra telescopes, respectively. The curves show mass density contours reconstructed by gravitational lensing [5]. Horizontal axes are the inclination angles, vertical axes are the ascention angles.

example, our solar system orbits the galactic center at a speed of roughly 220 km s^{-1}. According to Kepler's law, the total mass $M(r)$ inside a region of radius r and the orbital velocity $v(r)$ at the distance r from the galaxy center are related as

$$v^2(r) = \frac{G_\mathrm{N} M(r)}{r}\,,$$

where

$$M(r) = 4\pi \int_0^r \rho(r) r^2 \, \mathrm{d}r$$

and $\rho(r)$ is the distribution of matter density.

If we leave the area of the optically observable galactic disk, the orbital velocity of certain remote stars must decrease with increasing r as $v(r) \sim r^{-1/2}$. But observations do not confirm this dependence. Instead, 'flat' rotational curves, $v(r) \sim$ const, like those shown in Fig. 2a, have been obtained [4].

In the outer galactic region containing only cold neutral hydrogen and no stars, the gas rotation rate can also be measured. Such measurement is possible for galaxies seen from the 'side,' i.e., parallel to their plane. Radiotelescopes allow observing emission at the wavelength 21 cm corresponding to ultrathin splitting due to proton – electron spin interactions. The orbiting of a galaxy leads to a Doppler shift of the 21 cm line, which allows estimating the gas rotational velocity in the outer region of the galaxy. The orbital speed of the gas, like that of the stars, remains unaltered far beyond the limits of the visible galaxy.

Measurements of a few hundred spiral galaxies indicate that all of them are 'imbedded' into a massive DM halo. The actual size of the halo has until recently been impossible to measure. Analysis of the results of gravitational lensing made in the last few years has shown that the diameter of the dark galactic halo may be more than one order of magnitude greater than the visible diameter.

These findings suggest the existence of galaxies with a universal density profile: an exponentially thin stellar disk and a spherical DM halo with a smooth core of a radius r_0 and the density

$$\rho_0 = 4.5 \times 10^{-2} \, (r_0 \, [\mathrm{kpc}])^{-2/3} M_\odot [\mathrm{pc}^{-3}]\,,$$

where $M_\odot = 2 \times 10^{30}$ kg is the solar mass. The total amount of DM in the halo is difficult to estimate because we do not know its outer boundaries.

Studies of galactic clusters on large scales have revealed an even greater fraction of DM relative to the stars and the gas.

The results of independent investigations of virial speeds of the galaxies and velocities of the X-ray emitting gas gravitationally bound in clusters and data on gravitational lensing of background objects by the clusters yielded similar values of the DM mass. A characteristic example is presented in Fig. 2b, c showing cluster 1E0657-558 visualized at optical and X-ray wavelengths [5]. Analysis of the optical image indicates that the mass of the galaxies is only a few percent of the cluster mass. The X-ray image confirms localization of gaseous objects in the cluster. Finally, mass density contours reconstructed by means of gravitational lensing show that cluster 1E0657-558 probably consists of two galactic clusters containing both visible matter and spatially distributed DM [6].

Exploration of the Universe to cosmological scales, including detailed investigations of the anisotropy of the cosmic microwave background (CMB), observations of supernovae (SN) with large red shifts z, and studies of the large-scale distribution of galaxies, provide the basis for a cosmological model consistent with the mean matter density in the Universe deduced from observations of clusters and the primary distribution of light elements formed in the Big Bang nucleosynthesis. The same observations imply that DM had to be nonrelativistic by the moment when radiation and matter densities became equal. Such DM is referred to as cold.

Many recent astrophysical observations indicate that the exotic dark energy (DE) characterized by a virtually uniform density distribution and negative pressure [7, 8] dominates in the present Universe. The simplest candidate for the description of this DE is the cosmological term Λ in the Einstein field equations. Such a possibility has been considered throughout the entire history of relativistic cosmology. The main evidence of DE is derived from the observed temperature fluctuations of the CMB and formation of large-scale structures. Taken together with the results of other observations, this gives the picture of an almost spatially flat Universe having 70% of its energy in the form of DE. Consideration of DE is beyond the scope of this review. A detailed discussion of the DE problem can be found in [9].

In recent years, the Wilkinson Microwave Anisotropy Probe (WMAP) [10], Two Degree Field Galaxy Redshit Survey (2dFGRS) [11], and Sloan Digital Sky Survey (SDSS) [12, 13] experiments have provided highly accurate measures of major cosmological parameters. The totality of the results of these experiments are fairly well explained in the framework of a simple model of the Friedman – Robertson – Walker geometrically flat Universe in which 30% of energy density is in the form of nonrelativistic matter ($\Omega_{\rm M} = 0.30 \pm 0.04$) and 70% is in the form of DE with a negative pressure ($\Omega_{\Lambda} = 0.70 \pm 0.04$). Here and hereinafter, we use the standard notation: $a(t)$ is the scale factor in the Einstein equations, $H(t) = \big(\mathrm{d}a(t)/\mathrm{d}t\big)/a(t)$ is the Hubble parameter, $h = H/100$ [km s^{-1} Mpc^{-1}], and $\rho_{\rm c} = 3H/8\pi G_{\rm N}$ is the critical energy density at which the Universe is flat. Also, it is convenient to introduce the quantities $\Omega_i = \rho_i/\rho_{\rm c}$ and $\Omega = \sum \Omega_i = \sum \rho_i/\rho_{\rm c}$, where ρ_i is the density of the ith type of matter. All matter in the Universe can be described using three parameters: the Hubble constant $h = 0.70^{+0.04}_{-0.03}$, the matter density $\Omega_{\rm M}h^2 = 0.138 \pm 0.012$, and the baryonic density $\Omega_{\rm B}h^2 = 0.0230^{+0.0013}_{-0.0012}$, with the Universe containing only $\sim 4\%$ baryons and $\sim 26\%$ DM.

3. Candidates for DM particles

These findings account for a rather paradoxical situation in modern cosmology, that is, the amount of DM is fairly well known, but its nature remains virtually unknown. Elucidation of the nature of DM is the most challenging problem facing modern cosmology. The existence of DM in the Universe is deduced exclusively from its gravitational effect on the behavior of astrophysical systems on different cosmological scales, from galaxies to the cosmological horizon. The presence of still unobservable massive dark matter particles in the Universe is thus far the most natural explanation of this paradox despite alternative models of modified gravity proposed to account for the anomalous gravitational behavior of astrophysical objects [14]. We consider the most popular candidates for dark matter particles in Sections 3.1 – 3.6 below.

3.1 Neutrinos

3.1.1 Standard model neutrinos. Experimental studies of solar (Super-Kamiokande [15], Sudbury Neutrino Observatory (SNO) [16]), atmospheric (Super-Kamiokande [17], Main Injector Neutrino Oscillation Search (MINOS) [18, 19]), and accelerator (K2K [20, 21], MINOS [22, 23]) neutrinos have revealed oscillations, which imply nonzero neutrino masses; without a doubt, therefore, neutrinos contribute to DM. To date, the neutrino is the sole DM particle detected in experiment.

The cosmological background of relic neutrinos is predicted from the Big Bang cosmology. Being relativistic particles, neutrinos fall out of thermodynamic equilibrium and therefore comprise 'hot' DM. Such neutrinos may be the most widespread particles in the Universe after relic photons. The density of the number of neutrino light states in the Universe is presently estimated as [24]

$$n_{\nu}^0 + n_{\bar\nu}^0 \approx \frac{3}{4}\left(\frac{T_{\nu}^0}{T_{\gamma}^0}\right)^3 n_{\gamma}^0 \approx 112\ \mathrm{cm}^{-3}\,, \qquad n_{\nu}^0 = n_{\bar\nu}^0\,,$$

where n_{ν}^0, $n_{\bar\nu}^0$, and n_{γ}^0 are today's relic neutrino, antineutrino, and photon densities, $(T_{\nu}^0/T_{\gamma}^0)^3 \approx 4/11$, and $n_{\gamma}^0 \approx 400\ \mathrm{cm}^{-3}$. The maximum possible contribution of relic neutrinos of all i flavors to the Universe's matter is given by [24]

$$\Omega_{\nu}h^2 = \frac{\sum_i m_{\nu_i}}{94\ \mathrm{eV}}\,.$$

The best of the currently available experimental constraints on the electron neutrino mass have been achieved in the studies of the form of electron energy spectra in tritium β-decay: $m_{\nu} < 2.05$ eV (Troitsk [25]) and $m_{\nu} < 2.3$ eV (Mainz [26]) at a 95% confidence level. Practically speaking, these constraints hold for all mass states of neutrinos because the mass difference between them is very small: $\Delta m^2_{\rm solar} \approx \Delta m^2_{\rm reactor} \approx 7 \times 10^{-5}\ \mathrm{eV}^2$ and $\Delta m^2_{\rm atm} \approx \Delta m^2_{\rm acceler} \approx 3 \times 10^{-3}\ \mathrm{eV}^2$ as shown in experiments with solar (Homestake [27], GALLEX (Gallium Experiment) [28], SAGE (Soviet-American Gallium Experiment)[1] [29], GNO (Gallium Neutrino Observatory) [30], Super-Kamiokande [15], SNO [16], reactor KamLAND (Kamioka Liquid scintillator Antineutrino Detector) [31], atmospheric MACRO (Monopole Astrophysics and Cosmic Ray Observatory) [32], Soudan 2 [33], Super-Kamiokande [15, 34 – 36], MINOS [18, 19]), and long-baseline accelerator (K2K [20, 21], MINOS [22, 23]) neutrinos. The following constraint on the total relic neutrino density ensues from the experimentally found constraint on the neutrino mass:

$$\Omega_{\nu}h^2 < 0.07\,;$$

evidently, the neutrino cannot be the dominant component of DM.

In spite of the small contribution to the DM density, the neutrino plays an important role in cosmology by virtue of its large interaction length because it hampers evolution of minor objects formed in the Universe.[2] Simulation of the development of the Universe structure for different contributions of the neutrino component to matter have shown that $\sum_{\alpha} m_{\nu_{\alpha}} < 1$ eV [37].

Besides observation of the Universe large-scale structure, contributions of the neutrino component are estimated by measuring the CMB temperature fluctuations (WMAP [10]), Lyman-α forest energy spectra (SDSS [12, 13]),[3] and the luminosity of supernovae (Hubble Telescope [38]). Taken together, the results of these astrophysical measurements give several dissimilar cosmological constraints on the neutrino mass [10, 39 – 41]:

$$\sum_{\alpha} m_{\nu_{\alpha}} < (0.17 - 0.65)\ \mathrm{eV}\,.$$

This constraint is applicable to the whole body of hot DM, e.g., axions [39].

3.1.2 Sterile neutrinos. Sterile neutrinos were suggested as candidates for DM particles over 15 years ago [42]. They do not participate in weak interactions but, being massive particles, can mix with ordinary neutrinos. The overall result of oscillation studies gives evidence of the existence of one or several noninteracting sterile neutrinos into which ordinary-flavor neutrinos are converted as a result of oscillations. Experiments at the LEP (Large Electron – Positron) collider revealed only three generations of light

[1] The acronym SAGE is still in use, although 'Soviet' should have been substituted by 'Russian' some time ago.

[2] The neutrino – nucleus interaction length is expressed through the total cross section $\sigma^{\rm tot}_{\nu N}$ of this interaction: $L^{\rm int}_{\nu N}(E_{\nu}) = [\sigma^{\rm tot}_{\nu N}(E_{\nu})N_A]^{-1}$, where $N_A = 6.022 \times 10^{23}\ \mathrm{cm}^{-3}$ (water equivalent).

[3] Quasar spectra with relatively large red shifts contain many (a forest) of shifted Lyman-α H absorption lines attributable to the presence of hydrogen clouds at different line-of-sight distances (hence, the term Lyman-α forest).

neutrinos [43]. This means that three Δm^2 values can be measured in neutrino oscillation experiments, of which only two are independent. There are three groups of measurements in the following nonoverlapping ranges Δm^2 reported to date: $\Delta m^2_{21} \approx (10^{-5}-10^{-6})$ eV^2 in solar and reactor neutrino experiments, $\Delta m^2_{32} = 3.0 \times 10^{-3}$ eV^2 in experiments with atmospheric and long-baseline accelerator neutrinos, and $0.3 \text{ eV}^2 \leqslant \Delta m^2_{\text{LNSD}} \leqslant 2.2 \text{ eV}^2$ in LSND (Los Alamos Liquid Scintillation Neutrino Detector) experiments, whose results are still regarded as valid. Even if the three-flavor merging scenario proved unrealistic, we would have to recognize the existence of at least one sterile neutrino. Given the existence of more than three massive neutrinos, this fact should be regarded as a manifestation of physics beyond the Standard Model (SM).

The existence of DM in the form of sterile neutrinos has been discussed in many publications (see, e.g., [44–46]). Such neutrinos must have very small mixing angles with ordinary neutrinos. The mass of sterile neutrinos must have been relatively large (~ 10 keV) to enable them to smooth all fluctuations at scales smaller than their path length as they traveled across the early Universe. In other words, the mass had to satisfy the constraints ensuing from observations of the large-scale structure of the Universe. Sterile neutrinos must decay into ordinary SM neutrinos with the emission of photons whose energy roughly corresponds to half the mass of a decaying neutrino. The lifetime of sterile neutrinos may exceed the age of the Universe, which accounts for the considerable stability of sterile states. SDSS data on Lyman-α forest spectra [12, 13] and the failure to observe γ-emission from galactic clusters with characteristic energies ~ 10 keV enabled the authors of Refs [45, 46] to deduce the constraint on the sterile neutrino mass

$$m_{\text{ster}} \geqslant 14 \text{ keV}.$$

3.1.3 Heavy and very heavy neutrinos. Heavy neutrinos can exist as a superposition with light neutrinos ν_i [47]. They should only weakly merge with ordinary neutrinos and their decays should be apparent as additional peaks in the spectrum of charged leptons accompanying neutrinos in leptonic decays of mesons ($\pi \to \mu\nu$, $\pi \to e\nu$, $K \to \mu\nu$). The absence of extra peaks in the positron spectrum from the $\pi^+ \to e^+\nu_e$ decay excludes the existence of heavy neutrinos with masses of the order of $50 \text{ MeV} \leqslant m_\nu \leqslant 130 \text{ MeV}$ [48].

A number of scenarios have been proposed in which the appearance of very heavy neutrinos ν_H is expected. All these scenarios are beyond the scope of the SM [49–51]. Models with very heavy neutrinos postulate masses in the range of $45 \text{ GeV} \leqslant m_{\nu_H} \leqslant 1 \text{ TeV}$. The lower limit is given by the failure to observe pair creation of such neutrinos in LEP experiments and the upper limit arises from the requirement of perturbative unitarity of the neutrino pair production amplitude from the initial state of two longitudinally polarized W-bosons or Z-bosons [52].

3.2 Weakly interacting massive particles (WIMPs)

One of the leading candidates for DM particles are weakly interacting massive particles (WIMPs), supposed to have been born in the very first instants after the Big Bang. The term WIMP applies to a class of particles distinguished first and foremost by a mass and an annihilation cross section that enabled them to fall out of equilibrium in the early Universe with a density characteristic of DM. First, the appearance of WIMPs in theoretical physics was motivated by the problem of the electroweak symmetry breaking. Second, in accordance with standard cosmological assumptions, the thermal relic abundance of WIMPs naturally coincides with that necessary for DM. Finally, the requirement of a sufficiently effective annihilation of WIMPs implies that their interaction with matter must be strong enough to make them detectable in direct experiments.

The present WIMP density is estimated as [53]

$$\Omega_{\text{WIMP}}\, h^2 \approx \frac{3 \times 10^{-27} \text{ cm}^3 \text{ s}^{-1}}{\langle \sigma_{\text{ann}} v \rangle}.$$

For a particle of a given mass, the mean annihilation cross section times the velocity, $\langle \sigma_{\text{ann}} v \rangle$, has a maximum determined by the partial-wave unitarity of the S-matrix, $\langle \sigma_{\text{ann}} v \rangle_{\max} \approx 1/m^2_{\text{WIMP}}$ [54, 55]. The requirement $\Omega_{\text{WIMP}}\, h^2 \leqslant 1$ is compatible with the unitarity limit and provides a constraint on the mass of DM particles, $m_{\text{WIMP}} \leqslant 340$ TeV [54]. Results of WMAP experiments suggest more rigorous constraints [56]:

$$m_{\text{WIMP}} \leqslant 120 \text{ TeV}.$$

3.2.1 Supersymmetric particles. A few variants of extending the SM lead to WIMPs. The most popular of them is supersymmetry (SUSY), which extends the SM by including new particles and interactions. Unlike the SM, where fermions (components of matter) and bosons (carriers of interactions) are fundamentally different, the supersymmetric theories bring together particles of both types in the framework of a unified picture of matter and interactions. Supersymmetric theories postulate superpartners of ordinary particles, i.e., new particles whose spins differ by 1/2. A peculiar feature of supersymmetric theories is the unification of gauge coupling constants on the scale $M_U \sim 2 \times 10^{16}$ GeV.

The minimal supersymmetric standard model (MSSM) is the minimal supersymmetric extension of the SM. In this model, all gauge fields have fermionic superpartners. Gluons and gauge bosons B, W_3 (or γ and Z^0), and $W^\pm$ have fermionic partners called gluino ($\tilde{g}$), bino ($\tilde{B}$), and wino ($\tilde{W}^i$). They all are known under the generic name of gaugino. All fermions have scalar partners, such as squarks and sleptons for quarks and leptons. An additional Higgs field, besides two Higgs doublets, is introduced, and each neutral Higgs boson (H^0_1 and H^0_2) has a corresponding Higgsino ($\tilde{H}^0_1$ and $\tilde{H}^0_2$) with spin 1/2.

The R-parity introduced in the MSSM is a multiplicative number defined by the relation

$$R = (-1)^{3B+L+2s},$$

where B is the baryon number, L is the lepton number, and s is the particle spin. For all SM particles, $R = 1$, and for all their superpartners, $R = -1$. Due to the R-parity conservation, supersymmetric particles ('s-particles') decay only into an odd number of s-particles (plus SM particles). This means that the lightest s-particle (LSP) is stable and disappears only in the case of pair annihilation. It makes the LSP an appealing candidate for DM [57, 58].

The MSSM imposes many restrictions on the nature of the LSP. This particle may have neither the electric nor the color charge; otherwise, it would be able to create heavy isotopes with baryonic matter, at variance with experimental data. The fittest candidates for the LSP are neutralinos or a linear combination of the superpartners of the photon, Z^0, and Higgs H_1^0- and H_2^0-bosons [59],

$$\chi = N_{11}\tilde{B} + N_{12}\tilde{W}_3 + N_{13}\tilde{H}_1^0 + N_{14}\tilde{H}_2^0 ,$$

where N_{11}, N_{12}, N_{13}, and N_{14} are constants.

Pair annihilation reactions and elastic scattering from nucleons are crucial for the detection of neutralinos. Presently, neutralinos must be essentially nonrelativistic, with the main annihilation channels into fermion – antifermion pairs (largely heavy ones), pairs of gauge bosons (W^+W^-, Z^0Z^0), and final states containing Higgs bosons.

Other conceivable supersymmetric candidates for DM particles, besides neutralinos, might be sneutrinos and gravitinos. However, it was shown in [60] that the expected cross section of neutrino – nucleon interactions is too large and in conflict with results of the direct search for DM. Gravitinos are subject to gravitational interactions alone; therefore, they are of little interest as experimental objects for the direct and indirect search of DM [61].

3.2.2 Kaluza – Klein states. The early Grand Unification theories were based on the idea that unification of all interactions occurs near the Planck scale $M_{\mathrm{Pl}} \equiv G_4^{-1/2} \approx 10^{28}$ eV, where $G_4 = 6.707 \times 10^{-33}$ TeV^{-2} is the gravitational constant in the four-dimensional space – time world. A new TeV scale of the interaction unification proposed in certain recent publications includes gravitation [62 – 67]. Such a 'premature' unification may result from the manifestation of extra dimensions on this scale, first suggested by Kaluza and Klein [68]. Kaluza and Klein increased the number of spatial dimensions up to four in order to include electromagnetism into a 'geometric' theory of gravitation, i.e., to unify electromagnetism and gravity by identifying additional components of the metric tensor with ordinary gauge fields. It has long been believed that these extra dimensions are too small and therefore do not affect physics at relatively low energies. However, recent string models have given evidence that some of these dimensions may be greater than that (~ 1 mm) without contradicting observational data, e.g., the proton lifetime [69 – 72]. In this approach to gravity, space – time has the so-called brane – bulk structure. The brane space has the $(3+1)$ dimensions of the ordinary space – time in which all the usual SM particles and fields live. The brane space is embedded into a bulk space having n extra dimensions, besides the $(3+1)$ dimensions of Minkowski space; moreover, it contains gravity and probably unobservable SM gauge particles and singlets. The fundamental gravity scale in such a brane-world space is the new interaction unification scale $M_{n+4} \approx 1$ TeV rather than the macroscopic Planck scale M_{Pl}.

Theories with extra dimensions contain massive Kaluza – Klein (KK) gravitons that may emerge in the form of real and virtual particles. In our four-dimensional world, KK gravitons manifest themselves as towers of massive excited states (KK states). We note that the lightest Kaluza – Klein particles (LKKPs) were suggested as candidates for DM in [73] long before the appearance of quantum gravity theories with large extra dimensions and a TeV scale.

At present, theories with unified extra dimensions (UED theories) are being developed in which all SM particles and fields can propagate in extra dimensions [74]. KK excitations in UED theories are observable states, and the lightest of them corresponding to the first SM excitations are appealing candidates for DM. The mass of the lightest KK states is $m_{\mathrm{KK}} \approx 400 - 1200$ GeV [75].

The possibility of one more candidate for DM in a brane-world space was recently suggested in [76]. Because rigid objects are nonexistent in relativistic theories, the brane space must have a certain finite tension and fluctuate. These fluctuations are taken into account by introducing new fields related to the brane position in the bulk. These fields are Goldstone bosons corresponding to a spontaneous symmetry breaking of translational invariance caused by the presence of a brane space in the bulk. Branons are supposed to be responsible for the observed density of cosmological DM and comprise galactic halo matter. In this case, they can be detected in both 'direct' and 'indirect' experiments.

3.3 Superweakly interacting massive particles (SWIMPs)

A new class of nonbaryonic cold DM, superweakly interacting massive particles (SWIMPs), was postulated in Ref. [61]. Similarly to WIMPs, SWIMPs can be introduced based on a theory including supersymmetry and quantum gravity models with extra dimensions.

The main difference between WIMPs and SWIMPs is that the latter superweakly interact with ordinary matter and are not detected in any direct experiment proposed thus far. Moreover, the use of indirect detection techniques is also precluded by the suppression of annihilation cross sections of these particles. The sole observable proof of SWIMPs might be the decay of ordinary WIMPs into SWIMPs accompanied by the emission of photons and the emergence of cascades. The existence of SWIMPs might be just as well evidenced by a peak in the spectrum of diffuse γ-quanta with energies ~ 10 keV – 10 MeV.

Other candidates for SWIMPs currently under consideration are gravitinos in supersymmetric theories and KK gravitons in theories with extra dimensions, as well as axions and axinos. The axion appears to be a most popular SWIMP; it was introduced into particle physics many years ago to solve the problem of CP invariance. Superweak interactions of axions with matter may indicate that they were not in thermal equilibrium in the early Universe. Their relic abundance may be correlated with the DM cosmological density for masses about 10 μeV. The scenario of axionic DM is considered in Ref. [77]. One of the most important properties of axions is the two-photon interaction allowing axion – photon conversion in electromagnetic fields. Most attempts to search for axions are based on the use of this process [78].

3.4 Exotic baryonic candidates for DM particles

3.4.1 Massive compact halo objects (MACHOs). One of the most natural hypotheses regarding the nature of DM is the assumption of a certain class of astronomical objects that remain invisible because of their small size and low luminosity. Such hypothetical entities, known as massive compact halo objects (MACHOs), include, for example, black holes born in the Big Bang era [79].

Recent measurements using the gravitational microlensing effect [80] have permitted estimating the overall contribution of MACHOs to DM. MACHO and EROS collaborations [81] monitored about 55 mln stars in the Small and Large Magellanic Clouds. The gravity fields of MACHOs encountered on the line of sight at the moment of observation focused light and enhanced star brightness. The total mass of MACHOs in galactic halos calculated from the

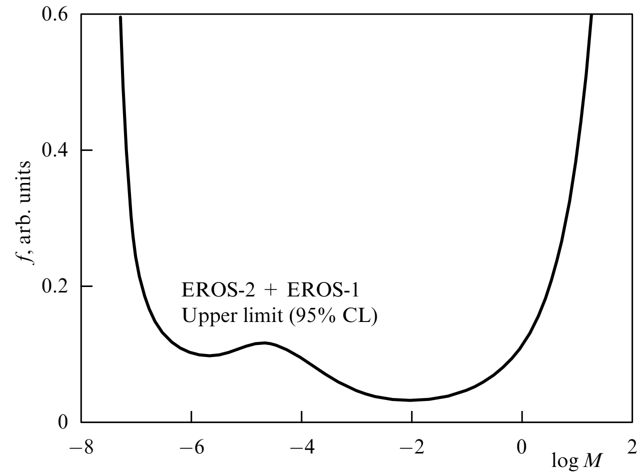

Figure 3. Limits for the halo mass fraction f enclosed in MACHOs with a mass M (EROS collaboration [81]).

results of monitoring proved to be less than 15% of the halo mass (Fig. 3).

3.4.2 Strangelets and nuclearites. Historically, the first 'exotic' candidates for DM were new particles and objects in the form of clumps of known or unknown quarks with an electric and/or baryonic charge [82, 83]. Strangelets are clumps of strange quark matter (SQM) composed of a roughly equal number of u-, d-, and s-quarks. Neutral SQM may exist as a strangelet surrounded by an electron cloud that compensates the charge. This quark – electron structure is called a nuclearite.

Strangelets and nuclearites are supposed to have emerged at an early stage of the Universe and persist until now as remnants of the Big Bang [83, 84]. SQM could form in both relic and modern epochs, e.g., from collisions of neutron and quark stars [85], giving rise to relatively light strangelets with $m_{\rm SQM} \approx 10^3 - 10^6$ GeV. A balloon experiment reported in Ref. [86] provides evidence of rapid massive charged strangelet-like particles in cosmic ray (CR) fluxes.

3.4.3 Technibaryons. Extension of the SQM concept to the technicolor theory gave rise to technibaryon matter (TBM) models [87]. The technicolor theory was in turn introduced to ensure the mechanism of spontaneous breaking of electroweak symmetry; this theory is very similar to the theory of quantum chromodynamics (QCD) but has an energy scale that is three orders of magnitude greater. Technibaryons predicted by this theory must have masses ~ 1 TeV. In analogy with SQM clumps (strangelets), TBM clumps are called technets. However, in contrast to strangelets with $m_{\rm QCM} < 10^4$ GeV, which presumably evaporated at an early stage of the Universe [84], technets are believed to survive until now because their binding energy is significantly higher than the critical temperature of transition from the quark – gluon phase to the hadron one.

3.4.4 CHAMPs. ChArge Massive Particles (CAMPs) were suggested as candidates for DM in [88]. The authors considered CHAMPs with a unit positive or negative charge. CHAMPs with the charge $Z = +1$ might exist as superheavy hydrogen and their antiparticles with $Z = -1$ might form bound states with protons or nuclei in the form of superheavy neutrons (neutroCHAMPs) or superheavy isotopes.

Later works were devoted to the estimation of the abundance of CHAMPs with different masses based on dynamic galactic models [88, 89], searches for anomalous hydrogen in seawater [90] and heavy isotopes [91], balloon and satellite CR experiments [92, 93], underground experiments [94], and analysis of stellar evolution [95]. The estimates thus obtained allow excluding the existence of CHAMPs with masses in the wide range $m_{\rm CHAMP} \approx 10^2 - 10^{16}$ GeV.

3.4.5 Superheavy X-particles. The constraint on the DM particle mass mentioned in Section 3.2, $m_{\rm DM} \leqslant 120$ TeV [56], was based on the unitarity limit assuming that DM particles are thermal relics from the early Universe. It is not impossible, however, that DM particles were not in thermodynamic equilibrium during the evolution of the Universe. Therefore, their mass may be as large as $10^{12} - 10^{19}$ GeV, much greater than the mass of thermal WIMPs. The possibility of gravitational formation of supermassive quasistable particles was first considered by Zel'dovich and Starobinskii [96].

Such superheavy particles (X-particles) might have emerged directly from vacuum fluctuations during inflation or transition between the inflation regime and the matter (radiation)-dominated regime due to nonadiabatic expansion of space – time in the early Universe [97, 98]. Because the X-particles are practically stable, they could probably have survived until now. However, it is difficult to account for such a long lifetime of X-particles comparable at least with the age of the Universe without knowing the symmetry necessary to support it. Approaches to the solution to this problem are discussed in several publications [97 – 100].

The primordial existence of superheavy particles (to be precise, their decays or annihilations in top – down scenarios) was suggested [101] as an alternative to the accelerator mechanism of cosmic ray (CR) formation with energies above the Greisen – Zatsepin – Kuz'min (GZK) cutoff [102, 103]. Because X-particles are not associated with any astrophysical object, they may decay or annihilate rather close to the Earth, e.g., in the halo of our Galaxy. Decay or annihilation products, i.e., CRs (nucleons and nuclei), neutrinos, and γ-quanta, may retain a large part of their energy until detection [97, 98, 104, 105]. If the CRs observed above the GZK cutoff originate from the decay of an X-particle, then its mass must be $m_{\rm X} \geqslant 10^{13}$ GeV.

For the minimal value $\tau_{\rm X} \approx 10^{10}$ years corresponding to the age of the Universe, the actual flux of superhigh-energy CRs corresponds to a low density of X-particles, $\Omega_{\rm X} \approx 10^{-12}$. If $\Omega_{\rm X} \approx 1$, X-particles may constitute an essential part of cold dark matter and the observed superhigh-energy CR flux corresponds to X-particles having a much longer lifetime, $\tau_{\rm X} \approx 10^{22}$ years [106, 107].

Weakly interacting WIMPZILLAs[4] [108] and strongly interacting neutral SIMPZILLAs [109] have been suggested as candidates for superheavy X-particles; the difference between the two amounts to the size of the cross section of their interaction with ordinary matter [110].

The main observational option for superheavy X-particles is registration of their decay and annihilation products, i.e., high-energy neutrinos and γ-quanta. We analyzed neutrino fluxes and γ-fluxes resulting from decays of superheavy

[4] Particles with the mass of 10 billion WIMP masses were named after the behemoth Wimpzillas.

X-particles of different types, as well as the possibilities of their detection in the new-generation neutrino and γ-telescopes and in DR detectors in [111].

3.4.6 Supersymmetric *Q*-balls. Supersymmetric generalizations of the SM, e.g., the MSSM, predict nontopological solitons called *Q*-balls [112]. Supersymmetric *Q*-balls are coherent states of squarks, sleptons, and Higgs fields with an arbitrary baryon number [113]. Such objects may have a number of interesting properties [114, 115]. Specifically, solitons with large baryon numbers are perfectly stable and might have been created in the early Universe [116]. Such objects are good candidates for DM. A soliton with a charge (baryonic number) $Q_{\rm B}$ has the mass $M_Q \approx (4\pi\sqrt{2}/3) m_0 Q^{3/4}$ and the radius $R_Q \approx 2^{-1/2} m_0^{-1} Q_{\rm B}^{1/4}$. It is believed that masses m_0 lie in the range from 100 GeV to 100 TeV.

The baryon number $Q_{\rm B}$ of a stable soliton must be higher than $10^{15}[m_0/(1\ \text{TeV})]^4$. Large solitons cannot decay into ordinary fermions because the energy per unit fermion number is smaller than the proton mass. *Q*-balls with a much larger total charge, e.g., in excess of 10^{20}, could probably have appeared in the early Universe from the decay of a coherent scalar condensate [116].

A flux of cosmic *Q*-balls toward the Earth can be estimated under the assumption that they make an important contribution to the DM of the Universe. Given the *Q*-ball density in the galactic halo $\rho_{\rm DM} \approx 0.3\ \text{GeV cm}^{-3}$, the particle number density is $n_Q \approx \rho_{\rm DM}/M_Q \approx 5\times10^{-5} Q_{\rm B}^{-3/4} (1\ \text{TeV}/m_Q)$ [cm^{-3}]. For the mean *Q*-ball speed $v_Q \approx 10^{-3}c$, its flux is

$$\Phi_Q \approx \frac{1}{4\pi} n_Q Q_{\rm B} v_Q \approx 10^2 Q_{\rm B}^{-3/4} \frac{1\ \text{TeV}}{m_Q}\ [\text{cm}^{-2}\ \text{s}^{-1}\ \text{sr}^{-1}].$$

Because solitons are able to retain the electric charge, relic solitons can be categorized into two classes: supersymmetric electrically neutral solitons (SENS's) and supersymmetric electrically charged solitons (SECS's). The coupling of *Q*-balls to matter and hence the methods of their detection essentially depend on whether DM is composed of SENSs or SECSs [117].

The passage of a *Q*-ball with the baryon number $Q_{\rm B} \approx 10^{24}$ through the detector is accompanied by the release of energy (~ 10 GeV per mm of path) and may leave a very bright signature. However, depending on the parameters m_0 and $Q_{\rm B}$, such events may be extremely rare [117].

Current experimental constraints on SECS fluxes follow from the results of MACRO experiments [118] for the search of nuclearites [83, 119], whose coupling to matter is similar: $\Phi_{\rm nuclearith} < 1.1\times10^{-14}\ \text{cm}^{-2}\ \text{s}^{-1}\ \text{sr}^{-1}$; this, in turn, gives the lower limit for the baryon number of DM composed of *Q*-balls, $Q_{\rm B} \geqslant 10^{21}$.

SENS signatures resemble those expected for Grand Unification monopoles responsible for the catalysis of proton decay. The corresponding constraint is $Q_{\rm B} \geqslant 10^{24}$ for $m_0 \approx 1$ TeV [117]. On the whole, *Q*-balls are appealing candidates for the DM predicted by supersymmetry.

3.4.7 Crypto-baryonic DM. Cryptons with the mass $\sim 10^{12}$ GeV are stable and metastable bound states of matter in the hidden sector suggested as candidates for superheavy DM in string and M-theories [120].

The concept of crypto-baryonic DM does not require the introduction of any new fundamental particles or interactions beyond the SM. This concept was developed in [121, 122] based on the assumption of at least one degenerate vacuum phase existing besides the ordinary vacuum. All DM, composed of a compressed cluster of atoms enclosed, e.g., in ~ 20 cm spherical regions, is concentrated in this phase. In this DM model, it is the ordinary baryonic matter or even atoms packed into small balls bounded by walls that separate the vacua. A similar model with QCD phases was discussed in [123].

We consider a representative ball with the radius 20 cm containing $N_{\rm B} = 3\times10^{37}$ baryons and with the mass of the order $M_{\rm B} \approx 10^{11}\ \text{kg} \approx 10^{-19} M_\odot$. Such clumps of DM cannot be detected by microlensing, which reveals only astrophysical compact objects with masses above $10^{-7} M_\odot$ [124]. Because the DM density is about 23% of the critical density $\rho_{\rm c} \approx 10^{-26}\ \text{kg m}^{-3}$, a volume of $10^{37}\ \text{m}^3 \approx (20\ \text{a.u.})^3$ contains a single DM ball on average. Crypto-baryonic balls comprising DM are difficult to observe, but they can expand inside dense stars. Disruption of their walls triggers a gamma-burst explosion. Such an explosive instability might have constituted the mechanism of birth of superhigh-energy CR particles from seemingly void regions of the Universe.

3.5 Magnetic monopoles

As is known, the monopole hypothesis was suggested by Dirac in 1931 to explain the electric charge quantization [125]. Dirac postulated a particle with a magnetic charge g related to an electric charge e by the quantization condition $eg = n\hbar c/2$, $n = 1, 2, \ldots$. But this relation does not fix the mass of the magnetic charge (monopole). Estimation based on the assumed equality of the classical monopole and electron radii gives $m_{\rm M} \sim g^2 m_{\rm e}/e^2 \approx n\,4700\, m_{\rm e} \approx n\,2.4$ GeV. These considerations have for a long time governed vain attempts to find light monopoles in accelerator experiments [126 – 128].

An understanding of the close connection between the monopole hypothesis and the theory of electromagnetic particles came after the work by 't Hooft [129] and Polyakov [130]. Magnetic monopoles arise in spontaneously broken non-Abelian gauge theories, which actually underlie all Grand Unified Theories (GUTs), in the form of a stable topological defect solution. If $m_{\rm X}$ is the mass of a typical gauge boson in the GUT, then the monopole mass can be written as $m_{\rm M} \propto \alpha_{\rm X}^{-1} m_{\rm X}$, where $\alpha_{\rm X}^{-1}$ is a dimensionless coupling constant on the $m_{\rm X}$ scale in the GUT model. In accordance with theories with the scale $m_{\rm X} \approx 10^{15}$ GeV, the assumption of $\alpha_{\rm X} \approx 0.025$ as a running coupling constant leads to a monopole with the mass $m_{\rm M} \approx 10^{17}$ GeV. This means that GUT monopoles will never be possible to investigate in an accelerator experiment.

As shown in Ref. [131], the massive monopoles that were formed in large numbers during phase transitions in the early Universe annihilated very slowly, and their density must now be of the same order as the baryon density. Because the monopole mass must be approximately 10^{16} times the proton mass, the matter density in the Universe with such a number of monopoles would have to be at least 10^{14} times the critical mass necessary to close the Universe, $\rho_{\rm c} \approx 10^{-29}\ \text{g cm}^{-3}$. Such a dense Universe would have inevitably collapsed. The problem of the abundance of relic GUT monopoles is resolved through the inflation mechanism, such that their content in the present Universe compares with the upper cosmological and experimental levels. It is supposed that the motion of heavy GUT monopoles is presently governed by gravity and magnetic fields, and their speeds must be close to the galactic speed ≈ 200 km s^{-1} [132].

Even lighter monopoles with masses $m_M \sim 10^7 - 10^{13}$ GeV are postulated that might have formed in the early Universe at a much later instant than that defined by the time scale of GUTs [133]. Such monopoles may accelerate to relativistic velocities in intergalactic magnetic fields [134] or acquire energy as they leave the surface of a neutron star [135]. Up to now, not a single event associated with monopoles has been documented in experiment. The best constraints on the monopole flux were obtained with the MACRO detector: $\Phi_{\text{monopole}} < 1.4 \times 10^{-16}$ cm^{-2} s^{-1} sr^{-1} [136].

3.6 Mirror particles

The ideas of 'mirror particles' and a 'mirror world' originated some 50 years ago and are currently discussed in the context of the DM problem. An introduction to the history of the mirror matter concept can be found in Ref. [137]. This model was created as a result of attempts to compensate the mirror asymmetry of weak interactions of ordinary particles despite the $V-A$ nature of such interactions [138, 139]. Another motivation for the introduction of mirror matter was the fact that all particles except gravitons have mirror partners. Mirror particles have the same masses as the ordinary ones and are coupled to one another as the usual particles, with the only difference that the mirror weak interaction is not left-handed but right-handed. The two sectors couple to each other gravitationally. Moreover, there are additional interaction channels. Possible nongravitational interactions involve the mixing of mirror and ordinary photons [139], mass states of mirror and ordinary SM neutrinos [140, 141], and mirror Higgs bosons and SM Higgs bosons [142].

Mirror protons and electrons must be stable for the same reason as ordinary protons and electrons. Mirror relic matter in the form of gas clouds, stars, planets, galaxies, etc. in the present-day Universe manifests itself as DM interacting gravitationally with the ordinary matter. The presence of mirror matter (in analogy with ordinary cold DM) might contribute to the formation of the Universe large-scale structure [143].

An important difference of mirror baryons from other candidates for DM is that mirror matter is coupled to itself. This property was used in [144] to resolve the problem of the DM density distribution.

In addition to mirror analogs of the ordinary SM particles, there may exist mirror superheavy DM X-particles decaying into mirror photons, leptons, and baryons. However, only mirror neutrinos turning into ordinary neutrino states as a result of oscillations can be detected [141]; all other decay products of mirror X-particles remain in the mirror world and are not observed in the ordinary one. Thus, mirror X-particles may be a hidden source of an intense neutrino flux [145] that might be detected by neutrino telescopes coming into operation in the near future.

4. The search for DM particles in collider experiments

The search for DM particles (WIMPs) is an important line of experimental studies currently underway at the Tevatron accelerator and designed to be conducted at the Large Hadron Collider (LHC). In CDF experiments (Collider Detector at Fermilab) [146] and the D0 experiment at Tevatron [147], at the energy $s_{pp}^{1/2} \approx 1.96$ TeV in the center-of-mass frame, the lower limits for gluino and squark masses were about 300 GeV. Energies $\sim s_{pp}^{1/2} \approx 14$ TeV are achievable in pp-interactions on the LHC, which allows observing the formation of new particles with large masses. The idea to study supersymmetric particles in LHC experiments was suggested in the mid-1990s [148] and their specific signatures are still the subject of extensive discussions [149, 150]. Specific conditions of KK-state detection in collider experiments are considered in detail in [151].

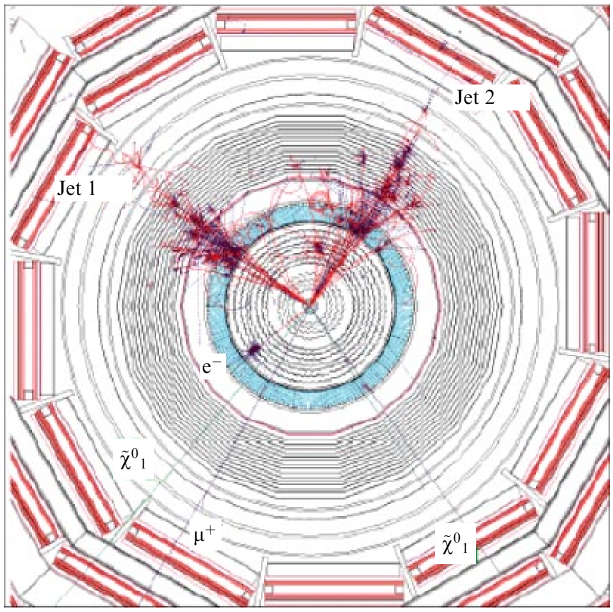

Figure 4. Simulated event giving rise to a pair of gluinos and their subsequent decay into WIMPs recorded with the SMS detector of LHC. The lacking transverse momentum with respect to the beam axis necessary for invisible WIMPs to form is denoted by $\tilde{\chi}_1^0$ [152].

Accelerator energies in excess of the WIMP rest mass are insufficient to observe these particles. Similarly to neutrinos, chargeless WIMPs generated in pp-interactions are invisible in detectors. The lacking energy (momentum) spent to the creation of a WIMP can be deduced only from the comprehensive kinematic analysis of visible products of the pp-interaction. An example of a simulated WIMP event in the CMS (Compact Muon Spectrometer) detector of the LHC is presented in Fig. 4 [152].

We note that only part of the pp-interaction energy is spent to form supersymmetric particles. Gluinos and squarks are born in interactions between individual quarks and gluons that transfer less than 10% of the total proton energy. For this reason, events giving rise to WIMPs with masses of the order 100 GeV are expected to occur at the LHC at energies 2000 GeV or higher.

Different variants of supersymmetric models and models with extra dimensions suggest a variety of candidates for WIMPs. In pp-collider experiments, this essentially complicates the problem of identifying the characteristic signatures of one WIMP type or another in a high-multiplicity final state [153]. Although some features of the final state of the interaction may in principle allow discriminating between the manifestations of supersymmetry and extra dimensions, the nature of WIMPs is not likely to be elucidated in LHC experiments [154]. However, the observation of heavy Higgs bosons (A, H, H$^\pm$) would substantially narrow the range of neutralino – nucleon cross sections determining the sensitivity of detectors necessary for direct identification of DM particles [155].

A more precise characteristic of WIMPs at energies $s_{ee}^{1/2} = 0.5-1$ TeV will be possible with the e^+e^- ILC (International Linear Collider) now under construction, [153–156]. High-energy e^+e^--annihilation processes give rise to pairs of new particles under better controlled conditions because it is much easier to identify final states of the e^+e^--reaction than to reconstruct all pp-interaction products. An attempt to observe Higgs bosons from e^+e^--interactions using the LEP collider at energies $s_{ee}^{1/2} \approx 200$ GeV in the center-of-mass frame has failed. The lower limit on the Higgs boson mass reported by the collaborations ALEPH (Apparatus for LEP physics), DELPHI (Detector with Lepton, Photon, and Hadron Identification), L3, and OPAL (Omni Purpose Apparatus at LEP) is $m_H > 114.4$ GeV [157]. Much higher energies to be achieved at the ILC may lead to the discovery of WIMPs and provide a good opportunity to separate the scenarios of their origin (SUSY or UED) [158–156]. However, an accelerator experiment does not permit estimating the contribution of new particles to DM even for a concrete scenario.

5. Indirect methods of the search for DM particles: detection of WIMP annihilation products

A number of experiments have been designed to observe hypothetical WIMP annihilation products in galactic halos, in the center of the Sun, and in other regions of the Universe. These products include neutrinos, positrons, antiprotons, and gamma-quanta.

5.1 Detection of neutrinos with neutrino telescopes

Modern neutrino telescopes are intended primarily for the detection of neutrinos from different astrophysical sources and cosmogenic fluxes (generated in interactions of super-high-energy CR and the microwave background). Moreover, neutrino telescopes may be used to indirectly detect cold DM in the form of WIMPs. Such studies are based on the assumption that WIMPs are captured by gravity fields of massive astrophysical objects, such as the Sun and the Earth, or accumulate in the central region of the Galaxy. The capture continues throughout the lifetime of a star or a planet and results in the accumulation of WIMPs in its shell. After the WIMP density becomes high enough, they begin to annihilate, giving rise to different particles. If the WIMP decay and annihilation products contain neutrinos, they can be detected with large neutrino telescopes.

All particles with the exception of neutrinos are rapidly absorbed in the interior of the Sun and the Earth. Part of the neutrino flux resulting from the WIMP annihilation inside the Sun or the Earth and even in the central region of the Galaxy may safely reach neutrino telescopes without any loss of energy. The proof of WIMP annihilation is an excess of neutrino events coming into the detector from the directions toward these objects (for the Earth, from the center of the lower hemisphere) over the atmospheric neutrino background.

The spectra of neutrinos resulting from annihilation of WIMPs captured inside the Earth and the Sun have been calculated in many works, e.g., [161–166]. The authors considered various WIMP annihilation channels, with the absorption of different neutrino flavors during their passage through the relic microwave and neutrino background and solar and terrestrial matter, as well as the effects of neutrino oscillations taken into account. WIMP annihilation channels contain heavy fermions, gauge and Higgs bosons, viz. $b\bar{b}$, $\tau^+\tau^-$, $c\bar{c}$, $t\bar{t}$, W^+W^-, ZZ, $H^{\pm}$, ZH, whose decays give rise to hadron jets composed largely of pi mesons. The decay chains of charged pions $\pi^+ \to \mu^+ + \nu_\mu$ and $\mu^+ \to e^+ + \bar{\nu}_\mu + \nu_e$ are responsible for the differential flux of neutrino flavors i [161]:

$$\frac{d\Phi_{\nu_i}}{dE_{\nu_i}} = \frac{\Gamma_{\rm ann}}{4\pi R^2} \sum_f {\rm BR}_f \left(\frac{dN_{\nu_i}}{dE_{\nu_i}}\right)_f ,$$

where summation ranges over all annihilation channels f with the partial contribution ${\rm BR}_f$, R is the distance from the neutrino source to the detector (e.g., the distance $R_{\rm SE}$ between the Sun and the Earth for the neutrino flux from DM particle annihilation products toward the Sun or the radius of the Earth $R_\oplus$ in the case of DM annihilation in its interior), and $(dN_{\nu_i}/dE_{\nu_i})_f$ is the differential spectrum of neutrinos formed in the annihilation channel f. The total number of annihilation acts per unit time, $\Gamma_{\rm ann}$, is related to the number of captured particles, $\Gamma_{\rm capt}$, by [166]

$$\Gamma_{\rm ann} = \frac{\Gamma_{\rm capt}}{2} \tanh^2 \frac{t_0}{\tau_A} ,$$

where t_0 is the age of the Sun and the Earth, and τ_A is the time scale of competing capture and annihilation processes proportional to the annihilation cross section.

The possibility of detecting neutrinos from WIMP annihilation depends on the number of particles captured by an astrophysical object and on their elastic scattering cross section. For the purpose of estimation, it can be assumed that $\Gamma_{\rm capt} \propto \sigma_{\rm scatt}\, \rho_{\rm WIMP}$ and that the capture and annihilation processes are in equilibrium (the condition $\tau_A \ll t_0$); this assumption holds only in the case of a large elastic cross section. The number of WIMP annihilation acts inside the Earth and the Sun can be estimated from the respective expressions [166]

$$\Gamma_{\rm ann}^{\rm Earth} = \frac{10^{14}}{c} \left(\frac{100\ {\rm GeV}}{m_{\rm WIMP}}\right)^2 , \qquad \Gamma_{\rm ann}^{\rm Sun} = \left(\frac{R_{\rm SE}}{R_\oplus}\right)^2 \Gamma_{\rm ann}^{\rm Earth} .$$

In neutrino telescopes, neutrinos with energies $E_\nu \approx 10$ GeV – 10 TeV are detected from the signatures of individual μ-tracks (in the case of the charged current interaction $\nu_\mu N \to \mu^- + X$ in the detector or in the adjacent volume). Modern neutrino telescopes contain natural volumes of pure water or ice (from fractions of a cubic kilometer to several cubic kilometers) that serve both as a neutrino target and as a radiator of Cherenkov radiation generated by secondary particles. Moreover, water and ice are optically transparent media for delivering the Cherenkov radiation to photodetectors mounted on suspended structures of different types. Operation details of neutrino telescopes and their potential for detecting high-energy neutrino fluxes are discussed in [167].

The Super-Kamiokande collaboration has recently obtained strong constraints on WIMPs with masses between 18 GeV and 10 TeV from the failure to observe high-energy ($E_\nu = 5$ GeV – 5 TeV $\approx (1/3-1/2)\, m_{\rm WIMP}$) neutrino fluxes from the Sun and the Earth toward the center of the Galaxy [168].

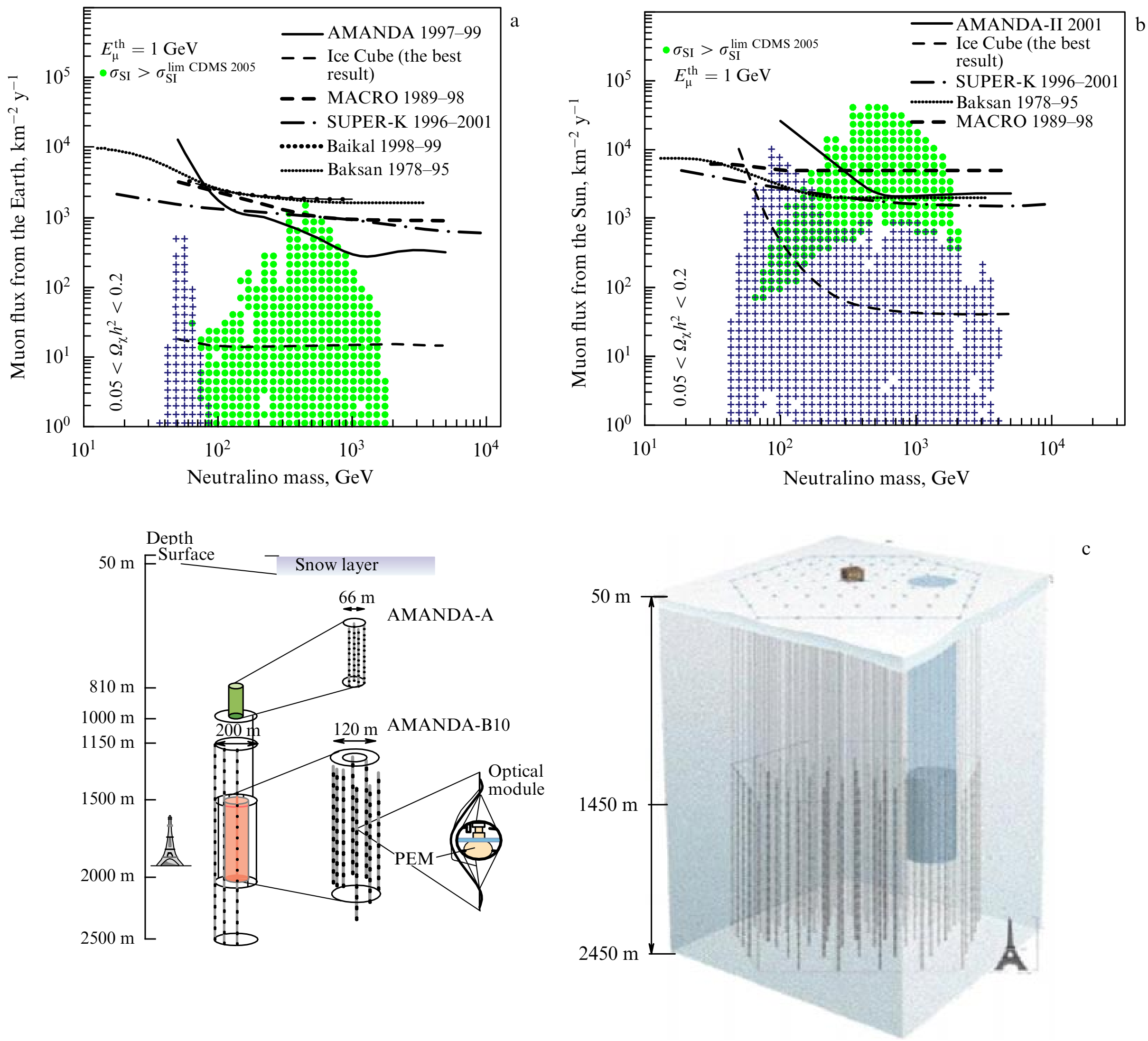

Figure 5. (a, b) Upper limits for the muon flux from the Earth (a) and the Sun (b) created in neutralino annihilation $\tilde{\chi}_1^0\tilde{\chi}_1^0 \to$ WW, depending on the neutralino mass, in the MACRO [169], Baksan [170], Baikal [171], and AMANDA [172] experiments. (Also presented are the results of the Ice Cube, Baikal, and Super-Kamiokande (Super-K) collaborations.) Dots show the forbidden parameter region in the CDMS experiment for direct DM detection, σ_{SI} is the spin-independent cross section of the WWIMP – nucleus interaction, and E_μ^{th} is the threshold muon energy [173]. (c) Schematic registration of astrophysical neutrinos in the AMANDA and Ice Cube telescopes [174].

The MACRO [169], Baksan (Baksan neutrino observatory) [170], Baikal [171], and AMANDA [172] collaborations also reported constraints on muon fluxes created in interactions of neutrinos from WIMP annihilation in the Earth and the Sun. These data are presented in Fig. 5a, b.

The above constraints can be significantly improved using the next-generation Ice Cube neutrino telescope under construction at the South Pole [165, 173]. The telescope features 80 strings frozen in Antarctic ice to the depth 1400 – 2400 m (Fig. 5c) [174]. Each string carries 60 optical modules regularly spaced by 17 m over its length. The detector volume in ice is ~ 1 km^3. The Ice Top shower detector consisting of 160 Cherenkov detectors is located at the ice surface on top of Ice Cube. Ice Top increases the sensitive volume of Ice Cube and will also be used for calibration, background subtraction, and investigation of atmospheric cascades. The construction of the telescope began in 2005 and will be completed in 2011.

Today, the ANTARES [175], Nestor [176], Nemo [177], KM3NeT (Cubic Kilometer Neutrino Telescope) [178] collaborations are carrying out studies aimed at collecting data for the substantiation of construction of a deep-water neutrino telescope with the instrumented volume 1 km^3 in the Mediterranean Sea. The prospects for indirect detection of high-energy neutrinos from the Sun in the ANTARES detector are discussed in Ref. [179]. It is shown that the detector can identify a few events in the mass range $m_{WIMP} \approx 100 - 800$ GeV over 3 years. The possibility of indirectly detecting neutrinos from WIMP annihilation has been significantly increased by the decision to enlarge several-fold the effective volume of the NEMO telescope designed and constructed with the support of the KM3NeT Consortium.

Experiments with neutrino telescopes allow obtaining model-independent constraints on annihilation cross sections of all kinds of DM particles under the assumption that annihilation leads to the final states

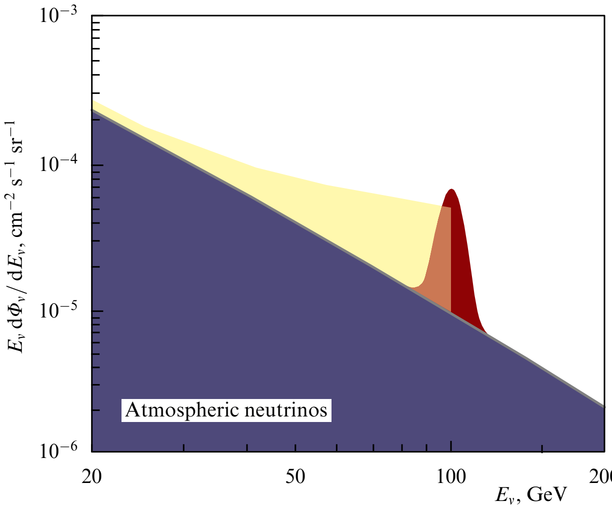

Figure 6. Spectrum of atmospheric neutrinos and the expected excess intensity due to an additional contribution from annihilation of DM particles, $\chi + \chi \to \nu + \bar{\nu}$. It is assumed that $m_\chi = 100$ GeV. The DM annihilation peak in the halo described by the Gaussian distribution with the width $\varepsilon = m_\chi/20$; excess over the atmospheric neutrino background in the case of diffusively distributed DM [181].

containing only SM particles. The upper bound of the total cross section corresponds to the limit case where neutrinos are the sole DM annihilation products, $\mathrm{BR}(\mathrm{DM} + \mathrm{DM} \to \nu + \bar{\nu}) = 100\%$.

A diffuse neutrino flux from DM annihilation is calculated from the relation [180, 181]

$$\frac{\mathrm{d}\Phi_\nu}{\mathrm{d}E_\nu} = \frac{\langle\sigma_\mathrm{A} v\rangle}{2}\,\frac{c}{4\pi H_0}\,\frac{\Omega_\mathrm{DM}^2\,\rho_\mathrm{c}^2}{m_\mathrm{WIMP}^2}\int\frac{\mathrm{d}N_\nu(E'_\nu)}{\mathrm{d}E'_\nu}\,\frac{(1+z)^3 f(z)}{h(z)}\,\mathrm{d}z\,,$$

where $\rho_\mathrm{c} = 5.3 \times 10^{-6}$ GeV s^{-1} is the critical density, $H_0 = 70$ km s^{-1} is the Hubble constant, and

$$h(z) = \left[(1+z)^3\Omega_\mathrm{DM} + \Omega_\Lambda\right]^{1/2}$$

with $\Omega_\mathrm{DM} = 0.3$ and $\Omega_\Lambda = 0.7$. The initial spectrum of annihilation products $\mathrm{d}N(E')/\mathrm{d}E'$ is modified by the red shift such that $E' = (1+z)E$; $f(z)$ is the evolution parameter of the source in which annihilation took place (e.g., the galactic halo).

The neutrino spectrum for annihilation into a neutrino pair is a monoenergetic line:

$$\frac{\mathrm{d}N_\nu}{\mathrm{d}E_\nu} = \frac{2}{3}\,\delta(E - m_\chi)\,.$$

The factor 2/3 is introduced to account for the fact that two neutrinos out of the three flavors are formed with equal probability in a single annihilation act. The delta-function regularizes the integration over the red shift. Figure 6 illustrates the possibility of determining the DM annihilation cross section limit based on the results of detection of high-energy neutrino fluxes from the galactic halo. It follows from Fig. 6 that the extraction of an annihilation signal is possible when its level is at least twice that of the atmospheric neutrino background [181].

Comparison of the theoretical diffuse neutrino signal from annihilation processes with the observed atmospheric neutrino background in Refs [180, 181] put a constraint on the total annihilation cross section in the range $m_\mathrm{DM} \approx 10 - 10^5$ GeV

$$\langle\sigma_\mathrm{A} v\rangle < 10^{-17}\left(\frac{m_\mathrm{DM}}{1\ \mathrm{GeV}}\right)\ [\mathrm{cm}^3\ \mathrm{s}^{-1}]\,.$$

5.2 Detection of photons with gamma-telescopes

Direct detection of cosmic γ-quanta with energies in the range from several GeV to several TeV is possible only in satellite experiments. The length of interaction between photons with such energies and matter during formation of $\mathrm{e}^+\mathrm{e}^-$-pairs is around 38 g cm^{-2}, which is much smaller than the depth of the Earth's vertical atmosphere, i.e., the total amount of atmospheric matter per cm^2 in the vertical direction,1030 g cm^{-2}. For this reason, photons with energies from several GeV to several TeV do not reach the Earth, unlike neutrinos. The operating principle of ground-based gamma-telescopes consists in detecting the Cherenkov radiation accompanying an electric cascade generated by high-energy photon interactions in the upper atmosphere. The main problem encountered in photon detection by a ground-based telescope lies in the difficulty of distinguishing electromagnetic showers from hadron cascades induced by CRs (mainly protons). The majority of modern Cherenkov gamma-telescopes produce light images of the transverse shower profile. Air showers of γ-quanta and CR particles are differentiated by comparing the observed Cherenkov light intensity and the results of calculations for atmospheric showers of different natures. Gamma-telescopes can reliably detect high-energy photons in the direction of an astrophysical source of γ-quanta in which the intensity of electromagnetic showers is much higher than the isotropic background of showers from hadron – hadron interactions in the atmosphere.

By analogy with neutrino telescopes, in which the existence of DM can be indirectly confirmed by recording neutrinos, gamma-telescopes detect γ-quanta from decays of the DM annihilation products:

$$\mathrm{DM} + \mathrm{DM} \to \mathrm{q} + \bar{\mathrm{q}} \to \text{fragmentation} \to \pi^0 \to 2\gamma\,.$$

There may be a direct channel of annihilation into quanta accounting for the appearance of a monoenergetic line:

$$\mathrm{DM} + \mathrm{DM} \to \gamma + \gamma \quad \text{or} \quad \gamma + \mathrm{Z}\,.$$

Similarly to neutrinos, γ-quanta do not deviate in galactic magnetic fields and carry information about the original annihilation region. This region can be seen by ground and satellite-based gamma-telescopes.

The EGRET experiment on board the satellite launched in 1992 [182] was the first to demonstrate excess diffuse γ-quanta in the ~ 10 GeV energy range of their spectrum over the theoretical γ-background for all known nuclear processes, inverse Compton scattering, and bremsstrahlung radiation.

In the last few years, practically all ground-based Cherenkov gamma-telescopes (CANGAROO, VERITAS, MAGIC, HESS) have registered γ-quanta with TeV energies coming from the vicinity of the galactic center. The nature of this source of γ-quanta remains to be clarified. A possible explanation is the γ-emission from the annihilation of DM particles.

The annihilation energy spectrum must extend continuously up to the energy corresponding to the mass of a DM particle and probably contains γ-lines associated with two-particle final states. A flux of γ-quanta from the DM particle annihilation near the galactic center is described by the expression [183]

$$\Phi_\gamma(\psi, E_\gamma) \approx 5.6 \times 10^{-12}\ \mathrm{cm}^{-2}\ \mathrm{s}^{-1} \times \frac{\mathrm{d}N_\gamma}{\mathrm{d}E_\gamma}\left(\frac{\langle\sigma_\mathrm{A} v\rangle}{3\times 10^{-26}\ \mathrm{cm}^3\ \mathrm{s}^{-1}}\right)\left(\frac{m_\mathrm{DM}}{1\ \mathrm{TeV}}\right)^{-2}\langle J(\Delta\Omega)\rangle\Delta\Omega\,,$$

where ψ is the angle between the line of sight and the galactic center and $\langle\sigma_\mathrm{A} v\rangle$ is the annihilation cross section averaged over DM particle velocities. The angular resolution, which is $0.5^\circ - 1^\circ$ for ground-based Cherenkov telescopes, determines the solid angle, $\Delta\Omega \approx 5\times 10^{-5}$ sr. The quantity $\langle J(\Delta\Omega)\rangle$ strongly depends on the DM distribution; values from 5.6×10^3 [184] to 1.9×10^6 [185] are used in different galactic halo models.

5.2.1 Satellite-based gamma-telescopes. ***EGRET*** (Energetic Gamma Ray Experiment Telescope) was one of the four detectors operating on board the GRO (Compton Gamma Ray Observatory) satellite for 9 years (1991 – 2000). The telescope measured γ-quantum fluxes in the energy range $E_\gamma = 30$ MeV – 30 GeV. Analysis of the observed γ-quantum spectrum in the direction toward the galactic center provided the upper limit on the existence of DM particles. Recently, a new analysis of the EGRET data [187, 188] confirmed the excess of γ-quanta with energies above 1 GeV compared with the number of γ-quanta with such energies predicted by the galactic model of diffuse γ-quanta [189]. Analysis of 180 directions in the celestial sphere revealed an excess in all of them. This suggests an additional source of γ-quanta, e.g., annihilation of DM particles. The shape of the spectrum is compatible with that expected for annihilation of nonrelativistic massive particles followed by their fragmentation into hadronic jets and decay of neutral pions into γ-quanta. The excess energy spectrum in EGRET is in accordance with the existence of neutralino WIMPs having an estimated mass in the range $m_\mathrm{DM} \approx 50 - 100$ GeV [187, 188]. The theory predicts $m_\mathrm{DM} \approx 500$ GeV [190].

GLAST (Gamma-ray Large Area Space Telescope) is a gamma-observatory launched in 2008. One of the principal goals of this experiment is to measure the extragalactic diffuse γ-quantum background. Another equally important objective is to obtain information about sources of the most intense γ-quanta in the Universe that might be directly associated with the existence of DM. GLAST will be continuously surveying different potential sources of DM, including the galactic center. The maximum effective area of the telescope in the energy range 1 – 10 GeV is almost 9000 cm^2, the field of view >2 sr, the detection energy range of γ-quanta is 20 MeV – 300 GeV, and the resolution is 30 times that of the EGRET experiment [191].

GLAST consists of segmented detector modules surrounded by a protective anticoincidence layer of a plastic scintillator that extracts charged components of CRs. Each module has a tracker shaped by 18 planes of silicon strip detectors interlayered with tungsten foil and a terminal electromagnetic calorimeter of 1536 CsI arranged in 8 layers. A photon passing through the tracker is with high probability converted in the tungsten foil to an e^+e^- pair, whose tracks are recorded in the next plane of the silicon detector. The direction and the energy of the incoming primary γ-quanta are deduced from the trajectory of the e^+e^- pair in the tracker and the energy release in the calorimeter.

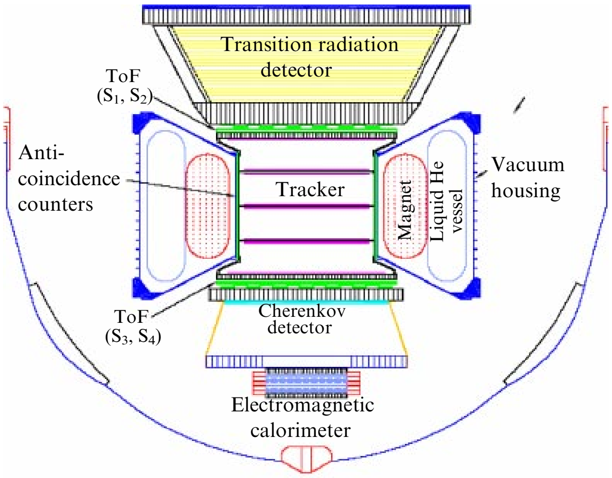

Figure 7. Block diagram of the AMS-2 spectrometer to be based on the International Space Station [194]. The figure shows the superconducting magnet, transition radiation gas detector, silicon tracker, time-of-flight (ToF) systems with $S_1 - S_4$ scintillation counters, Cherenkov detector (RICH), electromagnetic calorimeter, and anticoincidence system.

GLAST is expected to detect DM at a 5σ (3σ) confidence level when surveying the celestial sphere in the direction of the galactic center within a solid angle of $\sim 0.1^\circ$, if the DM annihilation products are heavy quarks or gauge bosons with the mass under 500 (750) GeV [192, 193]. The sensitivity of the annihilation cross section measurement of GLAST will be of the order $\langle\sigma_\mathrm{A} v\rangle = 10^{-24} - 10^{-27}$ cm^3 s^{-1} depending on the halo model. By increasing the solid angle within which the galactic center is observed, it will be possible to identify WIMPs with a mass in excess of several TeV with a high degree of confidence. However, GLAST will not differentiate between the γ-spectrum and the DM annihilation if the main annihilation products are electrons and muons.

AMS (Alpha Magnetic Spectrometer) is an experiment on board the International Space Station (ISS) designed to study antimatter of cosmic origin. AMS can detect γ-quanta in the energy range from 1 to 10 GeV [194].

AMS-2 (Fig. 7) is a combination of different detectors. A cylindrical superconducting magnet (length: 0.8 m, outer diameter: 1.2 m) creates a field strength of 0.8 T. Eight double-sided layers of silicon detectors are aligned in a plane normal to the magnetic field axis. The silicon tracker provides reliable measurement of the trajectory of a relativistic single-charged particle to within 10 μm. It is also used to measure energy losses, which is necessary for determining the size of a passing particle. The time-of-flight system containing 4 layers of scintillation detectors measures the arrival time of a charged particle up to 140 ps. The system is also used to measure the position and the energy losses. A transition radiation detector placed on top of the spectrometer consists of 20 layers of 12 mm thick porous plastic fabric alternating with 20 layers of detecting tubes 6 mm in diameter filled with an $Xe + CO_2$ mixture. The detector separates electrons from hadrons with the rejection coefficient $\sim 10^2$ at energies ~ 200 GeV. A ring imaging Cherenkov detector (RICH) located below the last plane of the time-of-flight system consists of a 3 cm thick air – helium radiator with the refractive index 1.05, a mirror, and a light-collecting pixel-matrix photodetector. The RICH detector measures the particle velocities with an error less than 1%. An imaging magnetic calorimeter at the bottom of AMS has the size

$65 \times 65 \times 17$ cm^3 and the depth $\sim 16X_0$, where X_0 is the radiation length. It consists of modules made of a sandwich of lead foils and layers of scintillating fibers 1 mm in diameter glued together.

AMS detects cosmic γ-quanta by two methods. One (conversion mode) implies reconstruction in the tracker of e^+e^- pairs formed as a result of γ-conversion in the substance above the track. The other (single-photon mode) implies detection of γ-quanta in the electromagnetic calorimeter.

The possibility of using AMS for the detection of γ-quanta was evaluated theoretically using the GEANT (GEometry ANd Tracking) software package designed to simulate the passage of elementary particles through matter, and experimentally in the first test flight of AMS-1 on board the Space Shuttle-1 [195].

AMS-2 with the aperture ~ 500 cm^2 sr to be installed on the ISS will measure fluxes of γ-quanta in the direction of the galactic center with GeV energies; these fluxes can be several times weaker than the fluxes recorded by EGRET. These measurements are required for detecting neutralinos with small masses. It is expected that AMS-1 will help to find constraints on low-mass DM in the galactic halo and exclude certain scenarios of its evolution with a high degree of confidence.

5.2.2. Ground-based imaging Cherenkov gamma-telescopes. ***MAGIC*** (Major Atmospheric Imaging Cherenkov), the world's largest Cherenkov telescope with a parabolic mirror 17 m in diameter situated on one of the Canary Islands at 2200 m above sea level, has been operating since 2005. The telescope is equipped with a high-resolution 576-pixel camera consisting of photomultipliers. MAGIC detects γ-quanta with energies from 30 GeV to several tens of TeV. The air shower collection area of MAGIC is $10^4 - 10^5$ m^2. The energy resolution ranges from 15 to 40%, depending on the zenith angle and the primary particle energy. The second telescope was installed 85 m from the first in 2007. As a result, the sensitivity of the MAGIC-II stereosystem increased two-fold, the energy threshold decreased, and the angular resolution improved [196].

The telescope is designed primarily to detect γ-quanta from WIMP annihilation [197]. It was used to measure the γ-quantum spectrum up to energies ~ 20 TeV in the direction of the galactic center [198]. Most SUSY scenarios of DM set the energy cut-off for the annihilation γ-quantum spectra below 10 GeV. Therefore, the high-energy part of the γ-quantum spectrum measured by MAGIC appears to be unrelated to DM decay.

HESS (High Energy Stereoscopic System) is an array of four telescopes recording atmospheric Cherenkov light (Fig. 8). HESS is situated at 1800 m above sea level in Namibia. Each telescope has a 107 m^2 optical reflector consisting of 382 mirrors [199]. Cherenkov light is collected by the reflector and focused onto the matrix of 960 photoelectron multipliers (PEMs). The full viewing angle is 5°. The stereoscopic technique enables HESS to exactly reconstruct the direction of the received primary γ-quanta and their energy while effectively suppressing cosmic background radiation. The energy threshold of the telescope is ~ 100 GeV and the angular resolution is $0.1°$.

HESS is designed to detect γ-quanta in the energy range 100 GeV – 100 TeV and elucidate their nature. It has already recorded TeV γ-quanta in the direction of the galactic center [200, 201]. High-energy γ-quanta from the galactic center are associated with the direction toward source J1745-290. The measured dependence of the $E_\gamma^2\, \mathrm{d}\Phi_\gamma/\mathrm{d}E_\gamma$ spectrum on the energy E_γ is not described by any annihilation mode hypothesis; this practically rules out the annihilation nature of high-energy γ-quanta [202]. Nor do high-energy γ-quanta from the M87 galaxy in the Virgo constellation and the Sagittarius Dwarf Galaxy detected by HESS carry γ-signals that might originate in DM annihilation [203].

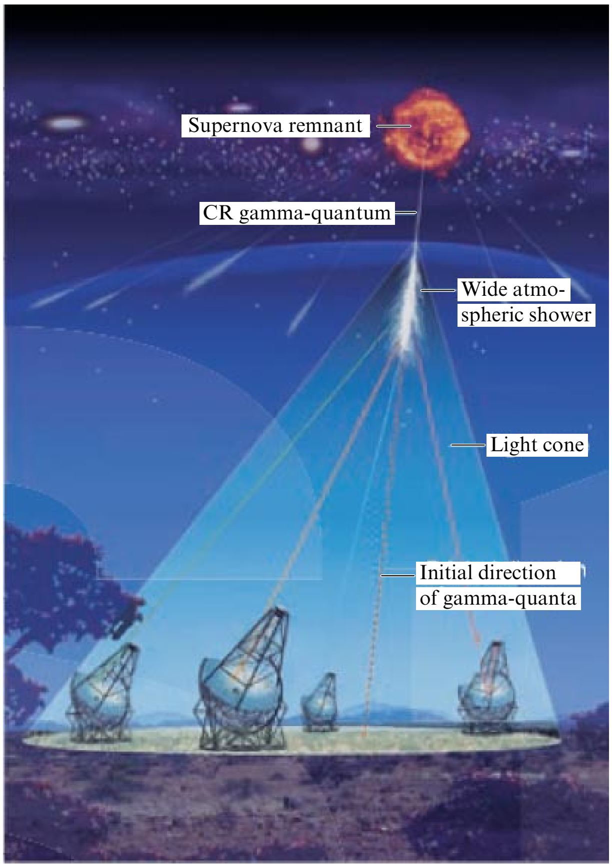

Figure 8. HESS array of four telescopes.

The constraint on the annihilation cross section in HESS is $\langle \sigma_{\mathrm{A}} v \rangle^{\mathrm{HESS}} < 10^{-24}$ cm^3 s^{-1} [204].

The search for DM will be continued based on a system of HESS2 telescopes to be completed in 2009. The second phase of the HESS project will comprise a new telescope with the mirror diameter 28 m situated in the center of the existing array. Such configuration will ensure the 80 GeV detection threshold and will make the HESS complex sensitive to most SUSY models.

CANGAROO (Collaboration of Australia and Nippon (Japan) for a Gamma Ray Observatory in the Outback) is the South Australia-based telescope for detecting TeV γ-quanta. In the first phase of the experiment (CANGAROO-I), initiated in 1992, a single telescope with a 3.8 m mirror was operated. The second phase (CANGAROO-II) started in 1999 with the construction of a 7 m mirror telescope; the mirror diameter was eventually enlarged to 10 m. CANGAROO-II recorded a significant excess of γ-quanta with energies above 250 GeV in the direction of the galactic center. The upper bound on the DM annihilation cross section (under the assumption of the mode $\chi\chi \to \gamma\gamma$) obtained with CANGAROO-II was $\langle \sigma_{\mathrm{A}} v \rangle^{\mathrm{CANGAROO-II}} < 10^{24}$ cm^3 s^{-1} [205].

In the third phase (CANGAROO-III), three more telescopes, each with a 10 m mirror, were built. Today, all four Cherenkov telescopes can be operated either jointly or independently.

VERITAS (Very Energetic Radiation Imaging Telescope Array System) is a γ-observatory in Arizona that comprises four Cherenkov telescopes with the mirror diameter 12 m. VERITAS succeeds the pioneering Cherenkov telescope (Wipple) that produced visible-light images of atmospheric lines [206]. In the period from 1995 to 2003, Wipple detected a flux of γ-quanta with energies above 2.8 TeV coming from the direction toward the galactic center.

VERITAS can record γ-quanta in the energy range 100 GeV – 30 TeV; it has a large effective area ($> 3 \times 10^4$ m^2) with a good energy (10 – 20%) and angular ($\sim 0.14°$) resolution. The total field of view of the system is 3.5°. Astronomical observations with VERITAS began in March 2007 [208].

The search for DM particles based on precision observations of γ-fluxes is one of the main lines of VERITAS studies.

5.2.3 Ground-based Cherenkov gamma telescopes without image visualization. ***Milagro*** (Spanish for miracle) is a ground-based water Cherenkov detector designed to observe TeV γ-quanta [209]. Milagro, based at the Los Alamos National Laboratory, USA, at 2630 m above sea level, is a reservoir containing 2.4×10^7 l of pure water. 723 PEMs aligned in two layers are imbedded in a volume of water $80 \times 60 \times 8$ m^3. The upper layer at the depth 1.4 m is used to determine the direction of air showers and the lower one submerged under 6 m of water separates primary γ-quantum and hadron showers.

Since Milagro was put into operation in 1999, it has detected γ-quanta with energies above 1 TeV from Crab Nebula and Mkr 421 [210]. For a total of 1165 hours, it recorded TeV γ-quanta in the direction of the Sun. However, it failed to detect high-energy γ-quanta that might have formed in the annihilation of neutralinos captured by the Sun [211].

CACTUS (Converted Atmospheric Cherenkov Telescope Using Solar-2) is a ground-based Cherenkov γ-telescope situated in California. It is actually a complex of mirrors intended to watch the Sun rather than carry out γ-astronomical research. For this reason, CACTUS is far from being an ideal device for detecting γ-quanta from astrophysical sources. Nevertheless, the telescope managed to record γ-quanta with the energy more than 100 GeV in the direction of the Draco constellation. It cannot be excluded that these γ-quanta originate from DM decays [212, 213].

CELESTE (Cherenkov Low Energy Sampling and Timing Experiment) is a ground-based Cherenkov γ-telescope built in the French Pyrenees at 1650 m above sea level. The telescope is made of 53 heliostats, each 54 m^2, that reflect light toward the collecting optical system. CELESTE has failed to detect any meaningful excess of γ-quanta with energies 50 – 500 GeV in the direction of the galaxies M31 and Draco [214].

5.3 Balloon and satellite experiments to observe positrons and antiprotons

Spectra of cosmic protons and antiprotons can also give evidence of DM annihilation [215 – 217]. However, these charged particles, unlike γ-quanta and neutrinos, are of little value for determining the direction to the source. The background level of antiparticles created in the terrestrial atmosphere from primary CR interactions must be known if their true nature is to be elucidated. Therefore, instruments measuring antiparticle spectra are launched on balloons or satellites outside the atmosphere.

HEAT (High Energy Antimatter Telescope) performed its virgin balloon flight in 1994 – 1995 and measured the positron spectrum at 1 – 50 GeV. The data obtained suggest an excess of positrons with energies above 9 GeV and therefore the presence of DM in the halo [218, 219].

BESS (Balloon-borne Experiment Superconducting Solenoidal spectrometer) measured antiproton spectra in the energy range 180 MeV – 4.2 GeV during several successful balloon flights in 1993 – 1998 [220]. The results show a relation between antiproton spectral changes and variations of solar activity. Nevertheless, an excess of antiprotons was documented in 1995 when solar activity was not the highest for the study period. Possible explanations may be the presence of an additional source of antiprotons, besides statistical fluctuations, such as annihilation of neutralinos [215].

CAPRICE (Cosmic AntiParticle Ring Imaging Cherenkov Experiment) is a balloon experiment in which a few tens of antiprotons with energies 3.2 – 49.1 GeV were registered in 1998 [221]. Analysis of these data does not unambiguously answer the question of their origin. The measured antiproton spectrum is indicative of the secondary nature of these particles, although their presence in primary CR composition cannot be excluded

Uncertainties in the interpretation of balloon measurements of positron and antiproton spectra may substantially diminish as the result of a statistical analysis of the events currently collected in the PAMELA satellite experiments and expected from the study with the use of AMS-2 on the ISS.

PAMELA experiment (Payload for Antimatter – Matter Exploration and Light-nuclei Astrophysics) is based on the Russian Resurs-DK 1 satellite launched into orbit in June 2006. The main objective of this study is to measure antimatter fluxes. PAMELA detects positrons and antiprotons in energy ranges 50 MeV – 170 GeV and 80 MeV – 190 GeV [222].

PAMELA is equipped with a variety of detectors measuring the particle charge, mass, and speed (Fig. 9) [223]. Its central component is a magnetic spectrometer with six planes of two-sided silicon microstrip detectors and a permanent magnet with the field strength 0.43 T. The spectrometer used to measure the particle charge and momentum is surrounded by a system of scintillation detectors necessary to receive a trigger signal and time-of-flight information. A calorimeter in which silicon detector layers alternate with tungsten plates separates hadrons and leptons. A neutron detector installed under the calorimeter enhances the reliability of separation. The total weight of PAMELA is 470 kg, the geometric factor is 21.5 cm^2 sr.

The instrument can detect excessive antiprotons in the spectrum being measured if the excess is consistent with neutralino annihilation models in the majority of supersymmetric scenarios [224]. The possibility of detecting DM particles in the positron channel strongly depends on the nature and local distribution density of DM. It is believed [225, 226] that positron spectrum studies with the use of PAMELA may contribute to the search for DM particles with the mass up to 550 GeV.

The possibility of detecting TM particles by measuring γ-quantum fluxes in ***AMS-2*** on board the ISS was discussed in

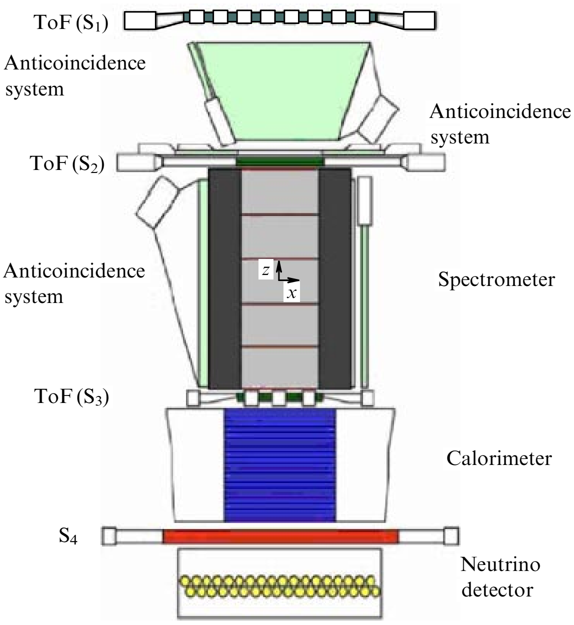

Figure 9. Block diagram of the PAMELA detector [223].

Section 5.2.1. The instrument is thought to be able to exactly measure positron spectra [117]. Precision measurements of positron energies by AMS-2 may uncover the subtleties of New Physics. Specifically, if antiprotons are actually products of DM annihilation, it may be possible to identify their annihilation channels, elucidate their origin, and propose an evolution scenario. The high reliability of the results is ensured by independent measurement of γ-quantum spectra in AMS-2.

6. Direct detection of WIMPs

The idea of the direct detection of WIMPs comes from the assumption that the Galaxy abounds in WIMPs and that many of them pass through the Earth. The main characteristics of the signal from directly detected WIMPs are their density distribution in the Galaxy, the distribution by velocities in the solar system, and the cross section of their scattering on nucleons. Based on these parameters, it is possible to estimate the event count rate R_{WIMP} using the expression

$$R_{\mathrm{WIMP}} \approx \sum_i N_i\, n_{\mathrm{WIMP}} \langle \sigma_{\mathrm{WIMP-nucleon}}\, v_{\mathrm{WIMP}} \rangle\,,$$

where $N_i = M_{\mathrm{detector}}/A_i$ is the number of nuclei in a target of the i type in a detector of mass M_{detector}, A_i is the atomic weight of a nucleus of the i type, n_{WIMP} is the WIMP flux density, and $\langle \sigma_{\mathrm{WIMP-nucleon}}\, v_{\mathrm{WIMP}} \rangle$ is the WIMP – nucleon scattering cross section averaged over WIMP velocities v_{WIMP} relative to the detector. A characteristic kinematic feature of the Earth's motion in the Galaxy is the annual revolution around the Sun, which gives the resulting velocity with respect to the galactic reference frame

$$v = 220\,\left(1.05 + 0.07\cos\left[2\pi(t - t_{\mathrm{m}})\right]\right)\ [\mathrm{km\ s^{-1}}]\,.$$

Here, time is measured in years and t_{m} roughly corresponds to early June. The result of this motion is approximately a 7% variation in the WIMP flux, and hence in the direct detection count rate during the year.

WIMPs travel with the typical speed $\langle v_{\mathrm{WIMP}} \rangle = 270\ \mathrm{km\,s^{-1}}$ and interact with nuclei in the processes of elastic and inelastic scattering. In the case of elastic scattering, the recoil spectrum has the typical energy $\langle E \rangle \approx 50$ keV [228]. In inelastic scattering, WIMPs interact with the target orbital electrons by exciting them or by ionizing the target. Also, a WIMP can excite a nucleus in the inelastic process such that the resulting nuclear recoil is followed by the emission of a photon (in about 1 ns). Such a signature should be separated from the signatures of background events. The mean nucleus recoil energy in the collision of a WIMP and a nucleus with mass m_{A} can be approximated as

$$\langle E \rangle \approx 1.6\,A \left(\frac{M_{\mathrm{WIMP}}}{M_{\mathrm{WIMP}} + m_{\mathrm{A}}}\right)^{1/2}\ [\mathrm{keV}]\,,$$

where A is the number of nucleons in the nucleus interacting with the WIMP.

WIMP scattering is usually considered in the context of two types of coupling. The axial – vector (spin-dependent) coupling is related to the spin content of the nucleon. Because $\sigma \sim J(J+1)$, where J is the nuclear spin of the target, the use of a target of heavy nuclei gives no advantage. Targets with medium and heavy nuclei appear more suitable in the case of the scalar (spin-independent) coupling $\sigma \sim A^2$ and in the search for WIMPs. Also, scattering through the vector coupling is possible for WIMPs that are not Majorana particles (neutralinos and KK states do not have this coupling). The cross section of the WIMP – nucleon interaction is very small, and therefore a large sensitive detector mass is needed.

In experiments for direct WIMP detection, it is necessary to somehow measure the energy released from WIMP scattering on the nuclear target. Ionization, scintillation, and/or heat detectors may be used to record recoil nuclei and measure their energy (Fig. 10). We recall that almost 100% of the energy of a recoil nucleus ΔE is converted into a thermal signal in heat detectors. In ionization detectors, the quenching factor for the transformation of the recoil energy into the energy spent to the creation of electron – hole pairs is below 30%. Less than 10% of the energy is converted into light in scintillation detectors. In this case, a detector of recoil nuclei must have the threshold of a few keV.

Importantly, ionization and scintillation outputs significantly increase if the primary interaction occurs with an electron, i.e., if its product is a recoil electron instead of a recoil nucleus. Such a situation occurs for all background events induced by photon scattering from electrons. Normally, they constitute the main component of the background. It follows from experimental practice that suppressing these background electrons is a most challenging and important task because they persist despite the use of highly sophisticated background suppression systems (underground laboratories for protection from CRs, passive and active protection, superhigh pure materials). In fact, sensitivity limits of experiments designed to directly detect WIMPs depend on solving this problem. One approach to suppressing this background component is to detect two signals simultaneously (e.g., phonon + ionization or ionization + scintillation) in 'hybrid' detectors (see Fig. 10). A neutron background can be suppressed by using the multiple scattering signature absent in the case of WIMPs.

Generally speaking, the difficulty of direct experiments in the search for WIMPs is determined by the following factors: (a) a very small WIMP – nucleon scattering cross section

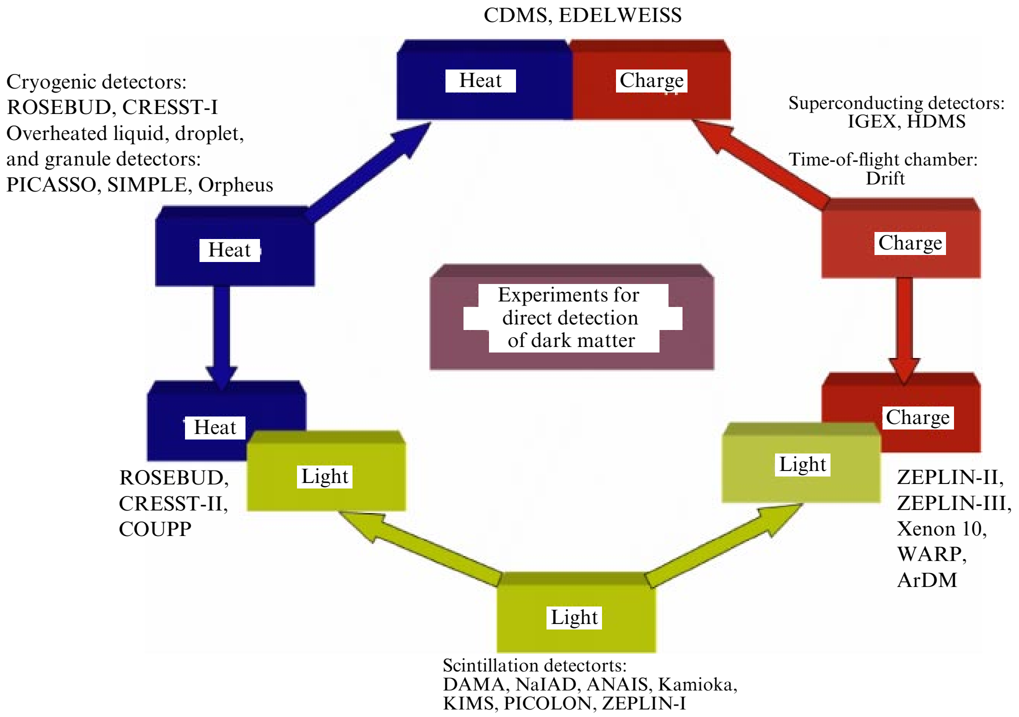

Figure 10. Principal detection methods and experiments designed to search for WIMPs.

($< 10^{-6}$ pb) necessitating a large sensitive detector mass; (b) the low efficiency of measurement of small energies of recoil nuclei ($\sim 10-100$ keV) necessitating the use of detectors with the threshold of several keV; (c) a very high CR and natural radioactivity background necessitating location of the detectors in underground laboratories and the use of protective shields or materials free from radioactive admixtures.

6.1 Charge detectors

6.1.1 Semiconducting detectors. Early WIMP experiments used germanium-based detectors having a low energy threshold and high resolution power. These detectors, initially optimized to study the double β-decay, were later used in search of DM particles. Time-of-flight chambers have recently come into use for WIMP detection.

IGEX (International Germanium EXperiment) in the Canfranc underground laboratory situated at the depth 2450 m of water equivalent (m.w.e.) in the Spanish Pyrenees [229]. The detector was protected by a lead shield and contained 2 kg of the pure germanium ^{76}Ge isotope. The event count rate 0.1 keV^{-1} kg^{-1} day^{-1} agrees with the theoretical background level.

HDMS (Heidelberg Dark Matter Search) was an experiment in the underground laboratory (3400 m.w.e.) of Gran Sasso, Italy [229]. The detector contained two ^{73}Ge crystals (one inserted into the other) with the weight about 2.3 kg. Both detectors recorded only background events unrelated to WIMP interactions. The detection threshold was $E_{\rm th} \approx 4-7.5$ keV and the energy resolution $2-4$ keV. Measurements were made at the recoil nucleus energies $10-50$ keV, and the event count rate did not exceed the background level 0.43 keV^{-1} kg^{-1} day^{-1}.

6.1.2 Time-projection chambers. ***Drift-II*** is an experiment based on a time-projection chamber at the depth 1100 m in the Boulby mine, North Yorkshire, UK. The 1 m^3 chamber filled with carbon disulfate (CS_2) works with negative ionic charge carriers [231]. A particle passing through the chamber interacts with the gaseous CS_2-target, giving rise to electron–ion pairs, which are separated in a strong electric field. CS_2 is an electronegative gas and the negative ions being formed drift toward one of the planes of the multiwire proportional chamber operated in the avalanche regime. Such a chamber detects recoil nuclei from WIMP interactions in the gas volume. Today, calibration of the instrument is underway with the use of radioactive sources.

MIMAC (MIcro-tpc Matrix of Chambers) is an experiment in a high-resolution time-of-flight chamber with He^3 as the target for detecting nonbaryonic DM. The chamber records ionization signals and electron track projection [232]. Movements of the recoil nucleus produced in WIMP scattering by He^3 generate ionization electrons that are detected at the threshold energy below 6 keV.

6.2 Scintillation detectors

A large detector mass can be obtained using NaI or liquid xenon scintillators in a very pure container.

DAMA (Dark Matter) is an experiment in the Gran Sasso underground laboratory with the use of approximately 100 kg of high-purity NaI(Tl) scintillator in nine independent 9.7 kg detectors [233]. The energy threshold of the experiment was $E_{\rm th} \approx 2$ keV and the recoil nucleus energy ≈ 22 keV. The energy resolution of the scintillator was evaluated using several radioactive sources (^{55}Fe, ^{109}Cd, ^{241}Am). The aim of the experiment was to study the effect of the Earth's motion around the Sun on DM particle interactions in the nuclear target. If DM is actually concentrated in the galactic halo, the Earth should cross its large flux in June (when the velocity vector of DM particles coincides with the direction of motion of the solar system relative to the Galaxy). In December, when the two

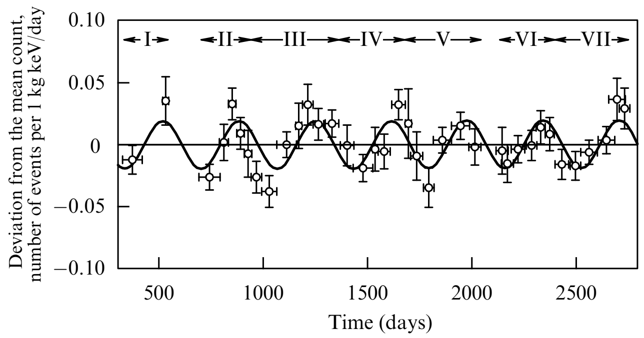

Figure 11. Annual modulation of event counts in the energy range 2 – 6 keV (DAMA experiment) [233].

velocities subtract, the number of interaction events in the detector should be very low.

DAMA collected data during 7 annual cycles. Measurements began before the expected minimum of events (December 2) and ended after the anticipated maximum (June 2). The total exposition time of detectors amounted to 107,731 kg day. Counting data in the energy range 2 – 6 keV suggest modulations at the 6.3σ confidence level (Fig. 11). This finding was interpreted by the DAMA collaboration as the evidence of a halo of WIMPs with the mass $m_{\rm WIMP} \approx 52$ GeV at the annihilation cross section $\sigma_{\rm WIMP-nucleon} \approx 7.2$ pb. However, the result is thus far unconfirmed in other DM experiments.

The second phase of the DAMA experiment (Large Sodium Iodide Bulk for Rare processor or DAMA/LIBRA) was initiated in 2003. This new experiment uses a 250 kg NaI(Tl)-scintillator (matrix of 25 crystals, 9.7 kg each) [234]. The total exposition was 1.5×10^5 kg day by early 2007. The DAMA/LIBRA collaboration has not yet reported the results on DM detection in the new experiment.

NaIAD (NaI Advanced Detector) was an experiment carried out in the Boulby mine [235]. The detector contained six NaI crystals (with the total weight 46 kg). PEMs attached to either end of a crystal recorded light signals. The detector was protected from bedrock radiation by a shield of copper and lead. Its energy threshold was ~ 2 keV, the data were analyzed in the range 2 – 30 keV, the exposition amounted to 10.6 kg y. No meaningful deviation from the background count rate was discovered.

ANAIS (Annual modulation with NaI's) is an experiment in the Canfranc underground laboratory [236] with the use of 14 NaI scintillator crystals of 10.7 kg each. The scintillators are assembled in a hexagonal structure protected by a shielding of 10 cm of lead, 2 mm of cadmium, and 40 cm of polyethylene. In addition, the detector was placed in a container filled with boron-containing water. The energy threshold was ~ 4 keV, events were analyzed up to the energy of 100 keV. The detector counted events at the rate 1.2 keV^{-1} kg^{-1} day^{-1}, the exposition amounted to 2070 kg day. No anomalous excess of events over the background was documented.

***Kamioka*-CaF$_2$(Eu)** is an experiment in the Kamiokande mine (2700 m.w.e), Japan. The detector contained a 310 g CaF$_2$(Eu) scintillator crystal protected by a shielding of 15 cm of copper, 15 cm of lead, and 20 cm of polyethylene [237]. Light output of CaF$_2$(Eu) crystals is approximately 50% of the NaI(Tl) light output; therefore, the energy threshold of CaF$_2$(Eu) detectors is slightly higher than in NaI(Tl) detectors. Light signals from the crystal were detected by PEMs and transmitted to the input of a digital oscillograph. Kamioka-CaF$_2$(Eu) counted events with energies $\leqslant 10$ keV at the rate 10 keV^{-1} kg^{-1} day^{-1}, in agreement with the background counting.

KIMS (Korea Invisible Mass Search) is an experiment in the Yang Yang mine, South Korea, at the depth 700 m. The detector contains four CsI(Tl) scintillator crystals (total weight 34.8 kg) [238]. Scintillation light enters the PEMs from two end surfaces of each crystal and is recorded by ultrafast analog – digital convertors. The total exposition is 3409 kg day. Subtraction of background events from their total count gives no meaningful events that could be associated with a recoil nucleus (i.e., no WIMPs were detected).

PICOLON (Planar Inorganic Crystals Laboratory for Low-background Neutralino) is an experiment designed to be conducted at the Oto Cosmo laboratory situated at a depth of 1200 m.w.e. 100 km from Osaka, Japan [239]. A new approach to recording WIMPs in a scintillation detector is planned. Several NaI crystal plates (6.6×6.6 cm^2) only ~ 0.05 cm thick will be used. It is assumed that all the energy will be released in a single plate due to the very short flight path of the recoil nucleus. At the same time, γ-quanta with an equivalent energy will go outside the plate in which interaction took place and enter the adjacent plates. A proper arrangement of the anticoincidence (veto) system will allow detecting an event whose signal is registered only in one plate. With high probability, it will then be possible to identify it with the signal from the recoil nucleus.

In the first phase of the experiment, only 3 thin crystals are to be used; in the second phase, 16 crystals will be arranged one above another. Scintillation light will be received by four PEMs in the corners of each crystal The detector will have the energy threshold ~ 2 keV and a linear response up to ~ 120 keV. It will be placed within a lead/copper shielding.

ZEPLIN (ZonEd Proportional scintillation in Liquid Noble gases) is an experiment in the Boulby mine. In its first phase (ZEPLIN-I), liquid xenon (3.1 kg) was used as the scintillator [240]. The study proved a failure because the electronic equipment produced too much noise and the energy resolution was insufficient to reliably detect meaningful signals. The experiment was extended based on ZEPLIN-II and ZEPLIN-III detectors with the use of liquid and gaseous xenon that recorded both charge and scintillation light signals.

6.3 Cryogenic heat detectors

Cryogenic detectors have been most extensively used in search of WIMPs during the last decade. This is because the thermal capacity at very low temperatures approximately obeys the Debye law ($\sim T^3$), which allows calorimetric measurements even at very small released energies. Specifically, a threshold of 1 keV has already been achieved in measuring the recoil energy. A decrease in the thermal capacity as $T \to 0$ may be used to record temperature responses of ~ 1 μK in a macroscopic working medium within technically attainable temperature ranges. Moreover, the energy value of an elementary phonon excitation in cryogenic detectors is much lower (less than 1 MeV) than in classical detectors based on semiconductors and oscillators. Due to this, cryogenic detectors permit achieving unprecedentally high sensitivity and energy resolution.

ROSEBUD (Rare Objects Search with Bolometers UndergrounD) is an experiment in the Canfranc underground laboratory using 3 sapphire bolometers with Ge-thermoresistors [241]. The total weight of sapphire crystals was about 100 g. Crystals surrounded by a thin sheet of high-purity copper and lead were imbedded in liquid helium at the temperature 20 mK. Peripheral protection was secured by lead blocks and cadmium foil. The detector was mounted on a vibroinsulating platform in a Faraday cage. The detection threshold was ~ 2 keV, the number of phonon events in the energy range 2 – 100 keV reached ~ 5 per 1 keV kg day (one order of magnitude greater than in a silicon detector). No anomalous changes in the phonon energy spectrum were documented.

ROSEBUD was extended to assess the possibility of using $CaWO_4$ and BGO bolometers for WIMP detection. Comparison of the spectra obtained with bolometers of different types permitted finding the dependence of event counts on the crystal atomic mass. However, BGO crystals turned out to be practically unsuitable for recording recoil nuclei from elastic WIMP scattering because of a very high detection threshold (~ 6 keV) [242].

***Kamioka*-NaF** is an experiment in the Kamiokande underground laboratory using eight NaF-bolometers (total weight 176 g) [243]. Each bolometer contained an NaF crystal $2 \times 2 \times 2$ cm^3 in size and a germanium thermistor. The constraint on the WIMP – nucleon cross section for WIMPs with the mass 27 GeV was $\sigma_{\mathrm{WIMP-nucleon}} \leqslant 27$ pb.

CRESST-I (Cryogenic Rare Event Search with Superconducting Thermometers) is an experiment at the Gran Sasso underground laboratory using a sapphire bolometer with a 262 g crystal [244]. The resolution of 133 eV was achieved at the threshold $E_{\mathrm{th}} \approx 500$ eV and the energy 1.5 keV.

6.4 Overheated droplet detectors and superconducting granule detectors

One approach to the development of WIMP detectors consists in the use of overheated liquids. Such detectors work as bubble chambers in which small energy release disturbs the metastable state of the liquid, thereby giving rise to bubbles recorded by optical devices or acoustic sensors. Minimal energy release is needed to trigger a phase transition; therefore, overheated droplet detectors are threshold instruments. The operating temperature and pressure are chosen such that only recoil nuclei could induce bubble formation. Recoil electrons from interactions of γ-quanta release less energy and fail to form bubbles.

COUPP (Chicagoland Observatory for Underground Particle Physics) is a detector analog of a bubble chamber filled with 2 kg of liquid CF_3I [245]. In 2005, the chamber was placed in the tunnel of the Tevatron NuMi neutrino channel at a depth of 300 m.w.e. Bubbles were detected by optical cameras and acoustic sensors. The use of the two signals ensured spatial reconstruction of a newly formed bubble up to 1 mm. These data allowed separation of recoil nuclei from events associated with multiple neutron scattering. However, the first phase of the COUPP experiment did not envisage minimization of the recoil nucleus background of alpha-particles created in the radioactive decay of radon present in small amounts in the environment. The total exposition of the detector was 250 kg day. No meaningful events were documented.

A new chamber is being designed to contain 80 kg of CF_3I and enable subtraction of the radon background [246]. The chamber will be installed in the Soudan underground laboratory, USA, which already operates the CDMS-II detector.

PICASSO (Project In Canada to Search for Supersymmetric Objects) is an experiment with a detector consisting of a polymerized gel that suspends liquid droplets in an overheated state [247]. The experiment was made in the world's deepest SNO underground laboratory (~ 6000 m.w.e.), Sudbury, Canada. The gel serves as the active target for WIMP interactions and overheated 10 – 100 μm droplets work as minibubbles in an ordinary chamber. The phase transition to the normal state is accompanied by drop bursting recorded by piezoelectric sensors at the outer surface of the detector walls. The phase transition is associated with a change in temperature and pressure in the gel surrounding each drop and depends on the specific character of energy loss by individual drops as they cross the sensitive detector volume. Due to this, it is possible to distinguish ^{19}F recoil nuclei from particles with a small ionization density. The energy threshold of nucleus detection can be varied by altering the detector temperature and pressure. The temperature dependence of the energy threshold was determined by calibration measurements using neutron, γ-, and α-sources and was compared with the results of calculations by the Monte Carlo method. Three 1.5 l detectors were commissioned in 2004. Each detector is a cylindrical polypropylene container filled with polymerized emulsion containing C_4F_{10} droplets. By varying the temperature in the range 20 – 47 °C, it was possible to detect the recoil nucleus with the energy 6 – 500 keV. The energy spectrum measured over a 1.98 kg day exposition period was in excellent agreement with the temperature dependence characteristic of α-particles, which differed significantly from that of WIMP-induced recoil nucleus. The constraint on the WIMP – nucleon cross section was 1.3 pb at the WIMP mass 29 GeV.

The number of detectors in the PICASSO experiment is gradually increasing. The instrument with 32 detectors will have the active mass 3 kg. With an exposition of 280 kg day, it is expected to achieve the sensitivity of the WIMP – nucleon cross section measurement of the order 5×10^{-38} cm^2.

SIMPLE (Superheated Instrument for Massive ParticLE searchers) is an experiment at the LSSB laboratory (Laboratoire Souterrain Bas Bruit), France, at a depth of 1500 m.w.e. with the use of a freon (C_2ClF_5)-based overheated droplet detector [248]. The SIMPLE detector works similarly to PICASSO. Its four 5 l modules contain a polymerized gel in which C_2ClF_5 droplets are suspended (the total active mass is approximately 43 g). The detectors are placed in a dewar with 700 l of admixture-free water surrounded by a triple layer of acoustic and thermal insulators. Sound waves accompanying the phase transition were recorded by submerged piezoelectric microphones and an acoustic monitor placed from the outside. Whenever a candidate for the sought event was recorded in any detector, the temperature, pressure, and shape of the signal in the form of a Fourier image were written into the computer memory.

The total exposition of the SIMPLE was 0.42 kg day. The signal count in the detector was compatible with the background contribution. Despite a smaller exposition than in PICASSO, the constraints on the WIMP – nucleon cross section were identical in both experiments. This result demonstrates the importance of using passive protection

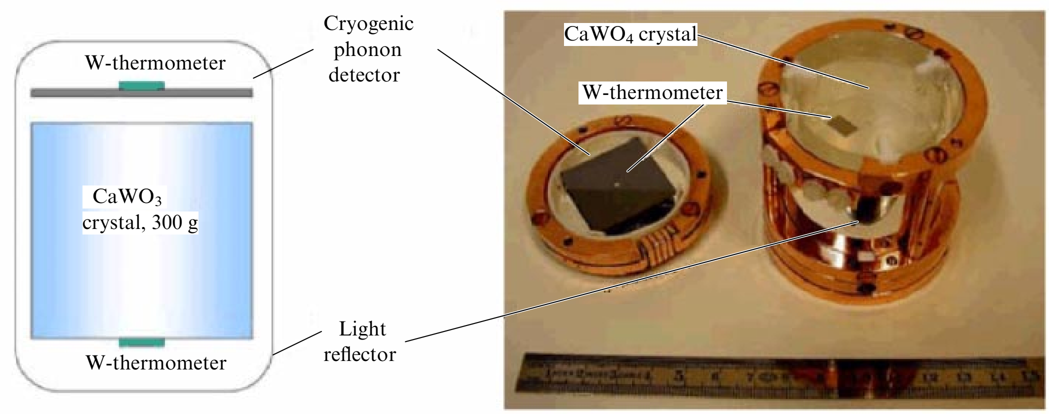

Figure 12. Diagram and photograph of the CRESST-II detector [250]. The W-thermometer is a tungsten thermometer.

and materials free from radioactive admixtures in WIMP experiments.

Orpheus (the name is borrowed from a Greek myth) is a detector in which the active target for WIMP interactions consists of superconducting Sn granules. It has been operating for a few years in the Berne underground laboratory at a relatively small depth (70 m.w.e.) [249]. Granules measuring 36 mcm on the average are uniformly distributed in an insulator placed in a magnetic field. The detector records changes in the magnetic flow caused by phase transitions induced by WIMP interaction with the superconducting granules in a metastable state. The detector operates at the temperature ~ 115 mK. A granule releasing several keV of energy passes from the superconducting to the standard state. A change in the magnetic flow following the disappearance of the Meissner effect is recorded in current windings of a SQUID quantum interferometer (Superconducting Quantum Interference Device).

Orpheus uses 4 cylindrical modules each with 14 containers filled up with Sn granules. Their total mass is ~ 420 g. The modules are surrounded by a superconducting NiTi solenoid creating a 40 mT magnetic field. External protection is secured by copper and lead layers of the respective thickness 5 and 15 cm that absorb γ-quanta. A sheet of boron-saturated polyethylene absorbs neutrons. The scintillation veto system separates muons passing through the detector.

Measurements have revealed a high noise level ($\sim 2 \times 10^3$ events per kg day) resistant to suppression, putting into question the expediency of further experimentation.

6.5 Combined light and heat detectors

CRESST-II is the first WIMP experiment with the use of cryogenic detectors based on $CaWO_4$ crystals that record both photons and light signals [250] (Fig. 12).

The detector is protected from natural background radiation by a sheet of copper and lead. Recoil nuclei with energies ~ 10 keV are effectively separated from background γ- and β-radiation. Four SQUID channels ensure independent operation in the phonon mode and in the scintillation regime.

One module of the detector consists of a 300 g $CaWO_4$ scintillation crystal working as a cryogenic calorimeter (phonon channel). A cryogenic detector close to the scintillation crystal is optimized to record scintillations (light channel). A phonon channel is intended to measure the energy transmitted by a recoil nucleus in the $CaWO_4$ crystal as it elastically scatters WIMPs. A recoil nucleus signal is different in terms of the light output from scintillation light emitted by an electron or a γ-quantum with the same energy, which allows effectively distinguishing background electrons and γ-quanta and independently measuring phonon and light signals.

A cylindrical $CaWO_4$ crystal 40 mm in diameter is used in the detector module. A light detector is placed at the top flat surface of the crystal and the module is surrounded by a multilayered polymeric light-reflecting foil. The instrument operates at about 10 mK. The tungsten thermometer is in the intermediate condition between superconducting and normal states. In this regime, even a small increase in the thermometer temperature leads to a relatively large increase in its resistance measured by two parallel windings. One end of the winding is attached to a superconducting film and the other is connected with the SQUID interferometer through a resistor. This ensures high sensitivity of current change measurements. Taken together, an increase in the thermometer resistance and an increase in the current strength are responsible for the enhanced output voltage of SQUID.

In the first measurements of 2004 with two detector modules, the signal count rate was 0.87 ± 0.22 kg^{-1} day^{-1}, in excellent agreement with the predicted signal from background electrons and γ-quanta. The next step in the development of the CRESST detector will be the installation of 33 additional modules with an updated 66-channel reading system, an antineutron protection system, and a muon veto system.

6.6 Combined heat and ionization detectors

CDMS (Cryogenic Dark Matter Search) was the first experiment in which independent measurement of ionization and thermal signals by a cryogenic germanium detector was used in the search for WIMPs. Up to 2002, the experiment was based at the Stanford laboratory, where the detector was rather poorly protected from neutrons and muons; therefore, the background could be separated only by normalization to the results of Monte Carlo simulation. Nevertheless, restrictions on the DM existence remained extremely strong for several years [251].

In 2003, a modified CDMS-II detector was installed at a depth of 2090 m.w.e. in the Soudan mine, Minnesota, USA. Four germanium crystals of 250 g each and two 100 g silicon detectors were cooled to below 50 mK (Fig. 13). They were protected from background neutrons and γ-radiation by

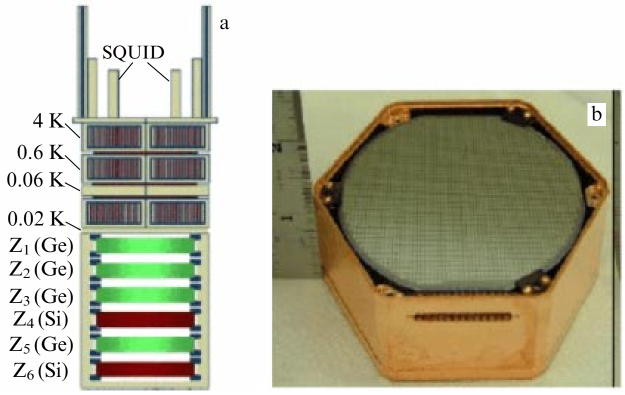

Figure 13. (a) Diagram of the CDMS-II detector. (b) Structural module of the SuperSDMS detector with the target containing 60 g of Ge crystals. $Z_1 - Z_6$, semiconducting detectors for charge measurement [252].

several layers of copper (0.5 cm), lead (22.5 cm), and polyethylene (50 cm). Charged particles (mainly muons) passing through the detector were separated by the veto system of scintillation counters.

In CDMS-II, recoil nucleus events are separated from electron scattering events via two independent channels. First, ionization is registered in a high-purity germanium crystal placed between the electrodes to which a voltage of several volts is applied. At a given energy, electrons have a greater ionizing capacity than nuclei. Second, thermal sensors measure heat release at low temperatures. A phonon signal from a recoil nucleus lasts longer and comes later than a signal from a recoil electron. Neutron-induced recoil nuclei are the main source of background signals that produce the required heat/ionization ratio calculated under the assumption of WIMP scattering by the germanium nucleus.

The detection threshold for recoil nuclei was 2 keV. Analysis of events with energies in the range from 10 to 100 keV recorded during the CDMS-III exposition of 19.4 kg day excluded, at a 90% confidence level, the existence of WIMPs with masses below 60 GeV at WIMP – nucleus cross sections greater than 4×10^{-43} cm^2. To date, this is one of the best constraints achieved.

It was proposed, by way of extension of the experiment, to create a new SuperCDMS detector and install it in the SNO laboratory, Canada, located in one of the world's deepest mines ($\sim$ 6000 m.w.e) [253]. There are plans to use CDMS-III analogs and gradually increase their number. Detectors with the total mass of germanium of approximately 27 kg will be used in the first phase, and detectors of the mass 145 and 1100 kg in the second and third phases, respectively. SuperCDMS is expected to measure WIMP – nucleus cross sections up to $10^{-44} - 10^{-46}$ cm^2.

EDELWEISS (Expérience pour Détector Les WIMPs en Site Souterrain) is a detector of the underground laboratory situated in the Modane tunnel connecting France and Italy. ($\sim$ 4800 m.w.e). Similarly to CDMS, the EDELWEISS experiment used cryogenic germanium detectors recording heat and ionization signals. In the first phase (the EDELWEISS-I experiment, 2000 – 2003), only three detectors were operated, each containing 320 g of the ^{73}Ge isotope [254]. Each detector was a germanium crystal shaped like a cylinder and had aluminum electrodes to record ionization signals and heat sensors glued to one of the electrodes for recording phonon signals. The detectors worked independently in a cryostat at 17 mK. The device was surrounded by layers of paraffin (30 cm), lead (15 cm), and copper (10 cm). The total exposition for 3 years was 62 kg day. The energy detection threshold was 13 keV. EDELWEISS-I detected 40 events with energies from 15 to 200 keV, which were regarded as candidates for signals of the recoil nucleus from WIMP interactions. Analysis of these results showed that the sources of signals resembling recoil nucleus signals could be neutrons and recoil electrons arising near the crystal surface. The constraint on the spin-independent cross section obtained in EDELWEISS-I was three times worse than in the CDMS-II experiment, where events with recoil electrons near the surface were easy to distinguish based on the arrival time of phonon signals.

The EDELWEISS experiment was extended to the second phase (EDELWEISS-II) in which the detector mass increased and background radiation sources were effectively suppressed [255]. The cryostat was protected from background γ-quanta by a lead layer 20 cm thick. Natural bedrock radiation and interactions of CR muons in the protective shielding can probably be a source of neutrons. The low-energy neutron background is reduced by three orders of magnitude using a polyethylene layer 50 cm thick. The muon veto system consists of 42 strips of plastic scintillator (total area 100 cm^2) surrounding the device. This system labels events involving muons that interacted in the lead shielding and gave rise to neutrons. High-energy neutrons resulting from interactions of muons unlabeled by the veto system are the sole source of undetectable background.

The EDELWEISS-II cryostat has the volume 50 l containing detectors of three types. First, there are 110 neutron-transmutation doped Ge (Ge-NTD) detectors weighing 330 g each, similar to those used in EDELWEISS-I. Detectors of the second type contain 400 g Ge crystals with new aluminum electrodes and two NbSi-insulating thermometric layers. The third type is detectors with Ge-NTD crystals weighing 400 g with an in-built electrode system. The new Ge-detectors were specially developed by the EDELWEISS collaboration for the reliable identification of near-surface events. It is planned to use 20 detectors of both the second and third types. EDELWEISS-II will be commissioned in late 2009.

The calculated number of events involving a recoil nucleus with energies over 10 keV to be detected in EDELWEISS-II is 10^{-3} per kg/day. This number is equivalent to the sensitivity necessary to measure a 10^{-8} pb WIMP – nucleon cross section for WIMPs with the mass $\sim$ 100 GeV, which is two orders of magnitude lower than in EDELWEISS-I.

6.7 Combined light and ionization detectors

ZEPLIN-II is the second phase of the ZEPLIN experiment, in which a detector based on liquid and gaseous xenon was used for the first time [256]. A particle passing though the liquid target ionizes the medium and triggers free electrons to move in the applied electric field toward the gaseous phase, enter it, and ionize gas atoms. Electroluminescence results in the elimination of atomic excitation and emission of light. The operating principle of such devices consists of different particles passing through the sensitive detector volume providing different contributions to the signals recorded as ionization light and energy losses (Fig. 14). The difference between these two signals permits discriminating between interactions with electrons and the recoil nucleus. If WIMPs are elastically scattered by the Xe nucleus, the signature of

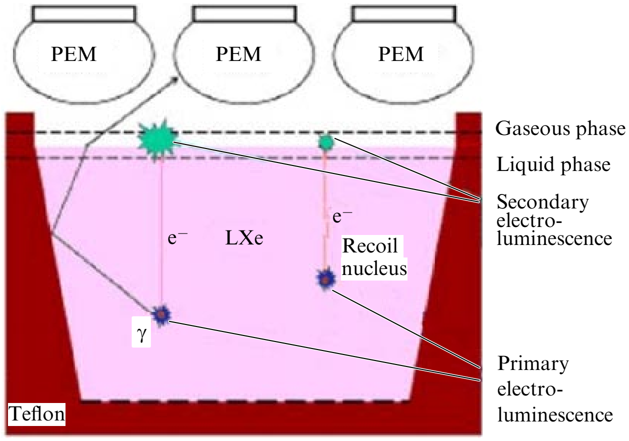

Figure 14. Principle of signal registration in a two-phase xenon detector. A particle entering the detector interacts in liquid xenon, giving rise to the primary scintillation signal. Secondary electrons drift toward the gaseous layer, where they generate the secondary electroluminescent signal. Both signals are recorded by the system of PEMs on top of the detector.

interactions between recoil nuclei is significantly different from that for γ-quanta and recoil electrons.

ZEPLIN-II contains 31 kg of liquid xenon filling a copper container 50 cm in diameter and 13 cm in height, whose interior is scanned by seven PEMs. The 2 cm gaseous phase overlies liquid xenon. The system of electrodes maintains the strength of the electric field at 1.8 kV cm^{-1} in the liquid phase and 2 kV cm^{-1} at the liquid – gas interface. The low detection threshold in this instrument is due to recording scintillation light by PEMs imbedded in the liquid phase. The lifetime of ions must be longer than that of free electrons if ionization losses in liquid xenon are to be measured. This condition is satisfied by using superhigh-pure xenon. During the first exposition of the detector (225 kg day), the number of measured events did not exceed the background count. The constraint on the WIMP – nucleon cross section was 6.6×10^{-7} pb.

ZEPLIN-III is the most recent version of the modified xenon detector with two-phase emission [257]. The detector has a matrix of 31 PEMs protected by a copper foil that scans a layer of liquid xenon 40 mm thick overlayed by a 5 mm gaseous phase. A voltage up to 40 keV is applied between the copper electrode bounding the gaseous phase and the grid bounding the active area of the liquid phase. This allows a fairly good reconstruction of an event in all three directions; specifically, the spatial resolution is ~ 10 mm in the horizontal plane and ~ 50 μm in the vertical direction. The copper container with the xenon target and PEMs is placed in a cryostat filled with liquid nitrogen. Calibration of the instrument and its preparation for searching for WIMPs are currently underway.

Xenon 10 is a xenon time-of-flight chamber operated by the Gran Sasso Laboratory [258]. The detector independently measures scintillation light in the liquid phase and ionization proportional to scintillation in the gaseous phase. The ratio of these two signals permits distinguishing events with recoil nucleus energies below 4.5 keV. The time-projection chamber is placed within a teflon cylinder 20 cm in diameter and 15 cm in height, functioning as both a light reflector and an insulator. The mass of the xenon target is 15 kg. Voltage applied to four steel mesh electrodes (two in the liquid and two in the gaseous phases) creates an electric field necessary for ionization electrons to drift in the liquid. The field strength in the liquid phase is 0.73 kV cm^{-1}. Electrons are expelled from the liquid surface and accelerated in the gaseous phase. Forty one compact PEMs in the bottom plane of the detector record direct scintillation light in the liquid phase and 48 PEMs in the top plane register proportional light response in the gas. A layer of liquid xenon (10 kg) outside the active volume has the temperature about $-93\,^{\circ}$C maintained by special cryogenic equipment. Peripheral protection of the detector consists of 20 cm thick polyethylene and lead sheets.

The detector was commissioned in 2006. During the first 58 days of exposition, 1800 events were detected, ten of which can be interpreted as recoil nucleus signals from WIMPs. This result implies the upper bounds $\sim 8.8 \times 10^{-44}$ cm^2 and $\sim 4.5 \times 10^{-44}$ cm^2 on the WIMP – nucleon cross section for WIMPs with the respective mass 100 GeV and 30 GeV.

WIMP experiments in the Gran Sasso Laboratory will be further extended by putting a Xenon 100 detector into operation in 2008. Its operating principle is analogous to that of Xenon 10, but the new detector will have an order of magnitude greater mass (150 kg of liquid xenon). Moreover, it will be additionally protected by liquid xenon. The inner target will be scanned by 250 PEMs. The sensitivity of the WIMP – nucleon cross section measurement will be of the order $\leqslant 9 \times 10^{-45}$ cm^2.

WARP (Wimp Argon Program) is a liquid argon drift chamber put into operation at Gran Sasso in 2006 [259]. The philosophy behind the development of liquid argon time-of-flight chambers with a system of electronic read-outs of information has for a long time been elaborated by the ICARUS collaboration (Imaging Cosmic and Rare Underground Signals) [260]. Such chambers ensure a precise measurement of relativistic and nonrelativistic particle momenta and calorimetry with high energy resolution. The search for WIMPs with liquid argon chambers, similar to xenon ones, requires knowledge of the light/charge signal ratio, measurement of rapid and slow components of scintillation light, and reconstruction of the event topology and the contributions of multiple scattering processes. The WARP collaboration used a two-phase 2.3 l argon drift chamber in which the gaseous phase over liquid argon contains 7 PEMs. The liquid argon surface is covered with a layer of a special additive that shifts the spectrum of UV photons emitted in the scintillation process in liquid argon toward the region surveyed by PEM photocathodes. The total drift length is 7.5 cm, the field strength 1 kV cm^{-1}, and the exposition 96.5 kg day. The constraint on the WIMP – nucleon cross section deduced from the lack of detected recoil nuclei with energies above 55 keV was $\leqslant 1.2 \times 10^{-42}$ cm^2 for WIMPs with masses of the order 100 GeV.

ArDM (Argon Dark Matter) is a liquid argon time-projection chamber being developed at CERN to contain 1 ton of liquid argon [261]. The maximum drift length of ionization electrons is 120 cm. Scintillation light is collected by 14 PEMs located in the liquid phase below the cathode grid. In the gaseous phase, electrons enter a large two-cascade electron multiplier, where their x and y coordinates are determined. The z coordinate is found from the electron drift time. After test measurements at CERN scheduled for 2007 and evaluation of the efficiency of separation of recoil nuclei from background electrons, the chamber will be transported to the Canfranc underground laboratory. It will be used to survey WIMP – nucleon cross sections in the range from 1×10^{-42} cm^2 to 1×10^{-44} cm^2, depending on the exposition time and the degree of background suppression.

7. Detection of strongly interacting DM

INCA (Ionization-Neutron CAlorimeter) is a multipurpose astrophysical orbital observatory being developed at the Lebedev Physical Institute (FIAN) jointly with the Institute of Nuclear Research (INR), the Russian Academy of Sciences, and the Research Institute of Nuclear Physics (RINP), Lomonosov Moscow State University. The observatory will be used to explore astrophysical aspects of primary cosmic radiation (PCR) and elementary particle physics at high energies ($E_{\rm CR} = 10^{12} - 10^{16}$ eV) [262, 263]. Special emphasis will be laid on the energy spectra of cosmic particles and the mass composition of PCR nuclear components (from energies $E_{\rm CR} \approx 10^{12}$ eV to $E_{\rm CR} \approx 10^{16}$ eV), the spectrum behavior of primary electrons at $E_{\rm e} \geqslant 10^{12}$ eV, diffuse γ-spectra at 30 GeV $\leqslant E_\gamma \leqslant$ 30 TeV, and discrete sources of γ-quanta at 10^{10} eV $\leqslant E_\gamma \leqslant 10^{12}$ eV [264 – 266]. Both ionization and neutron signals will be used to measure the cascade energy. On the one hand, this will allow markedly increasing the measurement accuracy and separating electrons and γ-quanta from the proton background. On the other hand, such an approach will give an opportunity to differentiate cascades from nonstandard exotic particles [267]. Taken together, the large aperture (~ 17.6 m^2 sr) of INCA and new technology for particle detection make this instrument a unique tool for searching for DM in the form of WIMPs and massive exotic particles with an unusually low charge-to-mass ratio, e.g., by means of recording signals from the annihilation of massive neutralinos [268, 269].

As noted in Section 3, strongly interacting DM particles may have a very large mass number $A = M_{\rm SIMP}/m_{\rm p} \gg 1$ and an abnormally low ratio $Z/A \ll 1$. It is believed that part of these particles can be accelerated to high energies, similarly to normal nuclei. The existence of such rapid exotic particles was confirmed in a Japanese balloon experiment some 15 years ago [86]. These rapid X-particles can be just as well recorded by INCA as superheavy nuclei with an abnormally low Z/A ratio. Their charge will be measured by the charge detector, and A values will be possible to find owing to the INCA ability to determine the baryonic number of a primary particle (assuming X-particles interact like massive nuclei). For example, this condition must be satisfied for strangelets.

Figure 15 shows theoretical distributions of events $N_{\rm event}$ by neutron numbers $N_{\rm neut}$ generated by different nuclei in an absorber approximately as thick as the interaction length. These distributions illustrate the INCA potential for measuring the mass number A of a 'superheavy nucleus.' If the spectrum profile of high-energy X-particles proposed in Ref. [86] is valid, about 10^{-6} of the particles detected by INCA must be exotic.

Another aspect of the problem of strongly interacting DM particles appears to be the so-called *centaur* phenomenon, i.e., interactions at high altitudes involving an unusually large number of high-energy hadrons and only a few or no electromagnetic particles. This phenomenon was first interpreted as a result of specific proton interactions at energies 3×10^{15} eV manifested as a kink (the so-called elbow) in the CR spectrum. Today, its astrophysical origin is conjectured and attributed to the decay of high-energy strangelets [270].

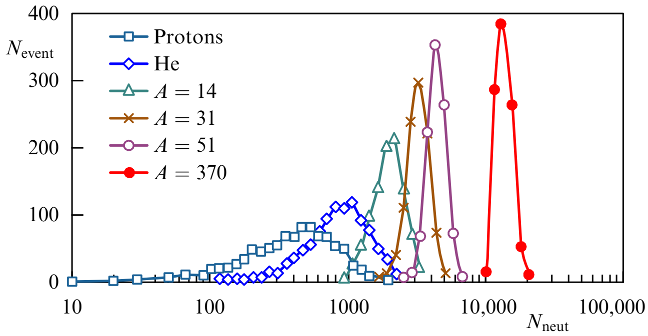

Figure 15. The number of events in INCA versus the number of neutrons generated by primary nuclei ($A = 1$, 4, 14, 31, 51) with $E = 1$ TeV. X-particles are assumed to interact as superheavy nuclei with $A = 370$.

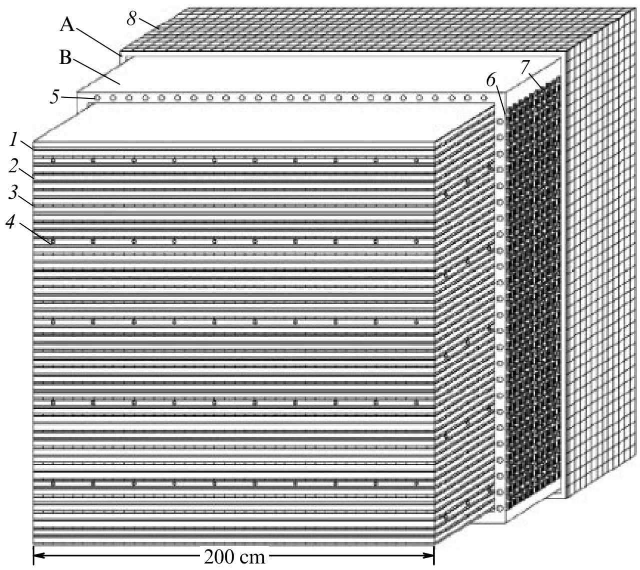

Figure 16. Schematic of the INCA detector: *1*, lead; *2*, polyethylene; *3*, plastic scintillators; *4*, SNM-17 counters; *5*, Gelii-3 counters; *6*, electronic plates; *7*, photodetectors (PEMs, phototriodes); *8*, charge detectors; A and B, outer layers.

The characteristics of INCA are such that they will probably allow calculating at least the upper limit for hadron interaction cross sections giving rise to centaur events.

The main elements of INCA are schematically represented in Fig. 16. Its inner part (calorimeter) has 48 layers made of a sandwich of lead foil (2 mm thick), a sheet of polyethylene (27.2 mm), and long (~ 2000 mm) blocks of plastic scintillators (10 mm). The weight of polyethylene and lead is 56 and 44% of the total, respectively, corresponding to $4.2\,\lambda^{\rm p}_{\rm int}$ and $0.3\,\lambda^{\rm p}_{\rm int}$ per unit proton path before interaction and to $4t_0$ and $17t_0$ if expressed in radiation units.

Plastic scintillator strips serve as position-sensitive detectors of neutron and ionization signals. Each strip has a PEM on the ends to measure amplitudes and thereby register the cascade ionization component. One hundred SNM-17 gas counters of slow neutrons (He^3, 7 atm, length 2000 mm) placed in every 5th polyethylene sheet 200 mm apart are intended to detect neutrons near their region of origin.

The outer part of INCA consists of two layers (A and B) spaced by a gap. The external layer A is 1 cm thick and encloses a 1 mm thick charge detector divided into 5.5×5.5 mm^2 sections and wrapped up in a 3 mm poly-

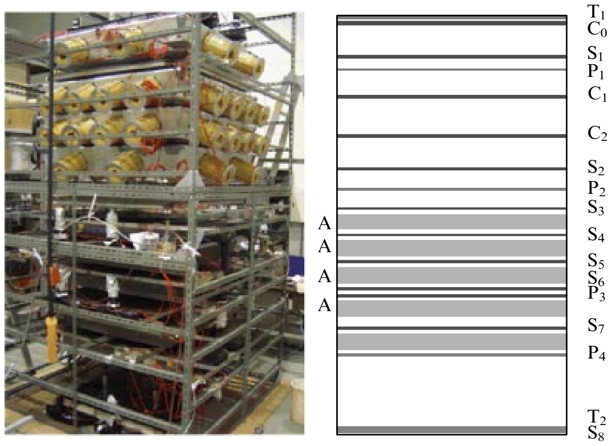

Figure 17. Photograph and diagram of OGAMA for searching for strange quark matter at the Lebedev Institute high-altitude station, Tien Shan: S_1 and S_2, charge-detecting scintillators; S_3-S_8, scintillators measuring the dE/dx ratio; C_0-C_2, Cherenkov detectors measuring the β-particle velocity; T_1 and T_2, direction scintillators (time-of-flight system); P, proportional chamber for coordinate detection; A, five planes of absorbent material.

ethylene film. Layer B is a polyethylene film 5 cm thick and has holes, where photodetectors are placed to collect light from the scintillators. Layer B serves as a reflector of neutrons and contains Gelii-2 counters measuring the neutron component.

The plastic scintillator detects neutrons by virtue of additives with a large thermal neutron absorption cross section, such as Cd (5300b) or Gd (60,000b) [271]. Scintillation detectors recording neutrons function as counters; energy release from the ionization component is registered by an amplitude measurement to determine x and y coordinates of cascade axes in each detector plane.

The INCA collaboration developed semiconducting silicon pixel charge detectors to be used instead of traditional semiconducting microstrip detectors. The new detectors are based on the original concept of the local-injection mechanism for strengthening the active bipolar n–p–n-transistor structure of the drift component of ionization current. The development of a matrix-structural detector with a large number of cells on the silicon substrate is in progress. This detector will have high temporal (~ 1 ns) and spatial (~ 10 μm) resolutions with the signal-to-noise ratio up to $\sim 10^2$.

Presently, work is underway to adjust the INCA equipment for installation on a spacecraft.

OGAMA (Objects in Galaxy from Anomalous MAtter) is an experiment at the Lebedev Institute high-altitude station in the Tien Shan Mountains having the aim to detect strongly interacting DM believed to exist in the form of exotic nuclei (like strangelets) with a small charge ($Z \sim 10$) and abnormally large mass ($A \geqslant 350$). The experiment uses a variant of the detector updated by Japanese physicists [86] for recording anomalously heavy nuclei. The detector was set up at the Lebedev Institute cosmic ray station situated 3500 m a.s.l. near Almaty. The experimental unit is an assembly of several types of detectors (Fig. 17). Scintillation planes S_1 and S_2 serve to measure the particle charge in the range $Z = 1-26$. Planes S_3-S_8 interleaved with an absorbing material are used to measure the energy from ionization losses dE/dx by a particle. Planes T_1 and T_2 constitute a time-of-flight system for determining the particle arrival direction. Cherenkov counters C_0-C_2 measure the β-particle velocity; its coordinates are detected by orthogonally positioned proportional chambers.

8. New promising methods for the detection of DM particles

8.1 Acoustic detection of massive charged DM particles in satellite experiments

It was proposed in [272] to detect massive charged DM particles, e.g., strangelets, by radiation acoustic methods with the help of balloon- and satellite-based instruments. The idea behind the experiment is to use an original technique developed at the Lebedev Institute [273]. The method registers charged particles using a sound pulse generated in the detector through a thermoelastic mechanism triggered by passing particles. The available state-of-the-art technology for manufacturing acoustic sensors gives hope that this method will be instrumental in the creation of a relatively light and cheap DM detector.

Detectors for searching for strongly interacting DM always contain sheets of absorbing material in which particles lose part of their energy E_d. A polystyrol-based plastic scintillator was used as the absorbent in the INCA and OGAMA experiments described in Section 7. The value of E_d calculated in relation to the mass number A of a particle with $A > 10^4$ propagating at the speed $v/c = 10^{-3}$ suggests that the particle loses 5 meV of energy in a 1 cm thick scintillator plate [272]. This energy release is easy to register, but for the purpose of DM experiments, these signals need to be distinguished from the heavy nuclear background created by CRs. The estimated maximum loss of energy by a uranium nucleus in the aforementioned plate is $E_d^{max} \approx 40$ GeV, meaning that the use of a 1 cm thick scintillator plate allows discriminating between signals from heavy nuclei and those generated by X-particles with mass numbers $A \geqslant 1.5 \times 10^8$.

Figure 18 shows the computed acoustic pressure as a function of the upper bound ν_{max} of the sensor sensitivity. It can be seen that in the frequency range under consideration, the X-particle signal exceeds the expected thermal noise level. In this case, the acoustic signal is respectively above 50 and 100 Pa for $\nu_{max} = 10^6$ and 10^7 Hz. Such signals can be

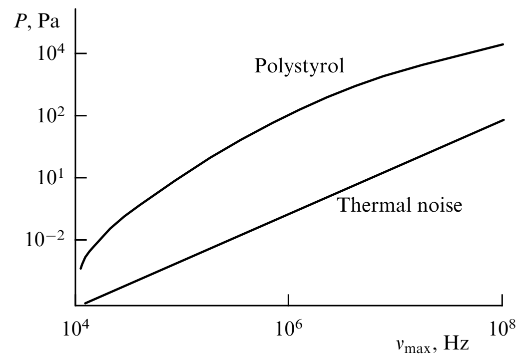

Figure 18. Acoustic pressure P created by DM particles passing through a 1 cm thick polystyrol plate 20 cm from the entry depending on the detector upper sensitivity limit ν_{max}. Calculation of the energy release of 100 GeV corresponding to the X-particle mass $m_X = 5 \times 10^8$ GeV. Straight line is the thermal noise level.

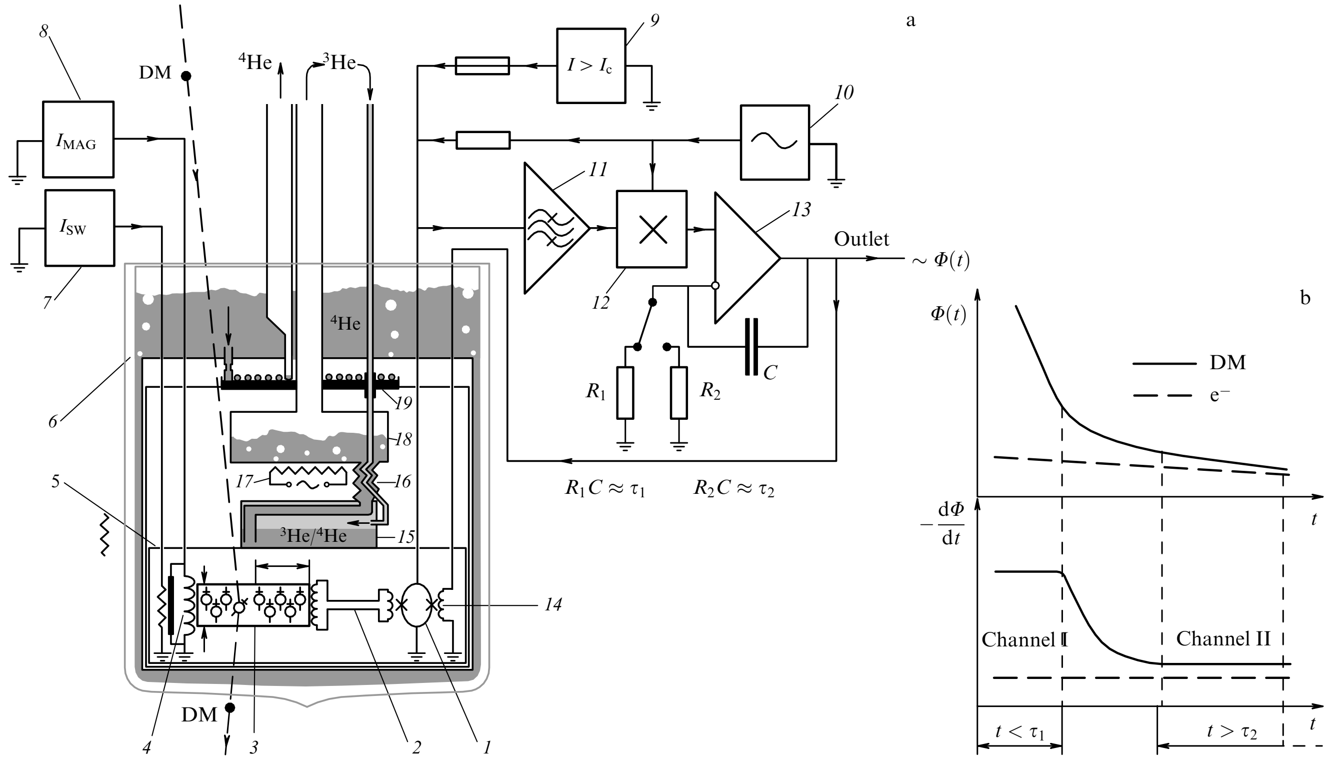

Figure 19. (a) Section sketch of the cryogenic magnetic calorimeter: *1*, direct count (DC) SQUID (crosses designate Josephson transitions); *2*, superconducting flux transformer; *3*, adsorber with a nuclear spin system; *4*, superconducting solenoid with a key to 'freeze' the magnetic field; *5*, superconducting screen; *6*, cryostat with liquid ^{4}He; *7*, source of key-driving current, I_{SW} is the superconducting key current; *8*, source of current feeding the superconducting solenoid, I_{MAG} is the superconducting solenoid current. Main elements of DC-SQUID electronics: *9*, source of the current shifting DC-SQUID operation point above the total critical current of the 1st and 2nd Josephson transitions; *10*, AC generator ($f = 100$ kHz); *11*, selective amplifier ($f = 100$ kHz); *12*, phase detector; *13*, integrator with an alterable time constant; *14*, actuating coil of the SQUID autocompensation system. Refrigerator for dissolution ^{3}He in ^{4}He: *15*, dissolution chamber; *16*, counter flow heat exchanger; *17*, evaporation chamber; *18*, evaporation chamber heater (^{3}He circulation lines are shown by arrows); *19*, plate with the attached single-degree thermal screen. (b) Time dependence of signals in two channels of the cryogenic magnetic calorimeter.

recorded by modern acoustic sensors. For example, piezoreceivers with active elements of a piezopolymeric polyvinylidene fluoride film widely used in dynamic deformation sensors are suitable for this purpose.

Such devices (size: 1×1 cm^2, thickness: ~ 10 μm, sensitivity: ~ 10 μV Pa^{-1}) record acoustic signals from X-particles in the mass range $A \geqslant 3 \times 10^7$. Sensors installed in the solar cell batteries of an Earth satellite or the outer walls of a space station, e.g., the ISS, would provide a very large effective detection area.

One more source of background events, i.e., cosmic dust hitting the detector, should be borne in mind when recording DM particles by the acoustic method. Comet-borne dust or meteoric matter forms a dust envelope around the Earth composed of particles with masses $10^{-17} - 10^{-3}$ g. The speed of such particles relative to the Earth does not exceed ~ 70 km s^{-1}. The generation of acoustic pulses by meteorite hits is mediated through a dynamic mechanism rather than a thermoacoustic one as is the case with X-particles and nuclei. The difference between the characteristics of acoustic pulses produced by these mechanisms may be used to reject the background noise. But the easiest way to suppress the acoustic background of dust particles is to use a thin screen or a shielding entrapping them.

Several layers of acoustic radiators are needed to record large-mass DM particles, which can easily penetrate deep into a material, in contrast to cosmic dust. For example, X-particles with $A > 10^9$ are known to pass through four 1 cm thick polystyrol plates. This fact can be used to detect their signals in a few plates and thereby obtain unique additional signatures.

8.2 Two-channel cryogenic magnetic calorimeter

Small ionization and scintillation outputs produced by recoil nuclei create a difficulty in the application of the hybrid technique to the region of small recoil energies. While high measuring efficiency in the thermal channel of a cryogenic detector allows registration of nuclear recoil up to several hundred electronvolts, it is impossible to use the second (light or ionization) signal at small recoil nucleus energies. But the region of low recoil energies is of special importance in the search for WIMPs due to the exponential dependence of the WIMP – nucleus interaction cross section.

A new two-channel scheme for direct detection of cosmic DM particles has recently been proposed [274] based on an ultralow-temperature calorimeter comprising a nuclear spin system whose magnetic response is measured by a SQUID. The scheme is free from the above drawbacks and ensures detection of recoil nuclei at low energies with the simultaneous suppression of background events caused by electron recoil. It allows measurements in the small nuclear recoil region, highly essential for WIMP searching.

We consider a cryogenic magnetic calorimeter (CMC) with a cylindrical absorber of height H (Fig. 19). A response to the energy release ΔE (induced, for instance, by nuclear recoil upon WIMP scattering in the absorber) in magnetic detectors is possible either at a fixed external field $B \neq 0$ or at $B = 0$ after a cycle of adiabatic demagnetization of the working medium [275]. Calculations [274] show that after achievement of thermal equilibrium in the absorber, the energy resolutions in both cases ($B \neq 0$ and $B = 0$) are roughly identical and independent of the paramagnetic base area:

$$|\delta E| \approx |T\,\delta S| \approx \left|\frac{HB_{\mathrm{r}}\,\delta\Phi}{\mu_0}\right|.$$

Here, B_{r} is the paramagnetic residual field, μ_0 is the vacuum magnetic permeability, and $\delta\Phi$ is the change in the magnetic flow caused by the energy release ΔE measured by a SQUID. The technically attainable SQUID resolution power is $\delta\Phi = 10^{-5}\Phi_0$ [$\mathrm{Hz}^{-1/2}$], where $\Phi_0 = 2\pi\hbar/2e = 2.07\times10^{-15}$ Wb [276]. Then the sensitivity of an electronic paramagnetic-based calorimeter ($B \approx B_{\mathrm{r}} \approx 100$ Oe) is $\delta E_{\mathrm{e}} = 3\times10^{-18}$ J $\mathrm{Hz}^{-1/2} \approx 20$ eV $\mathrm{Hz}^{1/2}$ and the sensitivity of a calorimeter containing a working agent with the nuclear spin system ($B \approx B_{\mathrm{r}} \approx 3$ Oe) is $\delta E_{\mathrm{N}} = 10^{-19}$ J $\mathrm{Hz}^{-1/2} \approx 0.6$ eV $\mathrm{Hz}^{1/2}$.

We now consider a variant for the use of a nuclear paramagnet that is quite promising in terms of the WIMP signal extraction. The above estimates imply that all the released energy uniformly spreads throughout the absorber volume. We now evaluate the sensitivity in the case before the thermal equilibrium is reached in the entire volume. As is known, the time τ_1 of reaching the local equilibrium in a nuclear spin system during nuclear demagnetization caused by energy release from a recoil nucleus is much smaller than the spin–phonon relaxation time τ_2 [274]. The time ratio τ_1/τ_2 can be written as

$$\frac{\tau_1}{\tau_2} \approx \frac{\eta_{\mathrm{e-n}}}{\eta_{\mathrm{n-n}}}\,\frac{C_{\mathrm{n}}}{C_{\mathrm{e}}}\,,$$

where $\eta_{\mathrm{e-n}}$ is the efficiency of the recoil nucleus energy transfer to the electron, $\eta_{\mathrm{n-n}}$ is the efficiency of energy exchange between the recoil nucleus and another nucleus, C_{n} is the magnetic heat capacity of the nuclear system, and C_{e} is the electron heat capacity. In the case of elastic scattering, $\eta_{\mathrm{e-n}}/\eta_{\mathrm{n-n}}$ is proportional to the electron/nucleus mass ratio $m_{\mathrm{e}}/m_{\mathrm{N}}$. For example, the ratio $C_{\mathrm{n}}/C_{\mathrm{e}}$ for a copper absorber at the temperature $T \sim 10$ mK in the field $B \sim 1$ T is roughly equal to unity: $C_{\mathrm{n}}/C_{\mathrm{e}} \sim 1$. Then, for such an absorber, $\tau_1/\tau_2 \sim m_{\mathrm{e}}/m_{\mathrm{N}}$, the relaxation time is $\tau_1 \sim 1$ ms, and $\tau_2 \sim 10$ s. It is during this time, τ_1, that the energy is transmitted onto the grid and nuclear demagnetization occurs in the entire absorber volume when the energy of a high-energy electron is transferred to conduction electrons. The same time is needed for complete equilibrium to be reached when the energy is released by a recoil nucleus from the WIMP interaction. A change in the flux $\Delta\Phi$ caused by the reduction in the moment $\Delta\mathbf{M}$ due to local heating for the time τ_1, in the case of a recoil nucleus, is registered by the input coil of a flux transformer with a radius R. A WIMP-triggered event leading to the energy release ΔE in a cylindrical absorber of the radius R and height H is detected at the initial instant under unsteady conditions with the resolution

$$\delta E(t < \tau_1) \approx \frac{RB_{\mathrm{r}}\,\delta\Phi}{2\pi\mu_0}\,.$$

Subsequently, after the thermal equilibrium is reached, the same event may be recorded with a different resolution (higher at $R > 2\pi H$ or lower at $R < 2\pi H$):

$$\delta E(t > \tau_2) \approx \frac{HB_{\mathrm{r}}\,\delta\Phi}{\mu_0}\,.$$

The respective responses in these conditions are

$$\Delta\Phi(t < \tau_1) = -\frac{2\pi\mu_0\Delta E}{RB_{\mathrm{r}}}\,, \qquad \Delta\Phi(t > \tau_2) = -\frac{\mu_0\Delta E}{HB_{\mathrm{r}}}\,.$$

In the case of an event from the electron interaction, there is only one relaxation time τ_2; therefore, the response of the magnetic flux for the time τ_1 for an electron is τ_1/τ_2 times smaller than $\Delta\Phi(t > \tau_2)$. This means that the electron recoil is suppressed in the rapid channel. This effect can be qualitatively assessed by introducing the rates of change of the magnetic flux in two recording channels. As shown in [274], the ratio of the rates of change before and after the thermal equilibrium is reached in the nuclear system,

$$\eta = \frac{\Delta\Phi(t < \tau_1)/\tau_1}{\Delta\Phi(t > \tau_2)/\tau_2} = \frac{2\pi H\tau_2}{R\tau_1}$$

can be made rather large by properly choosing times and sizes. For example, the relaxation time τ_1 for copper may be of the order of 1 ms and τ_2 not less than ~ 10 s, and hence $\eta = 10^4$ at $2\pi H/R = 1$. On the other hand, the ratio of the rates of change in an electron event with an energy ΔE transmitted to conduction electrons is of the order of $\eta \approx 1$ in both recording channels. This selecting events with the nuclear ($\eta \gg 1$) and electron ($\eta \approx 1$) recoil necessary in experiments for the search for WIMPs interacting with matter in the WIMP–nucleus scattering process.

The choice of $\tau_1 \approx 1$ ms is in line with the standard SQUID service band $\Delta f \approx 1/\tau_1 = 1$ kHz and the assumption of the standard flux resolution $\delta\Phi = 10^{-5}\Phi_0$ [$\mathrm{Hz}^{-1/2}$] yield noise constraint at the initial stage $\delta\Phi_1 = 10^{-4}\Phi_0$. Under nonequilibrium conditions, it corresponds to the energy resolution $\delta E(t < \tau_1) \approx 10^{-19}$ J ≈ 60 eV (here, $R = 100$ cm and $B_{\mathrm{r}}(\mathrm{Cu}) = 3$ Oe). During the relaxation towards thermal equilibrium ($\tau_2 \approx 10$ s), the energy release can be measured, with an increased integration time $\tau_2 = 10$ s in the narrowed working frequency range $\Delta f = 0.1$ Hz up to $\delta E(t < \tau_2) \approx 10^{-21}$ J ≈ 12 eV (here, $H = 20$ cm and $B_{\mathrm{r}}(\mathrm{Cu}) = 3$ Oe). With the above parameters, nuclear recoil events are selected based on the ratio of the rates of flux changes in the first and second channels $\eta \geqslant 10^4$.

We emphasize that a nuclear-magnetic calorimeter with a large-volume absorber allows a high accuracy of the WIMP energy release measurement and a strong suppression of recoil electron events. A specific feature of the DM detection scheme described in the preceding paragraphs is the registration of both signals (i.e., in nonequilibrium and equilibrium conditions) in a single nuclear-magnetic module.

For a copper absorber $2\pi H/R \sim 1$ in size, the ratio of demagnetization rates corresponding to a WIMP scattering event with recoil nucleus formation is $\eta_{\mathrm{WIMP}} \sim 10^4$. The ratio of demagnetization rates corresponding to a background electron is $\eta_{\mathrm{e}} \sim 1$; this allows selecting nuclear ($\eta_{\mathrm{WIMP}} \gg 1$) and electron ($\eta_{\mathrm{e}} \sim 1$) recoil events in WIMP-search experiments. The use of a copper absorber with $V \sim 0.25$ m^3 ($R = 75$ cm, $H = 12$ cm) and mass ~ 2 t would provide much more extensive statistics on WIMP interaction events compared to the statistics of all the experiments being planned.

The nuclear-magnetic calorimeter described in this section can be used to solve other fundamental problems related to the detection and precision measurement of small energy releases, such as determination of neutrino magnetic moments or measurement of low-energy solar neutrino fluxes.

9. Conclusion

In the last decade, practically all underground laboratories in the world have been experimenting with the direct detection of WIMPs. These low-background facilities are operating and developing a variety of detectors involving different methods of recording small energy releases from WIMP scattering by target nuclei (see Table 1).

The sensitivity attained in some of these experiments is sufficient to verify the predictions of the most realistic supersymmetric models in elementary particle physics. Recent progress in the development of cryogenic technologies, low-noise electronics, and hybrid methods for the suppression of phonon events has established the guidelines for future detector designers. How to detect WIMPs is no loner a question. New detectors must have various targets weighing from 100 to 1000 kg and use a combination of methods for the discovery of recoil nuclei by recording light, heat, ionization, and acoustic signals. Once a meaningful signal is detected, it will be possible not only to measure the WIMP mass but also to elucidate the nature of certain weakly interacting particles and to choose a plausible scenario of its origin from numerous options offered by theoretical models.

The creation of detectors of increasingly larger sizes is dictated by the smallness of the WIMP – nucleon cross section that determines the event count rate in a detector,

$$R \approx \sum_i N_i n_\chi \langle \sigma_{i\chi} \rangle \,.$$

Direct detection of WIMPs scattered from a scalar target implies a spin-independent WIMP – nucleus coupling. A spin-dependent coupling can be recorded in a target containing nuclei with a certain spin value. Constraints on the spin-dependent and spin-independent cross sections in different experiments are shown in Fig. 20. It can be seen that constrains on the WIMP – nucleon cross section in experiments with the use of scalar targets are several orders of magnitude smaller than in experiments designed to record spin-dependent interactions. However, experiments of either type provide an additional opportunity to identify the nature of DM with the use of different nuclear targets.

It is expected to obtain new information supporting the existence of WIMPs in experiments on the ILC pp-collider to be commissioned in the near future and thereafter on the ILC e^+e^--collider. However, collider experiments at superhigh energies are a nontrivial task given the multiplicity of final states. Even if new particles are discovered in these studies, their contribution to the total DM of the Universe will remain uncertain.

Finally, it is planned to examine different WIMP signatures by indirect methods using neutrino telescopes, ground- and space-based gamma-observatories, and specialized detectors launched on balloons or satellites to measure cosmic positron and antiproton spectra. Indirect experiments provide data for the estimation of the DM density in the halo of our Galaxy.

The combination of different experiments planned for the near future opens up prospects for the discovery of particles composing the dark matter in the Universe. In any case, the results of these experiments will map out the course of development of DM detectors of the next generation.

Table 1.

Experiment	Signal	Material	Exposition, kg day	Mass, kg	References
IGEX	Charge	^{76}Ge		2	[229]
HDMS	Charge	^{73}Ge	85.5	0.202	[230]
DAMA	Light	NaI	107,731	100	[233]
DAMA/LIBRA	Light	NaI	$\sim 1.5 \times 10^5$	250	[234]
NaIAD	Light	NaI	3879	46	[235]
KIMS	Light	NaI	3409	34.8	[238]
ZEPLIN-I	Light	Liquid Xe	293	3.1	[240]
ROSEBUD	Heat	Al_2O_3		0.1	[241]
Kamioka-NaF	Heat	NaF	3.38	0.176	[243]
CRESST-I	Heat	Al_2O_3	1.5	0.262	[244]
COUPP	Light & acoustic signal	Liquid CF_3I	250	2	[245]
PICASSO	Acoustic signal	C_4F_{10} droplets	1.98	0.00134	[247]
SIMPLE	Acoustic signal	C_2ClF_5 droplets	0.42	0.043	[248]
CRESST-II	Light & heat	$CaWO_4$	10.7	0.6	[250]
CDMS-II	Ionization & heat	Ge	19.4	1	[252]
EDELWEISS-I	Ionization & heat	Ge	62	0.96	[254]
EDELWEISS-II *	Ionization & heat	Ge		52	[255]
ZEPLIN-II	Light & ionization	Liquid & gaseous Xe	225	31	[256]
Xenon 10	Light & ionization	Liquid & gaseous Xe	316	15	[258]
WARP	Light & ionization	Liquid & gaseous Ar	96.5	3.2	[259]

* To begin in 2009.

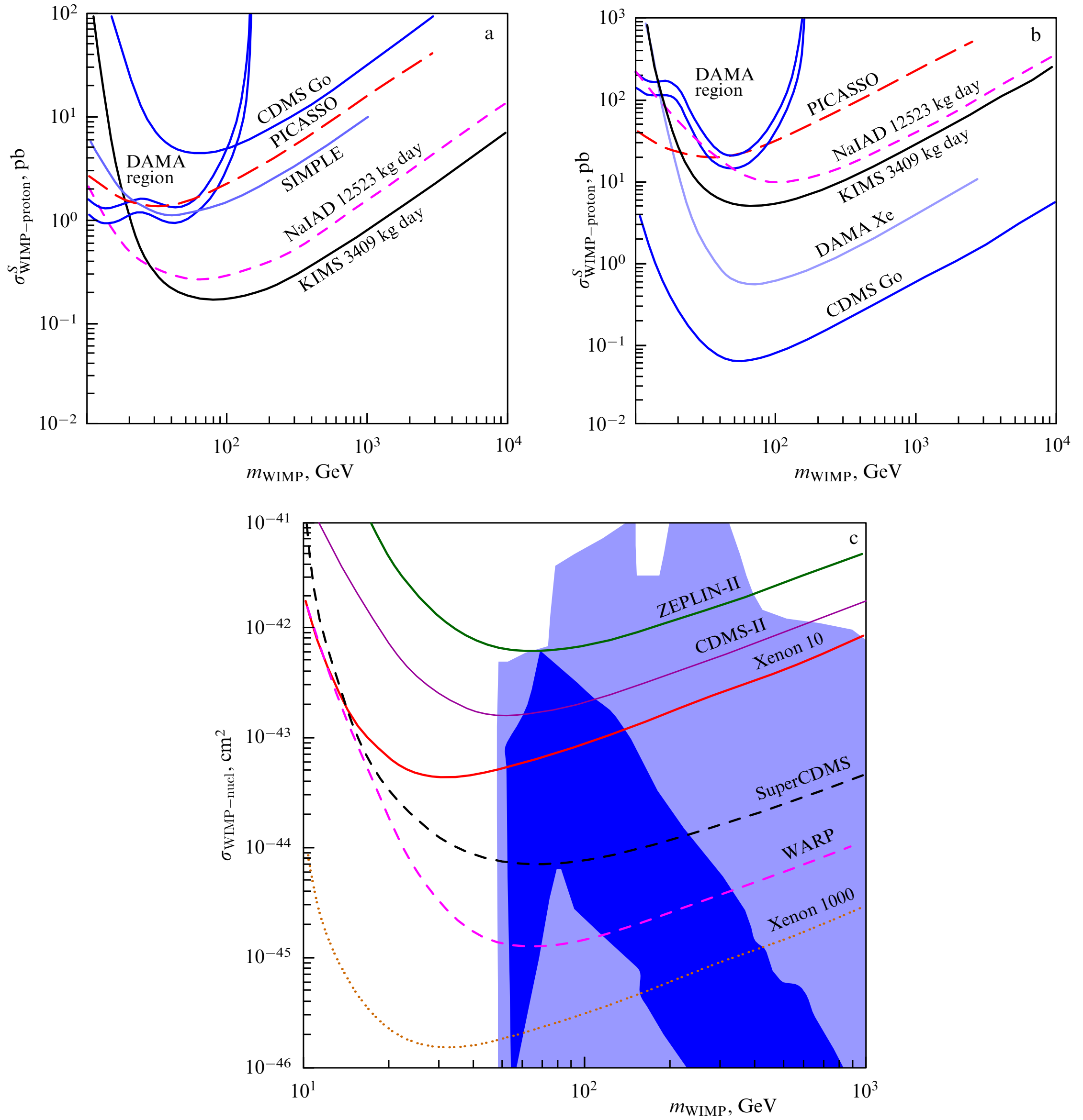

Figure 20. (a, b) Constraints on the spin-dependent cross section in WIMP-searching experiments [238] for WIMP interactions with a target proton (a) and neutron (b). (c) Constraints on the spin-independent cross section obtained in ongoing experiments and WIMP studies expected in the future [277]. WIMP – nucleon cross sections predicted in the models in [278] (grey area) and [279] (black area).

The authors thank A I Golovashkin, G A Gusev, T Saito, and A P Chubenko for enlightening discussions of certain issues addressed in the review.

The work was supported in part by the RFBR grant 08-02-00515 and the Neutrino Physics Program of the Russian Academy of Sciences.

References

1. Ginzburg V L *Usp. Fiz. Nauk* **174** 1240 (2004) [*Phys. Usp.* **47** 1155 (2004)]; *Rev. Mod. Phys.* **76** 981 (2004)
2. Zwicky F *Helv. Phys. Acta* **6** 110 (1933)
3. Gorbunov D S, Rubakov V A *Vvedenie v Teoriyu Rannei Vselennoi. Teoriya Goryachego Bol'shogo Vzryva* (Introduction to the Theory of Early Universe. The Theory of Hot Big Bang) (Moscow: Izd. IYaI RAN, 2007) (Moscow: URSS, 2008)
4. Corbelli E, Salucci P *Mon. Not. R. Astron. Soc.* **311** 441 (2002); astro-ph/9909252
5. Clowe D et al. *Astrophys. J. Lett.* **648** L109 (2006); astro-ph/0608407
6. Allen S W et al. *Mon. Not. R. Astron. Soc.* **353** 457 (2004); astro-ph/0405340
7. Spergel D N et al. *Astrophys. J. Suppl.* **148** 175 (2003); astro-ph/0302209
8. Tegmark M et al. *Phys. Rev. D* **69** 103501 (2004); astro-ph/0310723
9. Straumann N *Mod. Phys. Lett. A* **21** 1083 (2006); hep-ph/0604231
10. Spergel D N et al. *Astrophys. J. Suppl.* **170** 377 (2007); astro-ph/0603449
11. Cole S, Sánchez A G, Wilkins S *ASP Conf. Ser.* **379** 57 (2007); astro-ph/0611178
12. Tegmark M et al. *Phys. Rev. D* **74** 123507 (2006); astro-ph/0608632
13. Percival W J et al. *Astrophys. J.* **657** 645 (2007); astro-ph/0608636
14. Sanders R H, McGaugh S S *Annu. Rev. Astron. Astrophys.* **40** 263 (2002); astro-ph/0204521
15. Fukuda S et al. (Super-Kamiokande Collab.) *Phys. Rev. Lett.* **86** 5656 (2001); hep-ex/0103033
16. Aharmim B et al. *Phys. Rev. C* **72** 055502 (2005); nucl-ex/0502021
17. Fukuda S et al. (Super-Kamiokande Collab.) *Phys. Rev. Lett.* **85** 3999 (2000); hep-ex/0009001
18. Adamson P et al. (MINOS Collab.) *Phys. Rev. D* **73** 072002 (2006); hep-ex/0512036
19. Adamson P et al. (MINOS Collab.) *Phys. Rev. D* **75** 092003 (2007); hep-ex/0701045

20. Aliu E et al. (K2K Collab.) *Phys. Rev. Lett.* **94** 081802 (2005); hep-ex/0411038
21. Ahn M N et al. (K2K Collab.) *Phys. Rev. D* **74** 072003 (2006); hep-ex/0606032
22. Michael D G et al. (MINOS Collab.) *Phys. Rev. Lett.* **97** 191801 (2006); hep-ex/0607088
23. Adamson P et al. (MINOS Collab.) *Phys. Rev. D* **77** 072002 (2008); arXiv:0711.0769
24. Dolgov A D *Phys. Rep.* **370** 333 (2002); hep-ph/0202122
25. Lobashev V M *Nucl. Phys. A* **719** C153 (2003)
26. Kraus Ch et al. *Eur. Phys. J. C* **40** 447 (2005); hep-ex/0412056
27. Cleveland B T et al. *Astrophys. J.* **496** 505 (1998)
28. Hampel W et al. *Phys. Lett. B* **447** 127 (1999)
29. Abdurashitov J N et al. *Zh. Eksp. Teor. Fiz.* **122** 211 (2002) [*JETP* **95** 211 (2002)]; astro-ph/0204245
30. Altmann M et al. *Phys. Lett. B* **616** 174 (2005); hep-ex/0504037
31. Abe S et al. *Phys. Rev. Lett.* **100** 221803 (2008); hep-ex/0801.4589
32. Ambrosio M et al. *Eur. Phys. J. C* **36** 323 (2004)
33. Sanchez M et al. *Phys. Rev. D* **68** 113004 (2003)
34. Ashie Y et al. *Phys. Rev. Lett.* **93** 101801 (2004); hep-ex/0404034
35. Ashie Y et al. *Phys. Rev. D* **71** 112005 (2005); hep-ex/0501064
36. Desai S et al. *Astropart. Phys.* **29** 42 (2008); arXiv:0711.0053
37. Anchordoqui L, Halzen F *Ann. Phys.* (New York) **321** 2660 (2006); hep-ph/0510389
38. Riess A G et al. *Astrophys. J.* **659** 98 (2007); astro-ph/0611572
39. Hannestad S et al. *JCAP* (08) 015 (2007); arXiv:0706.4198
40. Seljak U, Slosar A, McDonald P *JCAP* (10) 014 (2006); astro-ph/0604335
41. Fogli G L et al. *Phys. Rev. D* **75** 053001 (2007); hep-ph/0608060
42. Dodelson S, Widrow L M *Phys. Rev. Lett.* **72** 17 (1994); hep-ph/9303287
43. Ting S C C *Phys. Rep.* **279** 203 (1997)
44. Asaka T, Blanchet S, Shaposhnikov M *Phys. Lett. B* **631** 151 (2005); hep-ph/0503065
45. Seljak U et al. *Phys. Rev. Lett.* **97** 191303 (2006); astro-ph/0602430
46. Viel M et al. *Phys. Rev. Lett.* **97** 071301 (2006); astro-ph/0605706
47. Berezhiani Z G, Vysotsky M I *Phys. Lett. B* **199** 281 (1987)
48. Britton D I et al. *Phys. Rev. D* **49** 28 (1994)
49. Hill C T, Paschos E A *Phys. Lett. B* **241** 96 (1990)
50. Altarelli G, Mele M, Ruckl R, CERN-ECFA Report 84-10, Vol. 2 (1984) p. 549
51. Babu K S, Pati J C, Stremnitzer H *Phys. Lett. B* **256** 206 (1991)
52. Bjorken J D, Llewellyn Smith C H *Phys. Rev. D* **7** 887 (1973)
53. Bertone G, Hooper D, Silk J *Phys. Rep.* **405** 279 (2005); hep-ph/0404175
54. Griest K, Kamionkowski M *Phys. Rev. Lett.* **64** 615 (1990)
55. Hui L *Phys. Rev. Lett.* **86** 3467 (2001)
56. Taoso M, Bertone G, Masiero A *JCAP* (03) 022 (2008); arXiv:0711.4996
57. Goldberg H *Phys. Rev. Lett.* **50** 1419 (1983)
58. Ellis J et al. *Nucl. Phys. B* **238** 453 (1984)
59. Jungman G, Kamionkowski M, Griest K *Phys. Rep.* **267** 195 (1996); hep-ph/9506380
60. Falk T, Olive K A, Srednicki M *Phys. Lett. B* **339** 248 (1994); hep-ph/9409270
61. Feng J L, Rajaraman A, Takayama F *Phys. Rev. Lett.* **91** 011302 (2003); hep-ph/0302215
62. Arkani-Hamed N, Dimopoulos S, Dvali G *Phys. Lett. B* **429** 263 (1998); hep-ph/9803315
63. Arkani-Hamed N, Dimopoulos S, Dvali G *Phys. Rev. D* **59** 086004 (1999); hep-ph/9807344
64. Randall L, Sundrum R *Phys. Rev. Lett.* **83** 3370 (1999); hep-ph/9905221
65. Randall L, Sundrum R *Phys. Rev. Lett.* **83** 4690 (1999); hep-th/9906064
66. Han T, Lykken J D, Zhang R-J *Phys. Rev. D* **59** 105006 (1999); hep-ph/9811350
67. Benakli K *Phys. Rev. D* **60** 104002 (1999); hep-ph/9809582
68. Klein O *Z. Phys.* **37** 895 (1926)
69. Witten E *Nucl. Phys. B* **471** 135 (1996); hep-th/9602070
70. Lykken J D *Phys. Rev. D* **54** R3693 (1996); hep-th/9603133
71. Antoniadis I, Dimopoulos S, Dvali G *Nucl. Phys. B* **516** 70 (1998); hep-ph/9710204
72. Dienes K R, Dudas E, Gherghetta T *Phys. Lett. B* **436** 55 (1998); hep-ph/9803466
73. Kolb E W, Slansky R *Phys. Lett. B* **135** 378 (1984)
74. Appelquist T, Cheng H-C, Dobrescu B A *Phys. Rev. D* **62** 035002 (2001); hep-ph/0012100
75. Servant G, Tait T M P *Nucl. Phys. B* **650** 391 (2003); hep-ph/0206071
76. Cembranos J A R, Dobado A, Maroto A L *Phys. Rev. Lett.* **90** 241301 (2003); hep-ph/0302041
77. Rosenberg L J, van Bibber K A *Phys. Rep.* **325** 1 (2000)
78. Picciotto C, Pospelov M *Phys. Lett. B* **605** 15 (2005); hep-ph/0402178
79. Carr B J *Astrophys. J.* **201** 1 (1975)
80. Paczynski B *Astrophys. J.* **304** 1 (1986)
81. Tisserand P et al. *Astron. Astrophys.* **469** 387 (2007); astro-ph/0607207
82. Witten E *Phys. Rev. D* **30** 272 (1984)
83. De Rújula A, Glashow S L *Nature* **312** 734 (1984)
84. Farhi E, Jaffe R L *Phys. Rev. D* **30** 2379 (1984)
85. Alcock C, Farhi E *Phys. Rev. D* **32** 1273 (1985)
86. Saito T et al. *Phys. Rev. Lett.* **65** 2094 (1990)
87. Frieman J A, Giudice G F *Nucl. Phys. B* **355** 162 (1991)
88. De Rújula A, Glashow S L, Sarid U *Nucl. Phys. B* **333** 173 (1990)
89. Dimopoulos S et al. *Phys. Rev. D* **41** 2388 (1990)
90. Kudo A, Yamaguchi M *Phys. Lett. B* **516** 151 (2001)
91. Hemmick T K et al. *Phys. Rev. D* **41** 2074 (1990)
92. Barwick S W, Price P B, Snowden-Ifft D P *Phys. Rev. Lett.* **64** 2859 (1990)
93. Snowden-Ifft D, Barwick S W, Price P B *Astrophys. J.* **364** L25 (1990)
94. Perl M L et al. *Int. J. Mod. Phys. A* **16** 2137 (2001); hep-ex/0102033
95. Gould A et al. *Phys. Lett. B* **238** 337 (1990)
96. Zel'dovich Ya B, Starobinskii A A *Zh. Eksp. Teor. Fiz.* **61** 2161 (1971) [*Sov. Phys. JETP* **34** 1159 (1972)]
97. Kuzmin V A, Rubakov V A *Yad. Fiz.* **61** 1122 (1998) [*Phys. Atom. Nucl.* **61** 1028 (1998)]; astro-ph/9709187
98. Kuzmin V A, Tkachev I I *Phys. Rep.* **320** 199 (1999); hep-ph/9903542
99. Hamaguchi K, Nomura Y, Yanagida T *Phys. Rev. D* **59** 063507 (1999); hep-ph/9809426
100. Hamaguchi K et al. *Phys. Rev. D* **60** 125009 (1999); hep-ph/9903207
101. Bhattacharjee P, Hill C T, Schramm D N *Phys. Rev. Lett.* **69** 567 (1992)
102. Greisen K *Phys. Rev. Lett.* **16** 748 (1966)
103. Zatsepin G T, Kuz'min V A *Pis'ma Zh. Eksp. Teor. Fiz.* **4** 114 (1966) [*JETP Lett.* **4** 78 (1966)]
104. Berezinsky V, Kachelrieß M, Vilenkin A *Phys. Rev. Lett.* **79** 4302 (1997); astro-ph/9708217
105. Berezinsky V, Blasi P, Vilenkin A *Phys. Rev. D* **58** 103515 (1998); astro-ph/9803271
106. Chung D J H, Kolb E W, Riotto A *Phys. Rev. D* **59** 023501 (1999); hep-ph/9802238
107. Chung D J H, Kolb E W, Riotto A *Phys. Rev. D* **60** 063504 (1999); *Phys. Rev. Lett.* **81** 4048 (1998); hep-ph/9805473
108. Kolb E W, Chung D J H, Riotto A, in *Dark Matter in Astrophysics and Particle Physics, 1998: Proc. of the 2nd Intern. Conf., Heidelberg, Germany, 20–25 July 1998* (Eds H V Klapdor-Kleingrothaus, L Baudis) (Philadelphia, PA: IOP, 1999) p. 592; hep-ph/9810361
109. Faraggi A E, Olive K A, Pospelov M *Astropart. Phys.* **13** 31 (2000)
110. Blasi P, Dick R, Kolb E W *Astropart. Phys.* **18** 57 (2002); astro-ph/0105232
111. Ryabov V A *Usp. Fiz. Nauk* **176** 931 (2006) [*Phys. Usp.* **49** 905 (2006)]
112. Coleman S *Nucl. Phys. B* **262** 263 (1985)
113. Kusenko A *Phys. Lett. B* **405** 108 (1997)
114. Dvali G, Kusenko A, Shaposhnikov M *Phys. Lett. B* **417** 99 (1998); hep-ph/9707423
115. Kusenko A *Phys. Lett. B* **406** 26 (1997); hep-ph/9705361
116. Kusenko A, Shaposhnikov M *Phys. Lett. B* **418** 46 (1998); hep-ph/9709492
117. Kusenko A et al. *Phys. Rev. Lett.* **80** 3185 (1998); hep-ph/9712212
118. Ahlen S et al. *Phys. Rev. Lett.* **69** 1860 (1992)

119. Re Rújula A *Nucl. Phys. A* **434** 605 (1985); Bakari D et al., hep-ex/0004019
120. Benakli K, Ellis J, Nanopoulos D V *Phys. Rev. D* **59** 047301 (1999); hep-ph/9803333
121. Froggatt C D, Nielsen H B *Phys. Lett. B* **368** 96 (1996)
122. Froggatt C D, Nielsen H B *Phys. Rev. Lett.* **95** 231301 (2005); astro-ph/0508513
123. Oaknin D H, Zhitnitsky A *Phys. Rev. D* **71** 023519 (2005)
124. Afonso C et al. *Astron. Astrophys.* **400** 951 (2003)
125. Dirac P A M *Proc. R. Soc. London A* **133** 60 (1931)
126. Abbiendi G et al. *Eur. Phys. J. C* **14** 187 (2000); hep-ex/9909051
127. Abulencia A et al. *Phys. Rev. Lett.* **96** 211802 (2006); hep-ex/0603006
128. Aktas A et al. *Eur. Phys. J. C* **41** 133 (2005); hep-ex/0501039
129. 't Hooft G *Nucl. Phys. B* **79** 276 (1974)
130. Polyakov A M *Pis'ma Zh. Eksp. Teor. Fiz.* **20** 430 (1994) [*JETP Lett.* **20** 194 (1994)]
131. Zeldovich Ya B, Khlopov M Yu *Phys. Lett. B* **79** 239 (1978)
132. Groom D E *Phys. Rep.* **140** 323 (1986)
133. Kolb E W, Turner M *The Early Universe* (Reading, Mass.: Addison-Wesley, 1990)
134. Kephart T W, Weiler T J *Astropart. Phys.* **4** 271 (1996); astro-ph/9505134
135. Harvey J A *Nucl. Phys. B* **236** 255 (1984)
136. Ambrosio M et al. *Eur. Phys. J. C* **25** 511 (2002); hep-ex/0207020
137. Okun L B *Usp. Fiz. Nauk* **177** 397 (2007) [*Phys. Usp.* **50** 380 (2007)]; hep-ph/0606202
138. Lee T D, Yang C N *Phys. Rev.* **104** 254 (1956)
139. Foot R, Lew H, Volkas R R *Phys. Lett. B* **272** 67 (1991)
140. Foot R, Volkas R R *Phys. Rev. D* **52** 6595 (1995)
141. Berezhiani Z G, Dolgov A D, Mohapatra R N *Phys. Lett. B* **375** 26 (1996); hep-ph/9511221
142. Ignatiev A Yu, Volkas R R *Phys. Lett. B* **487** 294 (2000)
143. Ignatiev A Yu, Volkas R R *Phys. Rev. D* **68** 023518 (2003); hep-ph/0304260
144. Mohapatra R N, Teplitz V L *Phys. Rev. D* **62** 063506 (2000)
145. Berezinsky V, Vilenkin A *Phys. Rev. D* **62** 083512 (2000); hep-ph/9908257
146. Abulencia A et al. *Phys. Rev. Lett.* **97** 171802 (2006); hep-ex/0605101
147. Abazov V M et al. *Phys. Lett. B* **638** 119 (2006); *Phys. Rev. Lett.* **97** 241801 (2006); hep-ex/0604046
148. Feng J L et al. *Phys. Rev. D* **52** 1418 (1995); hep-ph/9502260
149. Ellis J et al. *Phys. Rev. D* **62** 075010 (2000); hep-ph/0004169
150. Baer H et al. *JCAP* (09) 007 (2003); hep-ph/0305191
151. Hooper D, Profumo S *Phys. Rep.* **453** 29 (2007); hep-ph/0701197
152. Peskin M E, arXiv:0707.1536
153. Baltz E A et al. *Phys. Rev. D* **74** 103521 (2006); hep-ph/0602187
154. Datta A K, Kong K, Matchev K T *Phys. Rev. D* **72** 096006 (2005); hep-ph/0509246
155. Carena M, Hooper D, Vallinotto A *Phys. Rev. D* **75** 055010 (2007); hep-ph/0611065
156. Balazs C et al. *JHEP* (06) 066 (2007); hep-ph/0705.0431
157. Abbiendi G et al. (ALEPH, DELPHI, L3, OPAL Collab.) *Phys. Lett. B* **565** 61 (2003); hep-ex/0306033
158. Battaglia M et al. *JHEP* (07) 033 (2005); hep-ph/0502041
159. Bhattacharyya G et al. *Phys. Lett. B* **628** 141 (2005); hep-ph/0502031
160. Bhattacherjee B, Kundu A *Phys. Lett. B* **627** 137 (2005); hep-ph/0508170
161. Jungman G, Kamionkowski M *Phys. Rev. D* **51** 328 (1995); hep-ph/9407351
162. Hooper D, Kribs G D *Phys. Rev. D* **67** 055003 (2003); hep-ph/0208261
163. Crotty P *Phys. Rev. D* **66** 063504 (2002); hep-ph/0205116
164. Lundberg J, Edsjö J *Phys. Rev. D* **69** 123505 (2004); astro-ph/0401113
165. Halzen F, Hooper D *Phys. Rev. D* **73** 123507 (2006); hep-ph/0510048
166. Cirelli M et al. *Nucl. Phys. B* **727** 99 (2005); hep-ph/0506298
167. Ryabov V A *Fiz. Elem. Chastits At. Yadra* (2008) (accepted for publication)
168. Desai S et al. *Phys. Rev. D* **70** 083523 (2004); hep-ex/0404025
169. Ambrosio M et al. *Phys. Rev. D* **60** 082002 (1999); hep-ex/9812020
170. Boliev M et al., in *Proc. of the 24th Intern. Cosmic Ray Conf.: ICRC, Rome, 1995* Vol. 1 (Urbino, 1995) p. 722
171. Aynutdinov V et al. *Nucl. Instrum. Meth. Phys. Res. A* **588** 99 (2008)
172. Ackermann M et al. *Astropart. Phys.* **24** 459 (2006); astro-ph/0508518
173. Landsman H, in *Proc. of the 6th Intern. Workshop on the Identification of Dark Matter, IDM 2006, Greece*; astro-ph/0612239
174. Achterberg A et al. *Astropart. Phys.* **26** 155 (2006); astro-ph/0604450
175. Aguilar J A et al. *Astropart. Phys.* **23** 131 (2005); astro-ph/0412126
176. Aggouras G et al. *Astropart. Phys.* **23** 377 (2005)
177. Amore I et al. *Int. J. Mod. Phys. A* **22** 3509 (2007); arXiv:0709.3991
178. Katz U F *Nucl. Instrum. Meth. Phys. Res. A* **567** 457 (2006); astro-ph/0606068
179. Lim G, in *Proc. of the 15th Intern. Conf. on Supersymmetry and the Unification of Fundamental Interactions, SUSY 2007, Karlsruhe, Germany* Vol. 1 (Eds W de Boer, I Gebauer) (Karlsruhe: Univ. of Karlsruhe, 2007) p. 842; arXiv:0710.3685
180. Beacom J F, Bell N F, Mack G D *Phys. Rev. Lett.* **99** 231301 (2007); astro-ph/0608090
181. Yüksel H et al. *Phys. Rev. D* **76** 123506 (2007); arXiv:0707.0196
182. Hunter S D et al. *Astrophys. J.* **481** 205 (1997)
183. Hooper D et al. *JCAP* (09) 002 (2004); astro-ph/0404205
184. Navarro J F, Frenk C S, White S D *Astrophys. J.* **462** 563 (1996); astro-ph/9508025
185. Moore B et al. *Astrophys. J.* **524** L19 (1999); astro-ph/9907411
186. Hooper D, Dingus B L *Phys. Rev. D* **70** 113007 (2004); astro-ph/0210617
187. de Boer W et al. *Astron. Astrophys.* **444** 51 (2005); astro-ph/0508617
188. de Boer W et al. *Phys. Rev. Lett.* **95** 209001 (2005); astro-ph/0602325
189. Strong A W, Moskalenko I V, Reimer O *Astrophys. J.* **613** 962 (2004); astro-ph/0406254
190. Elsässer D, Mannheim K *Phys. Rev. Lett.* **94** 171302 (2005); astro-ph/0405235
191. Nuss E *Adv. Space Res.* **41** 2029 (2008); arXiv:0704.2738
192. Sellerholm A et al., in *Proc. of the 5th Intern. Workshop on Science with the New Generation High Energy Gamma-Ray Experiments* (Frascati Physics Ser., Vol. 45, Eds A Lionetto, A Morselli) (Frascati: INFN, 2007) p. 87; arXiv:0707.4126
193. Hooper D et al. *Phys. Rev. D* **77** 043511 (2008); FERMILAB-PUB-07-461-A; arXiv:0709.3114
194. Jacholkowska A et al. *Phys. Rev. D* **74** 023518 (2006); astro-ph/0508349
195. Aguilar M et al. *Phys. Rep.* **366** 331 (2002)
196. Goebel F, in *Proc. of the 30th Intern. Cosmic Ray Conf., Merida, Mexico, July 2007*; arXiv:0709.2605
197. Elsässer D, Mannheim K *New Astron. Rev.* **49** 297 (2005); astro-ph/0409563
198. Albert J et al. *Astrophys. J.* **638** L101 (2006); astro-ph/0512469
199. Aharonian F et al. *Phys. Rev. D* **75** 042004 (2007); astro-ph/0701766
200. Aharonian F et al. *Astron. Astrophys.* **425** L13 (2004); astro-ph/0408145
201. Aharonian F et al. *Nature* **439** 695 (2006); astro-ph/0603021
202. Aharonian F et al. *Phys. Rev. Lett.* **97** 221102 (2006); astro-ph/0610509
203. Moulin E et al., in *Proc. of the 30th Intern. Cosmic Ray Conf., Merida, Mexico, July 2007*; arXiv:0711.3682
204. Moulin E et al. *Phys. Rev. D* **77** 055014 (2008); arXiv: 0712.3151
205. Tsuchiya K et al. *Astrophys. J.* **606** L115 (2004); astro-ph/0403592
206. Holder J et al. *Astropart. Phys.* **25** 391 (2006); astro-ph/0604119
207. Kosack K et al. *Astrophys. J.* **608** L97 (2004); astro-ph/0403422
208. Maier G et al., in *Proc. of the 30th Intern. Cosmic Ray Conf., Merida, Mexico, July 2007*; arXiv:0709.3654
209. Atkins R et al. *Astrophys. J.* **604** L25 (2004); astro-ph/0311389
210. Atkins R et al. *Astrophys. J.*; astro-ph/0403097
211. Atkins R et al., astro-ph/0405291
212. Bergström L, Hooper D *Phys. Rev. D* **73** 063510 (2006); hep-ph/0512317
213. Profumo S, Kamionkowski M *JCAP* (03) 003 (2006); astro-ph/0601249
214. Lavalle J et al. *Astron. Astrophys.* **450** 1 (2006); astro-ph/0601298
215. Bottino A et al. *Phys. Rev. D* **58** 123503 (1998); astro-ph/9804137
216. Bergström L et al. *Phys. Rev. D* **59** 043506 (1999); astro-ph/9806072

217. Bergström L, Edsjö J, Ullio P *Astrophys. J.* **526** 215 (1999); astro-ph/9902012
218. Barwick S W et al. *Phys. Rev. Lett.* **75** 390 (1995); astro-ph/9505141
219. Barwick S W et al. *Astrophys. J.* **482** L191 (1997); astro-ph/9703192
220. Maeno T et al. *Astropart. Phys.* **16** 121 (2001); astro-ph/0010381
221. Boezio M et al. *Astrophys. J.* **561** 787 (2001); astro-ph/0103513
222. Casolino M et al. *Adv. Space Res.* **42** 455 (2008); arXiv:0708.1808
223. Picozza P, Galper A M, Castellini G *Astropart. Phys.* (submitted); astro-ph/0608697
224. Lionetto A M, Morselli A, Zdravkovic V *JCAP* (09) 010 (2005); astro-ph/0502406
225. Hooper D, Kribs G D *Phys. Rev. D* **70** 115004 (2004); hep-ph/0406026
226. Hooper D, Silk J *Phys. Rev. D* **71** 083503 (2005); hep-ph/0409104
227. Brun P *Eur. Phys. J. C* **56** 27 (2008); arXiv:0710.2458
228. Baudis L *Int. J. Mod. Phys. A* **21** 1925 (2006); astro-ph/0511805
229. Morales A et al. *Phys. Lett. B* **489** 268 (2000); hep-ex/0002053
230. Klapdor-Kleingrothaus H V et al. *Astropart. Phys.* **18** 525 (2003); hep-ph/0206151
231. Burgos S et al. *Astropart. Phys.* (submitted); arXiv:0707.1488
232. Santos D et al. *J. Phys. Conf. Ser.* **39** 154 (2006); astro-ph/0512220
233. Bernabei R et al. *Int. J. Mod. Phys. D* **13** 2127 (2004); astro-ph/0501412
234. Bernabei R, Contributed paper to Neutrinoless Double Beta Decay (NDBD07), Ahmedabad (India), February 2007; arXiv:0704.3543
235. Ahmed B et al. *Astropart. Phys.* **19** 691 (2003); hep-ex/0301039
236. Cebrián S et al. *Nucl. Phys. B Proc. Suppl.* **114** 111 (2003); hep-ex/0211050
237. Shimizu Y et al. *Phys. Lett. B* **633** 195 (2006); astro-ph/0510390
238. Lee H S et al. *Phys. Rev. Lett.* **99** 091301 (2007); arXiv:0704.0423
239. Fushimi K-I et al. *J. Phys. Conf. Ser.* **120** 042024 (2008); arXiv:0711.3053
240. Sumner T, in *Proc. of the 5th Intern. Symp. Sources and Detection of Dark Matter and Dark Energy in the Universe, Marina del Ray, 2002*
241. Cebrián S et al. *Astropart. Phys.* **15** 79 (2001); astro-ph/0004292
242. Cebrián S et al. *Nucl. Phys. B Proc. Suppl.* **110** 97 (2002); astro-ph/0112272
243. Takeda A et al. *Phys. Lett. B* **572** 145 (2003); astro-ph/0306365
244. Angloher C et al. *Astropart. Phys.* **18** 43 (2002)
245. Bolte W J et al. *Nucl. Instrum. Meth. Phys. Res. A* **577** 569 (2007); astro-ph/0503398
246. Bertone G et al. *Phys. Rev. Lett.* **99** 151301 (2007); arXiv:0705.2502
247. Barnabé-Heider M et al. *Phys. Lett. B* **624** 186 (2005); hep-ex/0502028
248. Girard T A et al. *Phys. Lett. B* **621** 233 (2005); hep-ex/0505053
249. Borer K et al. *Astropart. Phys.* **22** 199 (2004); astro-ph/0404311
250. Angloher G et al. *Astropart. Phys.* **23** 325 (2005); astro-ph/0408006
251. Akerib D S et al. *Phys. Rev. D* **68** 082002 (2003); hep-ex/0306001
252. Akerib D S et al. *Phys. Rev. Lett.* **93** 211301 (2004); astro-ph/0405033
253. Brink P L et al., in *Proc. of 22nd Texas Symp. on Relativistic Astrophysics, Stanford, 2004*, p. 2529; astro-ph/0503583
254. Sanglard V et al. *Phys. Rev. D* **71** 122002 (2005); astro-ph/0503265
255. Chantelauze A, in *Proc. of the 15th Intern. Conf. on Supersymmetry and the Unification of Fundamental Interactions, SUSY 2007, Karlsruhe, Germany* Vol. 1 (Eds W de Boer, I Gebauer) (Karlsruhe: Univ. of Karlsruhe, 2007); arXiv:0710.5849
256. Alner G J et al., astro-ph/0701858
257. Akimov D Yu et al. *Astropart. Phys.* **27** 46 (2007); astro-ph/0605500
258. Angle J et al. *Phys. Rev. Lett.* **100** 021303 (2008); arXiv:0706.0039
259. Benetti P et al. *Astropart. Phys.* (submitted); astro-ph/0701286
260. Amerio S et al. *Nucl. Instrum. Meth. Phys. Res. A* **527** 329 (2004)
261. Laffranchi M, Rubbia A *J. Phys. Conf. Ser.* **65** 012014 (2007); hep-ph/0702080
262. Alexandrov K V et al. *Nucl. Instrum. Meth. Phys. Res. A* **459** 135 (2001)
263. Aleksandrov K V et al. *Nucl. Phys. B Proc. Suppl.* **113** 344 (2002)
264. Aleksandrov K V et al. *Ozv. Ross. Akad. Nauk Ser. Fiz.* **66** 1624 (2002) [*Bull. Russ. Acad. Sci. Phys.* **66** 1795 (2002)]
265. Aleksandrov K V et al. *Nucl. Phys. B Proc. Suppl.* **122** 427 (2003)
266. Ammosov V V et al. *Nucl. Phys. B Proc. Suppl.* **151** 426 (2006)
267. Mukhamedshin R A *Nucl. Phys. B Proc. Suppl.* **97** 189 (2001)
268. Ammosov V V et al. *Nucl. Phys. B Proc. Suppl.* **166** 140 (2007)
269. Ammosov V V et al. *Nucl. Phys. B Proc. Suppl.* **175** 190 (2008)
270. Ohsawa A, Shibuya E, Tamada M, in *29th Intern. Cosmic Ray Conf., Pune, India, 2005* Vol. 9 (Mumbai Tate Inst. of Fundamental Res., 2005) p. 49
271. Zhukov A P et al. *Kratk. Soobshch. Fiz.* (10) 40 (2005) [*Bull. Lebedev Phys. Inst.* (10) 33 (2005)]
272. Kotelnikov K A et al. *Akust. Zh.* **44** 76 (1998) [*Acoust. Phys.* **44** 61 (1998)]
273. Askaryan G A *At. Energ.* **3** 152 (1957) [*At. Energy* **3** 921 (1957)]
274. Golovashkin A I et al. *Kratk. Soobshch. Fiz.* (10) 35 (2007) [*Bull. Lebedev Phys. Inst.* (10) 296 (2007)]
275. Lounasmaa O V *Experimental Principles and Methods Below 1 K* (New York: Academic Press, 1974)
276. Clarke J *Phys. Today* **39** (3) 36 (1986)
277. SUSY Dark Matter/Interactive Direct Detection Limit Plotter, http://dmtools.berkeley.edu/limitplots/
278. Baltz E A, Gondolo P *Phys. Rev. D* **67** 063503 (2003); astro-ph/0207673
279. Ellis J et al. *Phys. Rev. D* **71** 095007 (2005); hep-ph/0502001